R-06-109

# Mineralogy and geochemistry of rocks and fracture fillings from Forsmark and Oskarshamn: Compilation of data for SR-Can

Henrik Drake, Björn Sandström
Isochron GeoConsulting HB

Eva-Lena Tullborg, Terralogica AB

November 2006

**Svensk Kärnbränslehantering AB**
Swedish Nuclear Fuel
and Waste Management Co
Box 5864
SE-102 40 Stockholm Sweden
Tel 08-459 84 00
+46 8 459 84 00
Fax 08-661 57 19
+46 8 661 57 19

ISSN 1402-3091
SKB Rapport R-06-109

# Mineralogy and geochemistry of rocks and fracture fillings from Forsmark and Oskarshamn: Compilation of data for SR-Can

Henrik Drake, Björn Sandström
Isochron GeoConsulting HB

Eva-Lena Tullborg, Terralogica AB

November 2006

*Keywords:* SR-Can, Redox, Geochemistry, Fracture mineralogy, Density, Porosity.

# Abstract

This report is a compilation of the so far available data for the safety assessment SR-Can carried out by SKB. The data consists of mineralogy, geochemistry, porosity, density and redox properties for both dominating rock types and fracture fillings at the Forsmark and Oskarshamn candidate areas. In addition to the compilation of existing information, the aim has been to identify missing data and to clarify some conception of e.g. deformation zones. The objective of the report is to present the available data requested for the modelling of the chemical stability of the two sites. The report includes no interpretation of the data.

The data has been compiled from SKB reports in the R- and P-report series as well as from the SKB data base SICADA.

# Sammanfattning

Denna rapport är en sammanställning av den information som i nuläget finns tillgänglig för säkerhetsutvärderingen SR-Can som utförs av SKB. Informationen består av mineralogi, geokemi, porositet, densitet och redox-egenskaper hos de dominerande bergarterna och sprickfyllnaderna i platsundersökningsområdena Forsmark respektive Oskarshamn. Dessutom har målet varit att identifiera information som saknas och klargöra vissa begrepp såsom deformationszoner. Syftet med rapporten är att presentera tillgänglig data som efterfrågats vid modelleringen av de två områdenas kemiska stabilitet. Rapporten innehåller inga tolkningar av resultaten.

Data har sammanställts från SKB:s rapporter (R- och P-rapporter) och från SKB:s databas SICADA.

# Contents

# 1 Introduction

This report is a compilation of the so far available data for the safety assessment SR-Can carried out by SKB. The information compiled has been earlier published in a large number of SKB reports in the R- and P-report series. The data consists of mineralogy, geochemistry, porosity, density and redox properties for both dominating rock types and fracture fillings at the Forsmark and Oskarshamn candidate areas. All referred data has been extracted from SKB's database SICADA. In addition to compilation of existing information, the aim has been to identify missing data. In some cases ongoing studies will provide this data whereas in others, new studies need to be initiated.

The Forsmark and Laxemar/Simpevarp sites are treated in two separate sections of the report.

The focus for the Laxemar/Simpevarp site is on Laxemar but Simpevarp data has been included to get better statistic representation when appropriate. When data from Simpevarp and Laxemar has been used together this is always indicated.

Appendix 1 gives a list of minerals mentioned in this report and their chemical formula.

## 1.1 Characterisation of deformation zones

Rock types, wall rock alteration, fractures (open and sealed) and fracture minerals are initially documented during the mapping of the drill core according to the Boremap programme, which forms an integral part of the site characterisation protocol. When the drill core mapping is finished a single hole interpretation is conducted, whereby all available data from the drill core and borehole are used (including geophysical and flow logging) to distinguish deformations zones from more intact parts of the rock.

The deformation zone concept includes ductile as well as brittle zones. It is however common that brittle and ductile deformations are linked, often localised to the borders of mylonites (fine-grained, compact rock that formed by ductile deformation and recrystallisation as a response to shear stress) and less deformed rock.

Not all of the deformations zones recorded by the single-hole interpretations can be linked to deformation zones identified in other boreholes or at the surface as lineaments. This is more or less necessary to have a deformation zone upgraded to "deterministic", unless they are very clearly indicated geophysically.

According to this definition of deformation zones the width and extent of the zones can vary widely. This also means that the width and in the best case the length of a deformation zone is determined on geological grounds but does not for example imply that the zone is hydraulically conductive. Therefore, more detailed descriptions of the deformation zones may be needed for e.g. radionuclide transport modelling and performance assessment. Two different zone types, one from Forsmark and one from Laxemar are illustrated in Figures (1-1 and 1-2) showing core mapping, flow logging and BIPS images from each deformation zone.

Figure 1-1 shows the deformation zone ZFMNE0060 detected between 318 and 358 m in borehole KFM06A. Within this interval the bedrock is altered, with exception of a few meters at about 340 m core length. The fracture frequency is increased especially in the deeper part of the zone. The most hydraulically active part, in contrast, is located in the upper part of the zone. The flow rate is however relatively low; at maximum ~ 1,000 mL/hour, but mostly ~ 100 mL/hour or less. The water conducting fractures are relatively few, with the most conductive ones at 321.4 and 322.0 m core length. The BIPS image of this short section shows the water conducting fractures at ~ 322 m, which appear to be relatively simple fractures with widths around 1 mm or less. From a radionuclide transport point of view this deformation zone

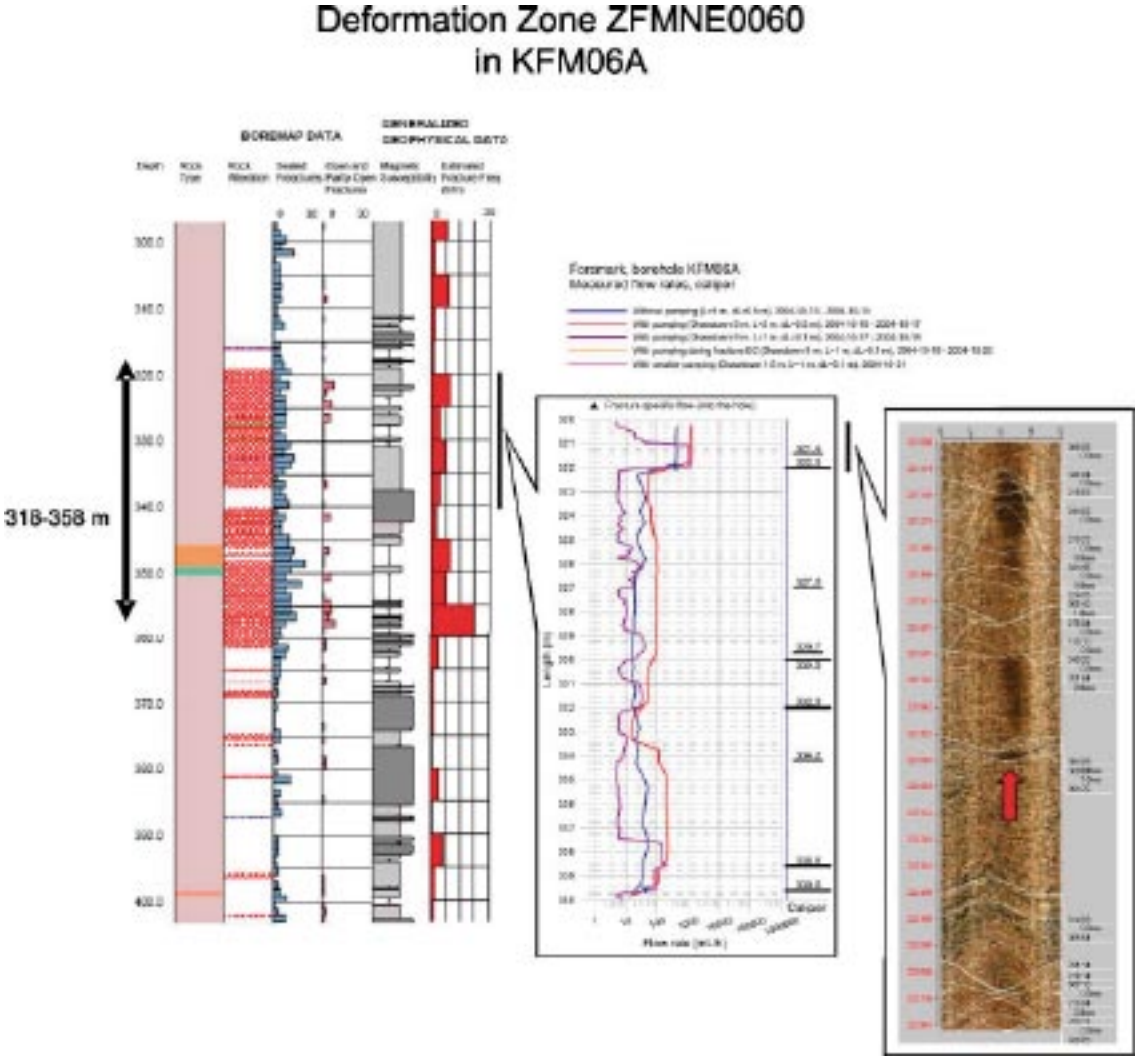


***Figure 1-1.*** *Deformation zone ZFMNE0060 in KFM06A at Forsmark, the zone is identified between 318–358 m. The left figure is the Boremap data from the drill core mapping, the middle figure is from the flow logging and the right figure is the BIPS image of a water conductive fracture.*

may not be a prominent conductor but it contains large amounts of fractures which can act as diffusion pathways with properties significantly different than the host rock.

Figure 1-2 shows the intersection of deformation zone ZSMEW007 in the borehole KLX04 at Laxemar. The zone is identified between 310 and 390 m core length where also the fracture frequency is enhanced. The wall rock alteration is most prominent between 340 to 385 m. The most intense brittle deformation is centred in the interval 345 and 353 m. Here both sealed fracture networks and high frequency of open fractures are documented and the detected flow in 5 m sections amounts to ~ 10 000 mL/hour. Around 15 different flow-log anomalies (conductive structures) are recorded in the interval 340 to 360 m. The BIPS image of the interval 352.3 to 353.8 m shows some of these structures which are either gouge filled faults, a few mm in width, or a number of fractures closely located.

It is important to note that the illustrated zones above are just examples and that larger and smaller and more or less hydraulically active deformation zones exist at both sites, which underlines the need for more detailed descriptions of the deformation zones focusing on properties important for radionuclide transport and retention.

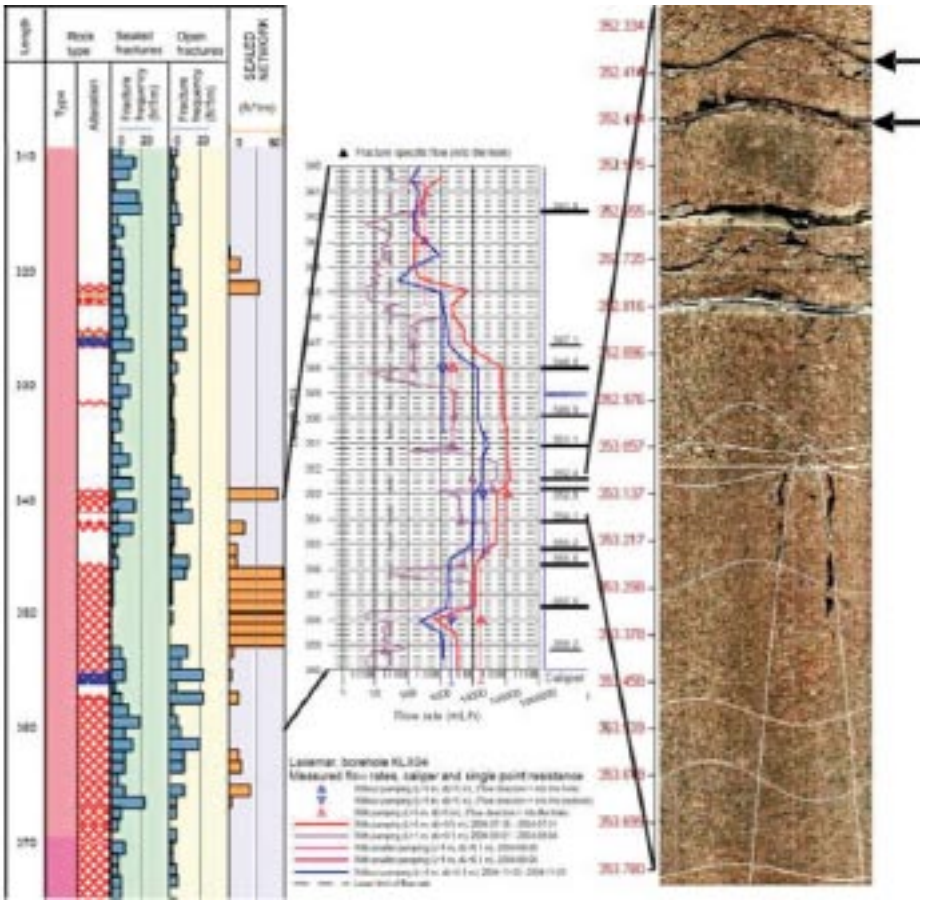

***Figure 1-2.*** *Deformation zone ZSMEW007 in KLX04 at Laxemar. The zone is identified between 310 and 390 m. The left figure is the Boremap data from the drill core mapping, the middle figure is from the flow logging and the right figure is the BIPS image with marked water conductive fractures.*

A number of potential problems concerning the description of the properties of a deformation zone can also be foreseen: for example, the determination of the hydraulically/non-hydraulically conductive fractures pointed out in /Byegård et al. 2006/. The flow-log can only identify features with transmissivities $\geq 10^{-9}$ m/s, but presumably a large part of the fractures mapped as open but not identified with the flow-log have transmissivities large enough to require their incorporation in the radionuclide transport modelling. During the mapping the fractures have been given different confidence levels: certain, probable and possible /SKB 2004c/. It looks as if the open fractures with confidence "certain" largely correspond to the fractures identified as water conducting, but for example at Laxemar these only constitute 3 to 10% of all the open fractures /Byegård et al. 2006/ and it is therefore likely that a portion of the fractures mapped as "probable" and "possible" should be considered as well. The parameterisation of the rock mass and the less conductive parts of the deformation zones in between the fractures is dependent on assumptions made on the number of open fractures that are included as flowing structures in the transport modelling. The rest of the fractures (the sealed and the open ones without flow) will contribute to the properties of the rock mass (alternatively in this case the deformed and altered rock) with a higher porosity and preferred diffusion pathways.

In conclusion; a better description of the deformation zones including parameters of importance for the radionuclide transport models and for the performance assessment analyses is suggested for the SR-Site project.

# 2 Forsmark

## 2.1 Rock mass

The candidate area at the Forsmark site is dominated by a granitic to granodioritic rock (rock code 101057) (Figure 2-1; 2-2) that occupies ~ 84% of the candidate site volume. 10% consists of granodioritic, tonalitic and granitic rock (rock code 101051) which occurs as lenses and dykes in the former rock type. Together, these two rock types occupy 94% of the candidate site volume. A description of these rock types and the subordinate rock types are presented in the following sections and summarized in Table 2-6. In the rock type descriptions, the mineralogy of all rock types is presented to give a broader geological view of the area. The volumetric numbers above are quantitative estimations and do not include occurrences less than 1 m in borehole length /SKB 2005a/. The rock codes are the standard rock codes used by the Geological Survey of Sweden (SGU) in their bedrock mapping.

### 2.1.1 Description of rock types

The following section is a description of the rock characteristics (compiled from /SKB 2005b/ when nothing else is stated). The rock types dealt with in this section are the ones making up a major component in the rock domain model. The mineralogical composition is based on point counting and the dominant minerals are presented for each rock type. Minor minerals (chlorite, epidote, allanite, prehnite, titanite, calcite, apatite, opaque) are normally only accounted for in this report when the mean content is ≥ 0.2%. The major mineral data is from /Stephens et al. 2003, 2005, Petersson et al. 2004b, 2005a/ and has been summarized in /SKB 2005b/. The minor mineral data has been compiled from /Petersson et al. 2004b, 2005a/. Where only trace amounts of minor minerals have been noted, the numeric value of 0.1% has been assign since it is below the detection limit since 500 points have been used during the point counting. This value has then been used in the calculations of mean and standard deviation thus causing a small systematic error in the values of the minor mineral content.

The pyrite content is not distinguished from other opaque minerals during the point counting. The amount of opaque minerals in the dominating granite (rock code 101057) is 0.3% ± 0.2, thus providing a theoretical maximum pyrite content of the rock. In reality, the main opaque mineral is magnetite and a lower pyrite content can be expected. A maximum pyrite content based on the S content in the rock has been calculated to ~ 0.4% (Section 2.1.2.1). In the subordinate granodiorite-tonalite-granite (rock code 101051), the opaque minerals make up less than 0.2%. Based on the S content in this rock type, a maximum pyrite content has been calculated to 0.75% (Section 2.1.2.2). During a rock alteration study which will be carried out during 2006, the pyrite content of both unaltered and altered will be analysed.

The grain size of typical biotite crystals in both rock type 101057 and 101051 varies but an estimation based on microscopy suggests a mean size of ~ 400×200µm (~ 0.08 $mm^2$) although aggregates of grains up to 2 $mm^2$ are also found (Figure 2-3).

Pyrite crystals occur only scattered in the both rock types, but an estimated normal grain size is ~ 0.03 $mm^2$ as shown in Figure 2-4.

The calcite content in the rock is low, 0.2% or less in all rock types in the Forsmark area according the point counting. Based on the C content in the two major rock types, a maximum calcite content of 0.08% in the granite to granodiorite (rock code 101057) and 0.25% in the granite-granodiorite-tonalite (rock code 101051) has been calculated (Section 2.2.1.1 and 2.2.1.2).

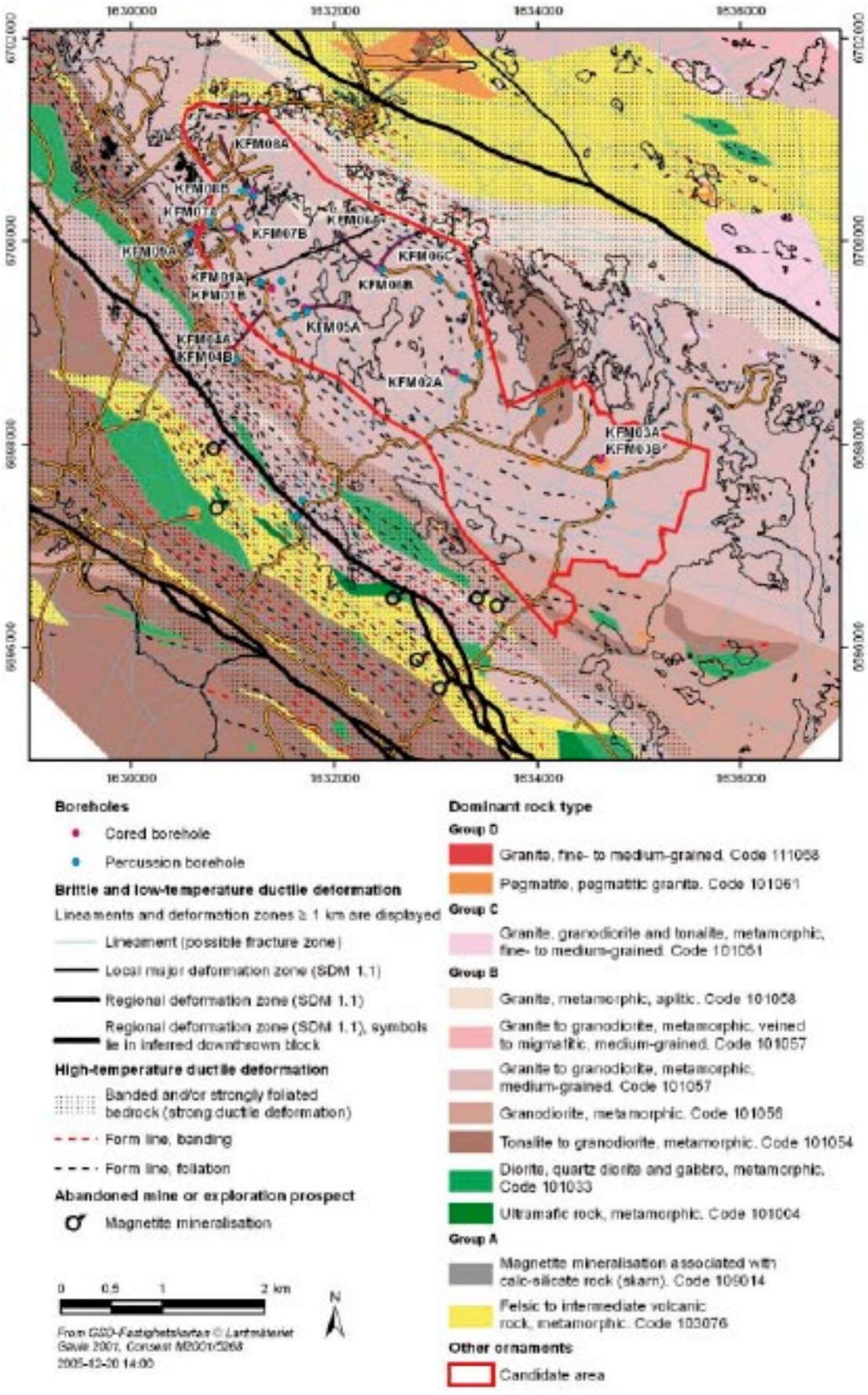


***Figure 2-1.*** *Bedrock geology map of the Forsmark site with surface projections of the boreholes dealt with in this report /SKB GIS 2005/.*

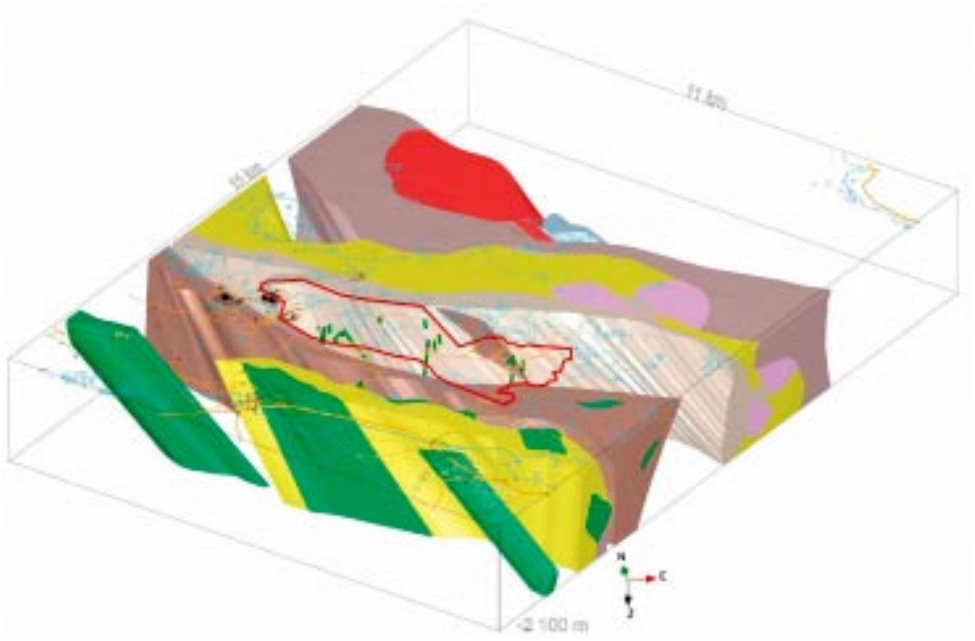

***Figure 2-2.*** *3D model of the Forsmark area (Rock domain model 1.2). The unshaded volume is the granite to granodiorite (rock code 101057), the other rock types have the same colour code as in legend in Figure 2-1. /Model provided by A. Simeonov SKB/.*

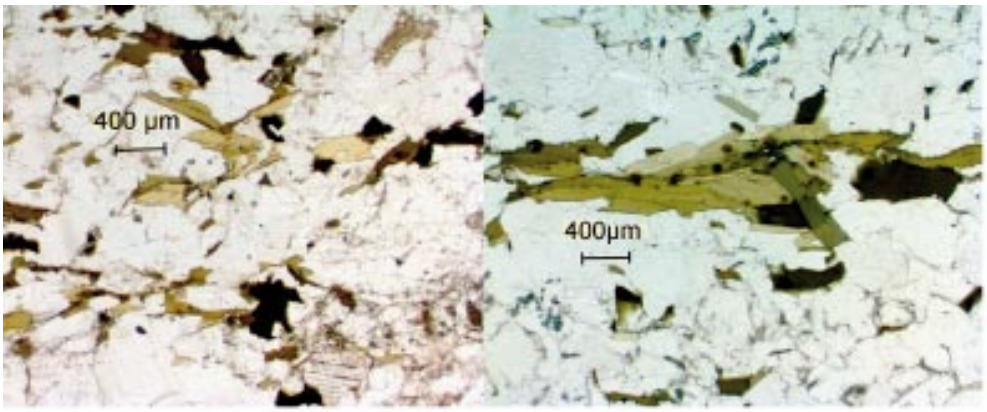


***Figure 2-3.*** *Photomicrograph of biotite crystals of normal size (left) and a larger aggregate of biotite crystals (right). All dark green to black minerals in the images are biotite crystals.*

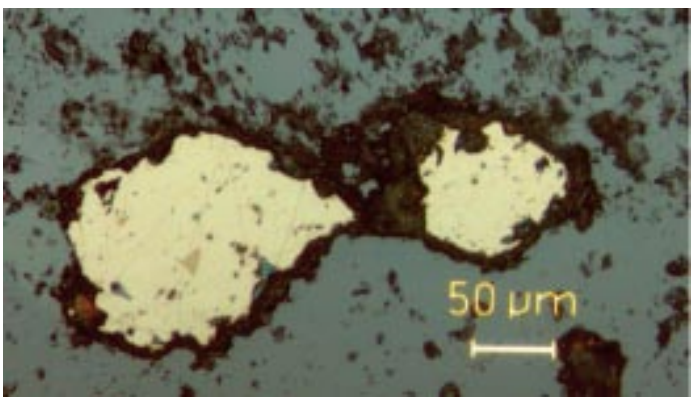


***Figure 2-4.*** *Photomicrograph in reflected light of normal sized pyrite grains surrounded by chlorite.*

The rock types in the Forsmark area are divided into four major groups (A–D):

- The oldest rocks belong to Group A and are dominated by metavolcanic rocks and iron oxide mineralizations older than 1,885 Ma.
- Group B consists of major plutonic rocks with variable composition and belongs to a suite of intrusive rocks between 1,865 and 1,886 Ma old.
- Group C and D are minor intrusive rocks and are younger than the rocks in Group A and most of the rocks in Group B. However, their absolute ages overlap with the youngest rocks in Group B.

Short descriptions of the texture and mineralogy of the rock types at the Forsmark site are listed below, obtained from /Petersson et al. 2004b, 2005a, SKB 2005b/. The two major rock types in the candidate area (rock code 101057 and 101051) are highlighted with grey. It is common that wall rock adjacent to fractures has undergone hydrothermal alteration creating changes in mineralogy and physical properties like e.g. porosity. Studies of hydrothermally altered rock which occurs adjacent to many fractures will be undertaken during 2006. A minor qualitative study of the wall rock alteration is available in /Sandström and Tullborg 2005/, which show replacement of biotite by chlorite and saussuritization of plagioclase (i.e plagioclase is replaced by albite, k-feldspar, epidote and hematite). This is in agreement with wall rock alteration studies carried out at the Oskarshamn site /Drake and Tullborg 2006ab/.

## Group A

***Felsic to intermediate volcanic rock – rock code 103076***

Fine-grained equigranular rock with a foliated, lineated and in part banded, folded structure. The mineral fabric consists of tectonic foliation/banding and mineral stretching lineation. The degree of inhomogeneity is high and the rock has been metamorphosed under amphibolite facies. In part, the rock has been K-Na altered pre-metamorphism.

*Mineralogical composition (vol%)*

| Mineral | Range | Mean | Std | |
|---|---|---|---|---|
| Quartz | 5.2–39.2 | 26.0 | 10.3 | N=15 |
| K-feldspar | 0–12.6 | 3.4 | 4.1 | |
| Plagioclase | 29.2–53.2 | 48.6 | 6.5 | |
| Biotite | 0–22.8 | 12.0 | 8.0 | |
| Hornblende | 0–35.6 | n.a. | n.a. | |
| Chlorite | 0.4 | n.a. | n.a. | N=1 |
| Allanite | 0.2 | n.a. | n.a. | |
| Apatite | 0.4 | n.a. | n.a. | |

***Sedimentary rock – rock code 106001***

Fine-grained equigranular rock with a banded, lineated and folded structure. The mineral fabric consists of mineral stretching foliation. The degree of inhomogeneity is high and the rock has been metamorphosed under amphibolite facies.

*Mineralogical composition*

No data available.

## Group B

### *Ultramafic rocks – rock code 101004*

The ultramafic rocks are a subordinate rock type part of the suite of intrusive rocks affected by ductile deformation (Group B) that dominate the Forsmark site. The ultramafic rocks are medium-grained and equigranular and have a low degree of inhomogeneity. They have been metamorphosed under amphibolite facies and locally show serpentinization.

*Mineralogical composition (N=2) (vol%)*

| Mineral | Range | Mean | Std |
|---|---|---|---|
| Pyroxene | 46.6–61.2 | n.a. | n.a. |
| Hornblende (actinolite) | 9.6–31.0 | n.a. | n.a. |
| Olivine (serpentine) | 0–35.2 | n.a. | n.a. |

### *Diorite, quartz diorite and gabbro – rock code 101033*

Medium-grained, equigranular rocks with a lineated and weakly foliated structure. Their mineral fabric consists of a mineral stretching lineation. They have a low degree of inhomogeneity and have been metamorphosed under amphibolite facies.

*Mineralogical composition (N=11) (vol%)*

| Mineral | Range | Mean | Std |
|---|---|---|---|
| Plagioclase | 40.4–64.6 | 51.3 | 5.0 |
| Hornblende | 10.6–50.6 | 27.6 | 11.5 |
| Biotite | 0–14.2 | 8.3 | 5.0 |
| Quartz | 0–24.6 | 8.3 | 7.7 |

### *Granitoid – rock code 111051*

A lineated and weakly foliated rock, the rock is poorly described and has only been mapped on under the Öregrundsgrepen.

*Mineralogical composition (N=0)*

No data available.

### *Granite (to granodiorite) – rock code 101057*

The main rock type at the Forsmark site and the main rock type of Group B is medium grained, equigranular with a lineated and weakly foliated structure. The mineral fabric consists of a mineral stretching lineation. The rock has a low degree of inhomogeneity and has been metamorphosed under amphibolite facies. For pyrite content, see Section 2.1.1.

*Mineralogical composition (vol%)*

| Mineral | Range | Mean | Std | |
|---|---|---|---|---|
| Quartz | 27.8-45.8 | 35.6 | 4.2 | N=46 |
| K-feldspar | 0.2–36.0 | 22.5 | 8.6 | |
| Plagioclase | 24.0–63.8 | 35.6 | 8.5 | |
| Biotite | 0.8–8.2 | 5.1 | 1.6 | |
| Chlorite | 0–1.2 | 0.2 | 0.3 | N=23 |
| Epidote | 0.1–3.2 | 0.6 | 0.7 | |
| Titanite | 0–1.0 | 0.2 | 0.2 | |
| Allanite | 0–0.6 | 0.2 | 0.2 | |
| Opaque | 0–0.8 | 0.3 | 0.2 | |

***Granite (to granodiorite) – rock code 111057***

Similar to the granite (to granodiorite) with rock code 101057, but with a veined to migmatic structure.

*Mineralogical composition (N=0)*

No data available, similar to 101057.

***Tonalite to granodiorite – rock code 101054***

Medium-grained and equigranular rock with a lineated and weakly foliated structure. The mineral fabric consists of a mineral stretching lineation. The rock has a low degree of inhomogeneity and has been metamorphosed under amphibolite facies.

*Mineralogical composition (vol%)*

| Mineral | Range | Mean | Std | N=25 |
|---|---|---|---|---|
| Quartz | 0–45.4 | 23.4 | 9.1 | |
| K-feldspar | 0–21.8 | 5.9 | 5.4 | |
| Plagioclase | 19.6–61.4 | 47.4 | 9.1 | |
| Biotite | 0–15.6 | 9.5 | 4.7 | |
| Hornblende | 0–41.8 | 10.0 | 9.1 | |
| Chlorite | 0.2 | n.a. | n.a. | N=2 |
| Epidote | 0.2–0.6 | n.a. | n.a. | |
| Titanite | 0.1–0.6 | n.a. | n.a. | |
| Calcite | 0.2 | n.a. | n.a. | |
| Apatite | 0.1–0.2 | n.a. | n.a. | |

## Group C

***Granodiorite, tonalite and granite – rock code 101051***

Fine- to medium-grained equigranular rocks with a lineated and weakly foliated structure. Their mineral fabric consists of a mineral stretching lineation. They have a low degree of inhomogeneity and have been metamorphosed under amphibolite facies. For pyrite content, see Section 2.1.1.

*Mineralogical composition (vol%)*

| Mineral | Range | Mean | Std | |
|---|---|---|---|---|
| Quartz | 15.4–35.4 | 27.3 | 5.6 | N=23 |
| K-feldspar | 0–38.0 | 12.2 | 12.0 | |
| Plagioclase | 29.4–67.0 | 46.4 | 10.0 | |
| Biotite | 1.8–19.4 | 9.1 | 4.8 | |
| Hornblende | 0–25.2 | n.a. | n.a. | |
| Epidote | 0.4–1.8 | 1.3 | 0.9 | N=7 |
| Titanite | 0–1.8 | 0.4 | 0.5 | |

## Group D

### *Granite – rock code 111058*

Fine-grained to medium grained equigranular granitic rock that occurs as dykes or locally larger bodies. The granite has been affected by penetrative ductile deformation under lower amphibolite facies metamorphism.

*Mineralogical composition (vol%)*

| Mineral | Range | Mean | Std | |
|---|---|---|---|---|
| Quartz | 25.4–42.8 | 32.4 | 6.4 | N=5 |
| K-feldspar | 22.6–37.8 | 29.6 | 5.6 | |
| Plagioclase | 22.0–46.2 | 33.0 | 9.3 | |
| Biotite | 0.6–4.4 | 2.7 | 1.6 | |
| Chlorite | 1.6–2.4 | n.a. | n.a. | N=2 |
| Epidote | 0.2–0.8 | n.a. | n.a. | |
| Opaque | 0.1–0.6 | n.a. | n.a. | |

### *Granite, aplitic – rock code 101058*

Fine-grained (and leucratic) equigranular rock with a lineated and weakly foliated structure. The mineral fabric consists of tectonic foliation/banding and mineral stretching lineation. The degree of inhomogeneity is high and the rock has been metamorphosed under amphibolite facies.

*Mineralogical composition (vol%)*

| Mineral | Range | Mean | Std | N=7 |
|---|---|---|---|---|
| Quartz | 30.8–44.4 | 37.3 | 4.4 | |
| K–feldspar | 4.0–47.0 | 22.9 | 15.9 | |
| Plagioclase | 18.8–58.2 | 37.1 | 15.8 | |
| Biotite | 0–2.0 | 1.1 | 0.9 | |
| Chlorite | 0.2–1.0 | 0.4 | 0.4 | N=5 |
| Epidote | 0.1–1.0 | 0.6 | 0.5 | |

### 2.1.2 Geochemistry

The geochemistry of the two dominating rock types within the Forsmark candidate area is described below. The geochemistry of altered rock found adjacent to many fractures will be analysed during 2006 as mentioned above.

#### *2.1.2.1 Granite to granodiorite (rock code 101057)*

The geochemistry of the most abundant rock type in the candidate area, the granite to granodiorite (rock code 101057), is characterized by a high $SiO_2$ content in agreement with the high quartz content in the rock. The total S content is 0.2 wt%, stoichiometric recalculation to pyrite gives a maximum pyrite content of ~ 0.4 wt%. The total C content is 0.01 wt% which gives a maximum calcite content (if all C is in the form of calcite) of ~ 0.08 wt%. Both S and C were analysed by volatization at > 1,650°C and the S and C content was determined by absorption of specific infrared wavelengths /Petersson et al. 2005a/, a more detailed S analyse will be carried out during 2006. The geochemistry of rock type 101057 is summarized in Table 2-1. The high Ba and low Cs content and the low LOI value are in accordance with the high alkali feldspar and relatively low mica content in the rock. The low Sr content supports the relatively low plagioclase content. The rock type has very low concentrations of almost all trace elements except the REEs. U and Th contents are both normal. Chondrite-normalized REE pattern show enrichment in the light REEs relative to the heavy REEs which is typical for granitic rocks (Figure 2-5). All the granite samples have negative Eu anomalies, probably due to fractional crystallization of plagioclase during the intrusion of the granites or inherited from the source of the granite.

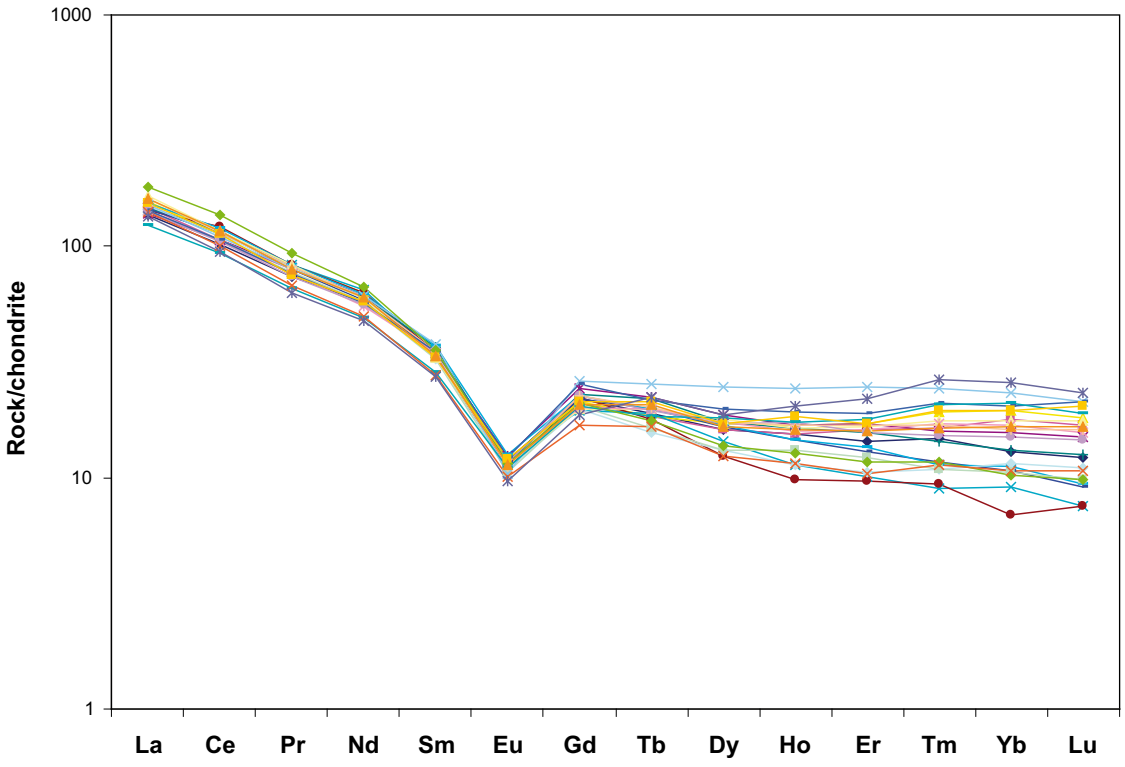


***Figure 2-5.*** *Chondrite normalized REE-pattern for granitic to granodioritic rock (rock code 101057). Data from /Petersson et al. 2005ab/. Chondrite values from /Evansen et al. 1978/ (N=23).*

**Table 2-1. Whole-rock geochemistry of granitic to granodioritic rock (rock code 101057). Mean and standard deviation values have been calculated based on data from /Petersson et al. 2004b, 2005a/. LOI = Lost on ignition, TOT/C = total C, TOT/S = total S. (*N23*).**

| Element | Mean (N=23) | Std | Element | Mean (N=23) | Std | Element | Mean (N=23) | Std | Element | Mean (N=23) | Std | Element | Mean (N=23) | Std |
|---|---|---|---|---|---|---|---|---|---|---|---|---|---|---|
| SiO2(wt%) | 74.38 | 0.78 | Sc (ppm) | 5.50 | 0.71 | Nb | 10.85 | 0.35 | Bi | <0.1 | n.a. | Tm | 0.53 | 0.21 |
| TiO2 | 0.20 | 0.02 | V | 6.00 | 2.83 | Mo | 0.75 | 0.07 | Th | 13.95 | 0.92 | Yb | 3.20 | 1.51 |
| Al2O3 | 12.92 | 0.13 | Cr | <7 | n.a. | Ag | <0.1 | n.a. | U | 4.20 | 0.14 | Lu | 0.45 | 0.20 |
| Fe2O3 | 2.67 | 0.37 | Co | 2.00 | 0.71 | Sn | <0.1 | n.a. | La | 33.30 | 0.42 | Au (ppb) | 2.55 | 1.63 |
| MnO | 0.04 | 0.00 | Ni | 2.20 | 0.14 | Cd | 1.03 | 1.38 | Ce | 63.10 | 3.11 | | | |
| MgO | 0.41 | 0.16 | Cu | 8.70 | 2.40 | Sb | 0.10 | 0.00 | Pr | 6.59 | 0.81 | | | |
| CaO | 1.57 | 0.22 | Zn | 23.00 | 2.83 | Cs | 0.55 | 0.07 | Nd | 24.95 | 3.32 | | | |
| Na2O | 3.55 | 0.22 | Ga | 15.00 | 0.28 | Ba | 1234.95 | 190.99 | Sm | 4.65 | 0.64 | | | |
| K2O | 3.39 | 0.04 | As | <0.5 | n.a. | Hf | 4.90 | 0.42 | Eu | 0.60 | 0.06 | | | |
| P2O5 | 0.04 | 0.00 | Se | <0.5 | n.a. | Ta | 0.70 | 0.42 | Gd | 4.15 | 0.50 | | | |
| LOI | 0.65 | 0.07 | Rb | 94.05 | 18.46 | W | 0.30 | 0.14 | Tb | 0.77 | 0.08 | | | |
| TOT/C | 0.01 | 0.00 | Sr | 94.95 | 7.85 | Hg | 0.01 | 0.00 | Dy | 4.41 | 0.48 | | | |
| TOT/S | 0.02 | 0.01 | Y | 30.65 | 7.85 | Tl | 0.20 | 0.00 | Ho | 1.01 | 0.20 | | | |
| SUM | 99.80 | 0.22 | Zr | 164.20 | 11.74 | Pb | 3.70 | 0.42 | Er | 3.00 | 0.88 | | | |

### 2.1.2.2 Granodiorite, tonalite and granite (rock code 101051)

In the second most abundant rock type in the candidate area, the granodiorite, tonalite and granite (rock code 101051), the inhomogeneity in chemical composition is larger due to the larger spread in mineralogy between the different types of rocks within this group. The total S content is 0.4 wt%, stoichiometric recalculation to pyrite gives a maximum pyrite content of ~ 0.75 wt%. The total C content is 0.03 wt% which gives a maximum calcite content (if all C is in the form of calcite) of ~ 0.25 wt%. S and C were analysed by volatization, as described above. A more detailed S analyse will be carried out during 2006. The geochemistry of rock type 101051 is summarized in Table 2-2. In the Chondrite normalized REE diagram (Figure 2-6), it can be seen that only two of eight samples show negative Eu anomalies and the spread is larger than in the granite to granodiorite (rock code 101057). Both the higher Eu content and the higher Sr content compared to rock type 101057 is due to the higher plagioclase content in rock type 101051.

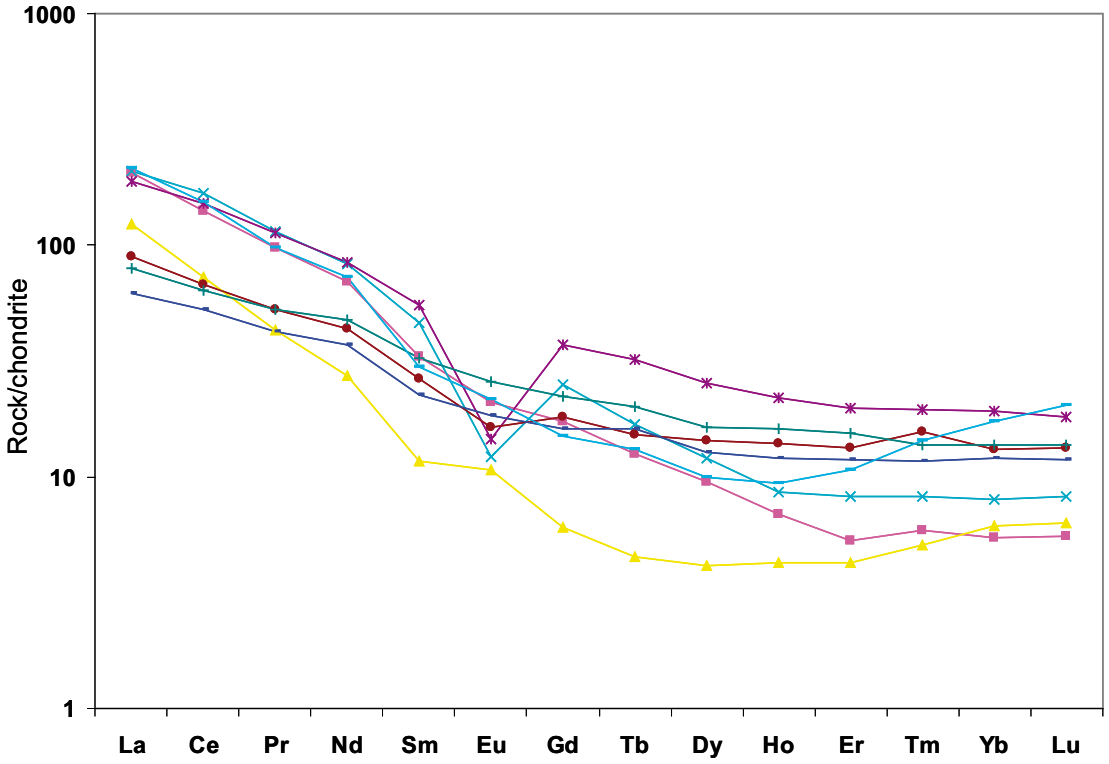


***Figure 2-6.*** *Chondrite normalized REE-pattern for granodiorite, tonalite and granite (rock type 101051). Data from /Petersson 2004b, 2005a/. Chondrite values from /Evansen et al. 1978/ (N=8).*

**Table 2-2. Whole-rock geochemistry of granite-granodiorite-tonalite (rock code 101051). Mean and standard deviation values have been calculated based on data from /Petersson, 2004b, 2005a/. LOI = Lost on ignition, TOT/C = total C, TOT/S = total S. (*N=8*).**

| Element | Mean (N=8) | Std | Element | Mean (N=8) | Std | Element | Mean (N=8) | Std | Element | Mean (N=8) | Std | Element | Mean (N=8) | Std |
|---|---|---|---|---|---|---|---|---|---|---|---|---|---|---|
| **SiO2(wt%)** | 67.69 | 6.45 | **Sc (ppm)** | 10.29 | 8.86 | **Nb** | 10.72 | 5.35 | **Bi** | 0.11 | 0.04 | **Tm** | 0.30 | 0.14 |
| **TiO2** | 0.42 | 0.26 | **V** | 41.71 | 47.13 | **Mo** | 0.46 | 0.21 | **Th** | 14.70 | 11.28 | **Yb** | 1.95 | 0.89 |
| **Al2O3** | 15.03 | 1.68 | **Cr** | 7.00 | n.a. | **Ag** | < 0.1 | n.a. | **U** | 4.04 | 2.44 | **Lu** | 0.31 | 0.15 |
| **Fe2O3** | 4.52 | 2.52 | **Co** | 7.81 | 6.31 | **Sn** | < 0.1 | n.a. | **La** | 38.83 | 14.58 | **Au (ppb)** | 0.84 | 0.50 |
| **MnO** | 0.07 | 0.05 | **Ni** | 3.56 | 2.39 | **Cd** | 2.83 | 0.41 | **Ce** | 74.50 | 29.52 | | | |
| **MgO** | 1.12 | 0.84 | **Cu** | 13.91 | 8.96 | **Sb** | 0.10 | 0.00 | **Pr** | 7.86 | 2.96 | | | |
| **CaO** | 3.98 | 2.24 | **Zn** | 52.00 | 16.57 | **Cs** | 0.80 | 0.16 | **Nd** | 29.03 | 10.37 | | | |
| **Na2O** | 3.70 | 0.48 | **Ga** | 18.69 | 2.64 | **Ba** | 746.17 | 195.75 | **Sm** | 5.17 | 2.15 | | | |
| **K2O** | 2.48 | 1.46 | **As** | 0.50 | 0.00 | **Hf** | 4.53 | 1.48 | **Eu** | 1.01 | 0.32 | | | |
| **P2O5** | 0.12 | 0.09 | **Se** | < 0.5 | n.a. | **Ta** | 0.74 | 0.34 | **Gd** | 4.11 | 1.97 | | | |
| **LOI** | 0.59 | 0.23 | **Rb** | 81.44 | 41.14 | **W** | 0.34 | 0.19 | **Tb** | 0.61 | 0.32 | | | |
| **TOT/C** | 0.03 | 0.02 | **Sr** | 377.11 | 276.55 | **Hg** | 1.54 | 3.28 | **Dy** | 3.32 | 1.69 | | | |
| **TOT/S** | 0.04 | 0.03 | **Y** | 20.19 | 10.01 | **Tl** | 0.24 | 0.13 | **Ho** | 0.66 | 0.34 | | | |
| **SUM** | 99.72 | 0.07 | **Zr** | 157.57 | 48.23 | **Pb** | 3.47 | 3.86 | **Er** | 1.83 | 0.94 | | | |

### 2.1.3 Porosity

Porosity measurements have been carried out on the rock types at Forsmark within several programs (e.g. the geology and transport programs). All determinations consider connected porosity and are measured as water saturation. The methods used differ however, between the different programs in terms of e.g. sample selection, sample size, water saturation time and drying time (More detailed information about the methods can be found in method descriptions SKB MD 160.002e, SKB MD 540.001, SKB MD 540.003 and SS EN 1936). The terminology used varies as well and the porosity measured is notified as effective, open or connected of which the latter is preferred in this compilation. The porosity results from the geology and transport program are briefly discussed below. A more thorough comparison of the different porosity measurement will be carried out during 2006 (pers. comm. E. Gustavsson, Geosigma AB).

*Geology program*

The porosity of surface and drill core samples has been measured as part of the Geology program and are presented in /SKB 2005b (p 145–148)/. The porosity measured in this project is the connected porosity measured by water saturation technique. For the different rock types in the Forsmark area, the porosity varies between 0.20 and 1.04% where the metavolcanic rock (rock type 103076) has the lowest porosity (Table 2-3) and the ultramafic rock (rock code 101004) has the highest. When only the major rock type within the Forsmark site is considered (rock code 101057) the porosity varies between 0.28 and 0.66% with a mean of 0.43% /SKB 2005b/. The surface samples are likely to have a higher porosity than the drill core samples due to weathering and a higher frequency of micro-fractures.

*Transport program*

The porosity of drill core samples has been measured as part of the Transport program and are presented in /SKB 2005b (p 492)/. The porosity is measured as the connected porosity by water saturation technique. The porosity is 0.24% ± 0.12 for the granite to granodiorite (rock code 101057) and 0.30% ± 0.27 for the granodiorite, tonalite and granite (rock code 101051) (Table 2-4).

**Table 2-3. Connected porosity measured by water saturation technique from the Geology program. Data from /SKB 2005b/.**

| Rock type Rock Code (SKB) | | Porosity (%) Range | Mean | Std |
|---|---|---|---|---|
| 101004 | Ultramafic rock | 1.04 | n.a. | n.a. |
| 101033 | Diorite. quartz diorite and gabbro | 0.25-0.54 | 0.37 | 0.07 |
| 111058 | Granite | 0.48-0.69 | 0.5 | 0.02 |
| 101051 | Granodiorite. tonalite and granite | 0.28-0.59 | 0.45 | 0.09 |
| 111051 | Granitoid | n.a. | 0.45(a) | n.a. |
| 101058 | Granite | 0.36-0.48 | 0.4 | 0.05 |
| 111057 | Granite (to granodiorite) | n.a. | 0.43 (b) | n.a. |
| 101057 | Granite (to granodiorite) | 0.28-0.66 | 0.43 | 0.08 |
| 101054 | Tonalite and granodiorite | 0.31-0.53 | 0.4 | 0.07 |
| 103076 | Felsic to intermediate volcanic rock | 0.20-0.62 | 0.37 | 0.11 |
| 106001 | Sedimentary rock | 0.48 | n.a. | n.a. |
| 101056 | Granodiorite | n.a. | 0.42 (c) | n.a. |

**Table 2-4. Connected porosity measured by water saturation technique from the *Transport program*. Data from /SKB 2005b/.**

| Rock type Rock Code (SKB) | | Porosity (%) Mean | Std | N |
|---|---|---|---|---|
| 101051 | Granodiorite, tonalite and granite | 0.30 | 0.27 | 30 |
| 101057 | Granite (to granodiorite) | 0.24 | 0.12 | 105 |
| 103076 | Felsic to intermediate volcanic rock | 0.78 | n.a. | 1 |
| 101056 | Granodiorite | 0.34 | 0.21 | 2 |

The porosities from the Transport program are lower than from the Geology program. This difference could partly be due to different measurement methods, although a lower porosity is expected since no surface samples have been used in the Transport program measurements.

The porosities from the Transport program are therefore suggested to be more representative for the connected porosity at depth. The porosities from the Transport program are therefore recommended for use in modelling until the results from the comparison study mentioned above is available.

The porosity in hydrothermally altered rock, which often occurs adjacent to fractures, has not yet been analysed in Forsmark, this will be done during 2006.

### 2.1.4 Density

The rock type with the highest density in the Forsmark area is an ultramafic rock (rock code 101004) with a density of 3.045 kg $m^{-3}$ while the rock type with the smallest density is a granite (rock code 101058) which has a mean density of 2.635 kg $m^{-3}$. The dominating granite to granodiorite (rock code 101057) has a density between 2.639 and 2.722 kg $m^{-3}$ with a mean of 2.657 kg $m^{-3}$ /SKB 2005b/. Densities for all rock types are summarized in Table 2-4. The density of hydrothermally altered rock, which often occurs adjacent to fractures, has not yet been analysed but will be carried out during 2006. In studies at the Oskarshamn site by /Drake and Tullborg 2006ab/ the decrease in density in altered rock has been showed to be ~ 0.01 kg $m^{-3}$.

### 2.1.5 Redox – Whole rock

No Mössbauer analyses have yet been carried out on whole rock samples from the Forsmark site. Also this will be done as part of a rock alteration study during 2006. Therefore, an estimation of the oxidation factor ($Fe^{3+}/Fe_{tot}$) of the rock types can only be based on the mineralogy.

Biotite is the major ferromagnesian mineral in granitic rocks which contain biotite. Other Fe-bearing silicates are e.g. epidote, titanite, hornblende, allanite and chlorite. Of these minerals, epidote contains almost exclusively $Fe^{3+}$ (oxidation factor ~ 1) while the other minerals have a low $Fe^{3+}/Fe_{tot}$ ratio /Deer et al. 1992/. The most important $Fe^{3+}$ bearing oxides are magnetite and hematite (magnetite has an oxidation factor of ~ 0.667 and hematite 1). To summarize, a high content of magnetite, hematite and epidote results in a high oxidation factor in granitic rock while a high biotite and/or chlorite content result in a lower oxidation factor.

To obtain a quantitative estimate of the $Fe^{3+}/Fe_{tot}$ ratio of the dominating granitic to granodioritic rock type in Forsmark (rock code 101057), its mineralogical composition has been compared to the Ävrö granite (spanning from granite to monzonite) from the Simpevarp subarea at the Oskarshamn site (Table 2-5), where Mössbauer analyses and point counting have been carried out /Drake and Tullborg 2006ab/.

**Table 2-5. Mineralogical composition of the major granite (to granodiorite) rock type in Forsmark and the Ävrö granite. The Forsmark values have been compiled from /SKB 2005b, Petersson 2004b, 2005a/. The Ävrö granite values are based on data from unaltered rock in /Drake and Tullborg 2006ab/.**

| | Forsmark granite (rock code 101057) Mean ±Std | Ävrö granite Mean ±Std |
|---|---|---|
| Quartz | 35.6 ± 4.2 | 18.8 ± 7.3 |
| K-feldspar | 22.5 ± 8.6 | 16.6 ± 8.8 |
| Plagioclase | 35.6 ± 8.5 | 43.9 ± 9.7 |
| Biotite | 5.1 ± 1.6 | 6.2 ± 5.5 |
| Amphibole | – | 3.4 ± 4.3 |
| Chlorite | 0.2 ± 0.3 | 4.4 ± 4.4 |
| Epidote | 0.6 ± 0.7 | 3.2 ± 3.1 |
| Titanite | 0.2 ± 0.2 | 1.6 ± 1.0 |
| Allanite | 0.2 ± 0.2 | – |
| Opaque | 0.3 ± 0.2 | 1.3 ± 0.4 |

*Ävrö granite*

The oxidation factor ($Fe^{3+}/Fe_{tot}$) for the Ävrö granite is 0.42 ± 0.09 /Drake and Tullborg 2006ab/. The oxidation factor (total) for all analysed unaltered rock types in the Oskarshamn studies varies between 0.26 and 0.54 (covering rocks from granite to quartz diorite). The large span is due to a higher hematite/magnetite ratio and an overall higher Fe-oxide content in the samples with the highest oxidation values.

*Forsmark granite*

The major ferromagnesian mineral in the metamorphic granite to granodiorite (rock code 101057) which makes up the absolute majority of the rock volume at the Forsmark site /SKB 2005b/ is biotite, comprising between 0.8 and 8.8 vol% (mean 5.1%). The other Fe-bearing silicates are epidote, titanite, hornblende, allanite and chlorite, all only present as accessory minerals (< 0.6%). The opaque minerals in the Forsmark granite are magnetite, pyrite, hematite, ilmenite and chalcopyrite (magnetite dominates) /Petersson et al. 2004b, Stephens et al. 2005/.

The Forsmark granite (rock code 101057) contains less $Fe^{3+}$ bearing minerals like magnetite, hematite and epidote than the Ävrö granite – thus, a lower oxidation factor can be expected. The lower content of biotite and chlorite (both with low oxidation factors) in the Forsmark granite might somewhat compensate this, but the oxidation factors for magnetite, hematite and epidote are so high that the later have been assumed to dominate the oxidation factor in these rocks. This assumption is supported by data in /Drake and Tullborg 2006ab/.

- Based on the mineralogical differences between the Forsmark granite (rock code 101057) and the Ävrö granite, an oxidation factor of approximately 0.3 is estimated for the Forsmark granite.
- This value has been assigned for all major rock types at the Forsmark site since the uncertainty in the estimated $Fe^{3+}/Fe_{tot}$ ratio probably is higher than the difference between major rock types (Table 2-6).

### 2.1.6 Summary

**Table 2-6. Summary of density, porosity, oxidation factor, $Fe_{tot}$ and $Fe^{2+}$ content for different rock types at the Forsmark site. The shaded lines represent the two rock types that together make up more than 94% of the volume in the candidate area.**

| Rock type Rock Code (SKB) | | Density (kg/m³) Range | Mean | Std | Porosity (%) (d) Mean | Std | N | Oxidation factor | Fe tot% | $Fe^{2+}$ % |
|---|---|---|---|---|---|---|---|---|---|---|
| 101004 | Ultramafic rock | 3,045* | * | * | *** | *** | *** | n.a. | | |
| 101033 | Diorite. quartz diorite and gabbro | 2,738–3,120 | 2,934 | 100 | *** | *** | *** | n.a. | | |
| 111058 | Granite | 2,627–2,645 | 2,638 | 9 | | | | 0.3** | | |
| 101051 | Granodiorite. tonalite and granite | 2,642–2,832 | 2,715 | 52 | 0.30 | 0.27 | 30 | 0.3** | 3.16 | 2.21 |
| 111051 | Granitoid | n.a. | 2,715(a) | n.a. | | | | 0.3** | | |
| 101058 | Granite | 2,620–2,646 | 2,635 | 9 | *** | *** | *** | 0.3** | | |
| 111057 | Granite (to granodiorite) | n.a. | 2,657(b) | n.a. | | | | 0.3** | | |
| 101057 | Granite (to granodiorite) | 2,639–2,722 | 2,657 | 15 | 0.24 | 0.12 | 105 | 0.3** | 1.87 | 1.31 |
| 101054 | Tonalite and granodiorite | 2,674–2,831 | 2,737 | 43 | | | | 0.3** | | |
| 103076 | Felsic to intermediate volcanic rock | 2,648–2,946 | 2,732 | 79 | 0.78 | n.a. | 1 | 0.3** | | |
| 106001 | Sedimentary rock | 2,691* | * | * | *** | *** | *** | n.a. | | |
| 101056 | Granodiorite | n.a. | 2,697 (c) | n.a. | 0.34 | 0.21 | 2 | 0.3** | | |

Density and porosity from /SKB 2005b/.

(a) No data available - based on similarity to rock type 101057 (Low confidence).

(b) No data available - based on similarity to rock type 101057 (Low confidence).

(c) No data available - mean of rock type 101057 and 101054.

(d) Section 2.1.3 for details.

* Data from single outcrop sample (Low confidence).

** Estimated value with low confidence (se text for details).

*** Values from different method in section 2.1.3.

## 2.2 Fracture mineralogy

### 2.2.1 Description of sampled boreholes and fracture zones

Fracture data is obtained during the Boremap mapping of the drill cores /Petersson and Wängnerud 2003, Petersson et al. 2003ab, 2004ac, 2005b/ the data is exported to the SKB database SICADA. The quantitative statistical analyses of fracture data in this report are based on this data extracted from SICADA and analysed using Microsoft Excel. The more qualitative fracture mineral data, chemical analyses and Mössbauer analyses have been obtained from the detailed fracture mineralogy studies /Sandström et al. 2004, Sandström and Tullborg 2005/. The fracture data used in this report is from boreholes KFM01A–8B (Figure 2-1 and Table 2-7). Boremap data from KFM06C has only been used for the uppermost 100 m in Figure 2-13 and 2-14 due to that the data was obtained in a late stage of the writing of this report.

The confidence of the Boremap data is classified as certain, probable or possible based on how certain the drill core mapping geologists are on whether a fracture was open in the borehole or not. In the data here used, 57% of the fractures have been classified as certain, 31% as probable and 12% as possible. Data of all confidence levels has been used in this report which introduces a larger uncertainty but provides a larger statistic base.

### 2.2.2 Variation of fractures with depth

The total numbers of fractures per 100 m drilled borehole (open, partly open and sealed) show a decreasing trend towards greater depth (Figure 2-7 and Table 2-10), the irregularity in this trend is at least partly a result of that the boreholes cut zones with a higher fracture frequency at different depths. Detailed fracture frequency data for each of the boreholes KFM01A, KFM01B, KFM02A, KFM03A, KFM03B, KFM04A and KFM05A is available in /SKB 2005b/ (p 197–198).

The total number of fractures in the available data is 26,498 of which 19,896 or 75% are sealed, 5,731 or 22% are open and 871 or 3% are partly open. The open fractures are concentrated to the upper 400 m where the fracture frequency is between 200 and 80 open fractures per 100 m. under this depth the number of fractures is between 60 and 17 per 100 m (Figure 2-8 and Table 2-9).

**Table 2-7. Summary of length and orientation of the boreholes used in this report. Data from /SKB 2005b, SICADA/. The boreholes named KFM0xA are 1,000 m telescopic drilled boreholes which start at ~ 100 m below the bedrock surface (above 100 m the boreholes are drilled by percussion, thus no Boremap data is available) while the boreholes named KFM0xB are shorter and drilled telescopically from the bedrock surface to obtain information of the upper part of the bedrock.**

| Borehole | Borehole length (m) | Borehole orientation |
|---|---|---|
| KFM01A | 1,000 | 318/–85° |
| KFM01B | 500 | 268/–79° |
| KFM02A | 1,000 | 276/–85° |
| KFM03A | 1,000 | 272/–86° |
| KFM03B | 100 | 272/–86° |
| KFM04A | 1,000 | 045/–60° |
| KFM05A | 1,000 | 081/–60° |
| KFM06A | 1,000 | 300/–60° |
| KFM06B | 100 | 300/–85° |
| KFM07A | 1,000 | 260/–60° |
| KFM08A | 1,000 | 320/–60° |
| KFM08B | 200 | 320/–85° |

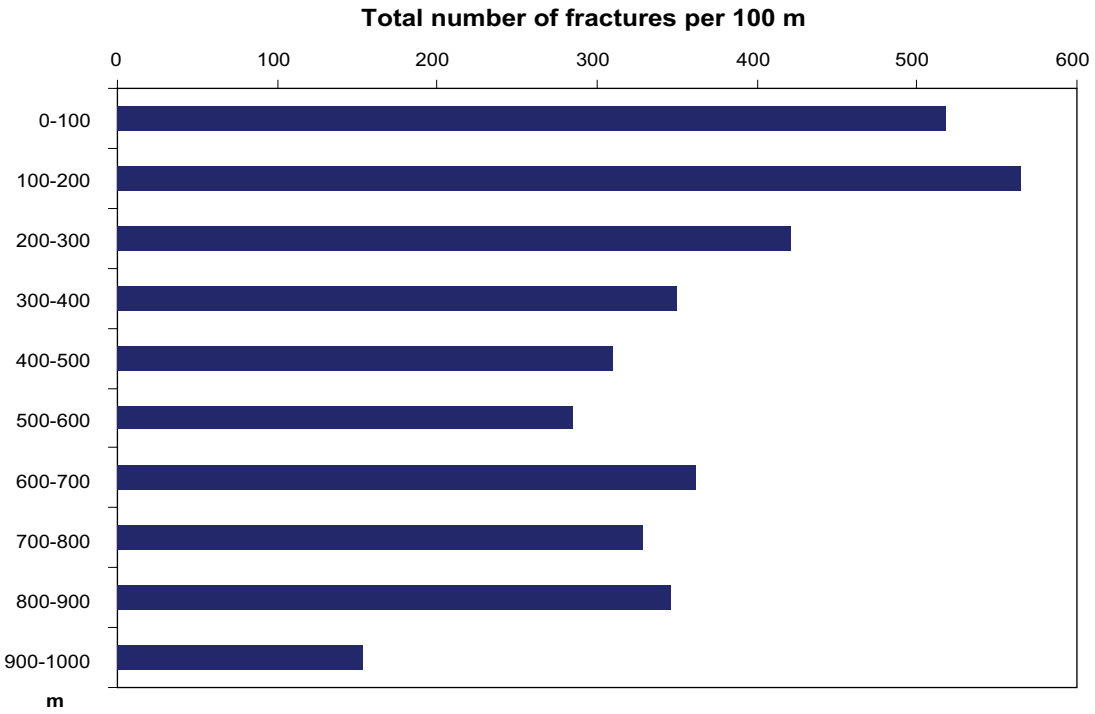


***Figure 2-7.*** *Total number of fractures per 100 m drilled borehole. Data from KFM01A–08B.*

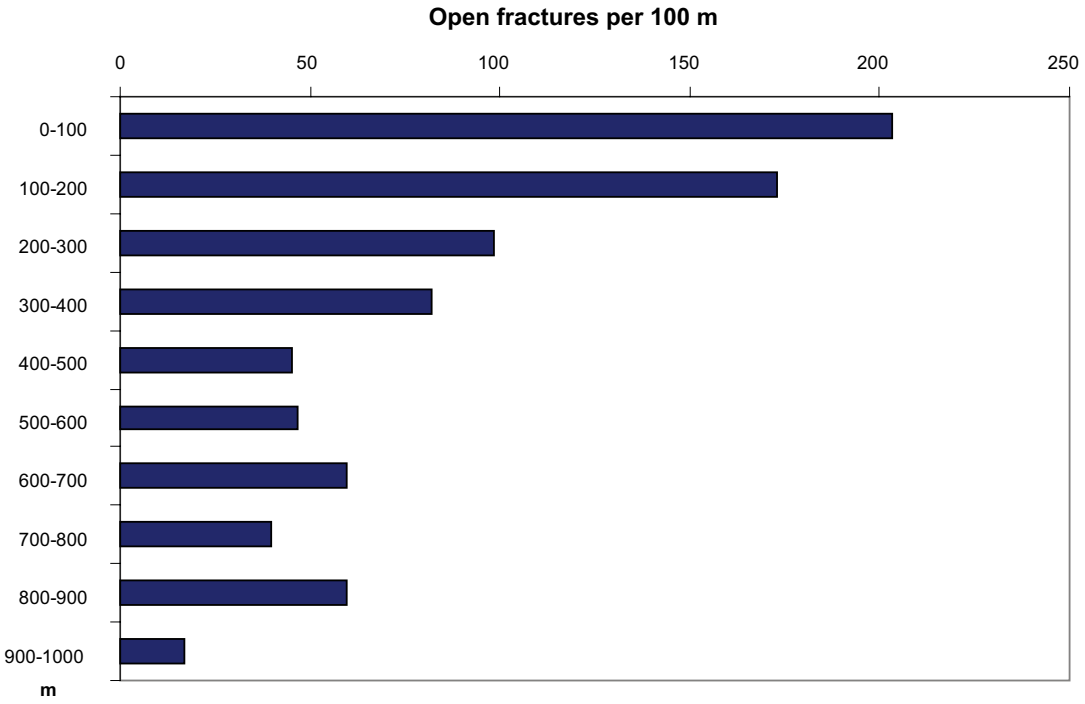


***Figure 2-8.*** *Number of open fractures per 100 m drilled borehole. Data from KFM01A–08B.*

**Table 2-8. Total number of fractures per 100 m drilled borehole. Data from KFM01A–08B.**

| m | Fractures/100 m |
|---|---|
| 0–100 | 519 |
| 100–200 | 564 |
| 200–300 | 422 |
| 300–400 | 349 |
| 400–500 | 309 |
| 500–600 | 285 |
| 600–700 | 362 |
| 700–800 | 329 |
| 800–900 | 347 |
| 900–1,000 | 153 |

**Table 2-9. Number of open fractures per 100 m drilled borehole. Data from KFM01A–08B.**

| m | Open fractures/100 m |
|---|---|
| 0–100 | 203 |
| 100–200 | 173 |
| 200–300 | 98 |
| 300–400 | 82 |
| 400–500 | 45 |
| 500–600 | 47 |
| 600–700 | 60 |
| 700–800 | 40 |
| 800–900 | 60 |
| 900–1,000 | 17 |

### 2.2.3 Abundance of fracture filling minerals

In this report “fracture filling” is used as a collective term for both coating and loose material in open fractures and for all material in sealed fractures. The collective term “fracture filling” for material in open fractures is used since the chemical analyses are usually carried out on both filling and coating material which are difficult to separate during sampling. When the term “coating” is used it refers only to the solid material coated to the fracture surface. Based on drill core samples, thin sections and Boremap data, the typical width of a chlorite filling has been estimated to ~ 0.5 mm. this would give a volume of $0.5\times10^{-3}$ $m^3$ chlorite per $m^2$ chlorite coated fracture surface. The specific gravity for chlorite varies between 2.6 and 3.3 g $cm^{-3}$ /Deer et al. 1992/ which gives a chlorite mass between 1.30 and 1.65 kg $m^{-2}$. A typical chlorite coated fracture is showed in Figure 2-9. A minimum estimate of the chlorite content in a chlorite bearing open fracture is a 0.1 mm thick coating covering 5% of the fracture surface. A minimum estimate of chlorite in a chlorite bearing fracture is thus between 0.013 and 0.017 kg $m^{-2}$. Observe that this number and the ones below are estimations and that the amount of fracture filling material differs highly between different fractures.

The width of a typical calcite fracture varies more than for chlorite, from less than a millimetre up to more than 10 cm in rare cases. The mineral is also more irregularly spread across the fracture surfaces (Figure 2-10). Base on drill core samples, Boremap data and that small amounts of calcite is easily recognizable due to reaction with HCl, a rough estimation of open calcite coated fractures is that the average thickness is ~ 0.5 mm and that the mineral covers ~ 50% of the fracture surface. This would give a volume of $0.25\times10^{-3}$ $m^3$ calcite per $m^2$ calcite coated fracture surface. Based on the specific gravity of calcite of 2.715 g $cm^{-3}$ /Deer et al. 1992/, this would

***Figure 2-9.*** *Chlorite coated fracture. The diameter of the drill core is ~ 5 cm (KFM07A 118.18–118.35 m).*

***Figure 2-10.*** *Calcite coated fracture surface. The diameter of the drill core is ~ 5 cm (KFM06A 743.39–743.52 m).*

give a calcite mass of 0.7 kg $m^{-2}$ in calcite coated fractures. A minimum estimate of the calcite content in a calcite bearing open fracture is a 0.1 mm thick coating covering 1% of the fracture surface. A minimum estimate of calcite in a calcite bearing fracture is thus $2.7\times10^{-3}$ kg $m^{-2}$.

A quantitative estimation of the pyrite content in fractures is difficult due its scattered occurrence. In pyrite carrying fractures, the mineral occurs as small cubic crystals unevenly distributed on the fracture surface. A rough estimation of the maximum amount of pyrite is based on an surface coverage of 1% and a crystal side of 1 mm, given the specific gravity of pyrite (4.95–5.03 g $cm^{-3}$ /Deer et al. 1992/, a maximum pyrite content in an average pyrite carrying fracture is estimated to 0.05 kg $m^{-2}$ fracture surface. A minimum estimate of the pyrite content in a pyrite bearing open fracture is 0.1 mm big crystals covering 0.1% of the surface. A minimum estimate of pyrite in a pyrite bearing fracture is thus between 0.0005 kg $m^{-2}$.

Some of the fracture minerals occur as small grains or in small amount which make them difficult to identify during the drill core mapping. Examples of fracture minerals that are underrepresented in the Boremap data due to difficulty to identify them macroscopically or with hand lens are clay minerals. Another mineral probably underrepresented in the Boremap data is quartz, since it often occurs as a very thin transparent coating in many fractures and is

often covered with later minerals and therefore is difficult to identify. This quartz occurs mostly in open fractures and consists of very small euhedral crystals. Hematite, which is a common mineral in Forsmark, does not occur in the quantities suggested by the Boremap data. This is a result of its ability to colour other minerals when present only as trace amounts. The hematite often occurs as submicroscopic grains not larger than a few microns and yet colour the fracture filling red (Figure 2-11). Many of the sealed fractures mapped with hematite as the major fracture mineral are probably hematite stained adularia ± quartz and albite.

Histograms of the mineralogy of sealed and open fractures can be seen in Figure 2-12 and 2-13. Observe that most of the fractures contain more than one mineral and that the sum of all fractures in the histograms therefore is higher than the total number of individual fractures.

#### *2.2.3.1 Sealed fractures*

About 75% (19,896) of the fractures in the analysed Boremap data are sealed. The most abundant fracture minerals are calcite and chlorite which occur in 40 and 38% respectively of all sealed fractures (Figure 2-12 and Table 2-10). Calcite occurs as fracture fillings up to more than a decimetre in width but are commonly between 0.5 and 2 mm. X-ray diffraction analyses show that many fractures mapped as chlorite often consist of chlorite and corrensite which is a chlorite-like mixed layer clay with layers of chlorite and smectite or vermiculite /Sandström et al. 2004, Sandström and Tullborg 2005/. Chlorite occurs mostly as thin fracture coatings although several centimeters wide chlorite coatings also are found.

Laumontite (Ca-zeolite) is found in 21% of all sealed fractures and hematite in 14%. The quantities of hematite in these fractures are often small, see discussion in Section 2.2.3. 19% of the sealed fractures in the Boremap data have been mapped as “no mineral”. According to the drill core mapping geologists, the basis for mapping a fracture as “no mineral” is that no mineral can be seen when the drill core is examined, this could be due to that a) in fact no minerals are present. b) that minerals exist inside the fracture and therefore can not be seen in the drill core or c) that the fracture coating is so thin that it can not be seen macroscopically (pers. comm. Jesper Petersson).

Quartz, adularia and prehnite are found in between 8 and 5% of the sealed fractures while pyrite and epidote occur in 3% of the fractures. Clay mineral, biotite, goethite and asphaltite are found in 1% or less of all sealed fractures.

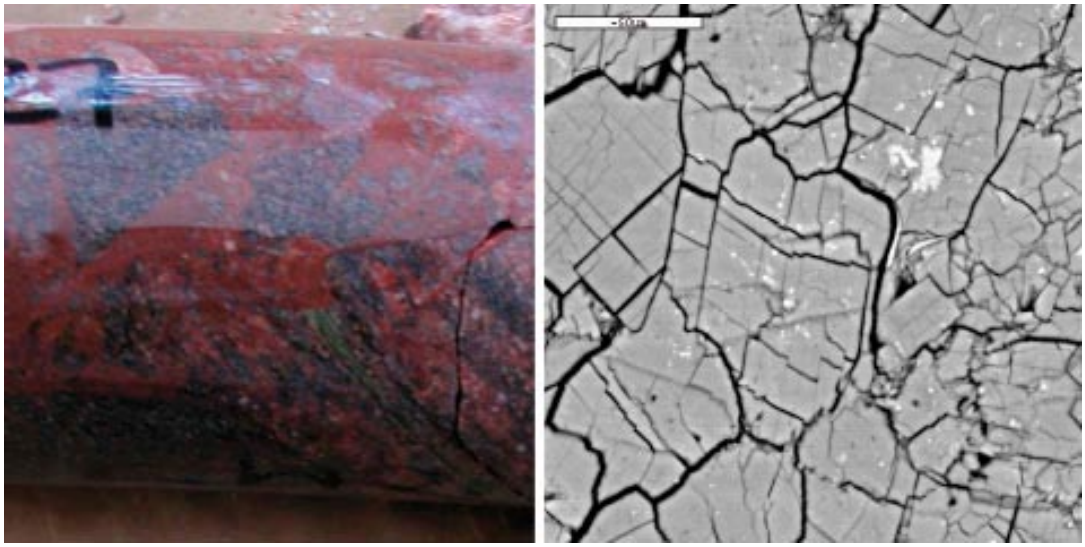

***Figure 2-11.*** *Red-stained breccia sealed with laumontite and hematite from sample KFM04A 226.98 m, the diameter of the drill core to the left is ~ 5 cm and the scale bar in the BSE image is 50 µm. Observe the small quantities of hematite grains in the Backscattered electron image to the right (bright spots) responsible for the red colour of the sealing, the grey mineral is laumontite. The hematite grains are often only a few microns in diameter.*

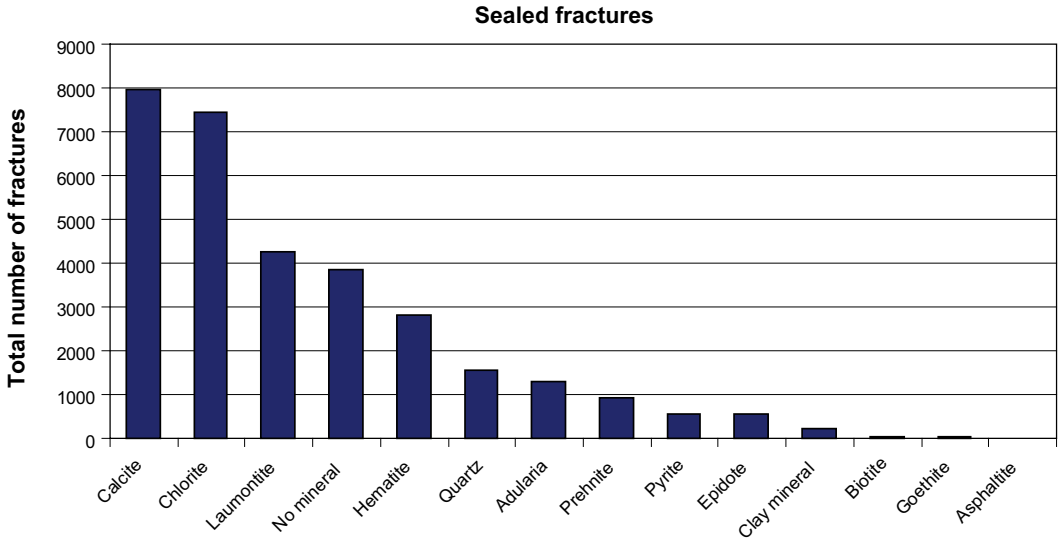


***Figure 2-12.*** *Histogram of fracture minerals in sealed fractures. Data from KFM01A–08B, total number of sealed fractures = 19,896.*

**Table 2-10. Relative abundance of fracture minerals in sealed fractures. The percentage value represent in how many of the sealed fractures a specific mineral has been identified. Data from KFM01A–08B.**

| Mineral | % |
|---|---|
| Calcite | 40 |
| Chlorite | 38 |
| Laumontite | 21 |
| No mineral | 19 |
| Hematite | 14 |
| Quartz | 8 |
| Adularia | 7 |
| Prehnite | 5 |
| Pyrite | 3 |
| Epidote | 3 |
| Clay minerals | 1 |
| Biotite | 0.3 |
| Goethite | 0.2 |
| Asphaltite | < 0.1 |

### *2.2.3.2 Open fractures*

Approximately 22% (5,731) of the fractures in the analysed Boremap data are open. The open fractures are dominated by chlorite and calcite which occur in 71 and 50% respectively of all open fractures (Figure 2-13 and Table 2-11). Compared to the sealed fractures, clay minerals are much more abundant in the open fractures and are found in 16% of these fractures. Hematite, pyrite and laumontite occur in between 15 and 9% of the open fractures and 11% has been mapped as “no mineral”. The “no mineral” occurrences are discussed in Section 2.2.3.1, the difference in the open fractures is that a few fractures in KFM01A and B got mapped as “no mineral”-fractures although they were drill induced (pers. comm. Jesper Petersson). Goethite, quartz, prehnite, asphaltite, adularia and epidote all occur in 2% or less of all open fractures. Quartz is probably underrepresented since it in open fractures often occurs as a very thin coating difficult to identify in hand sample.

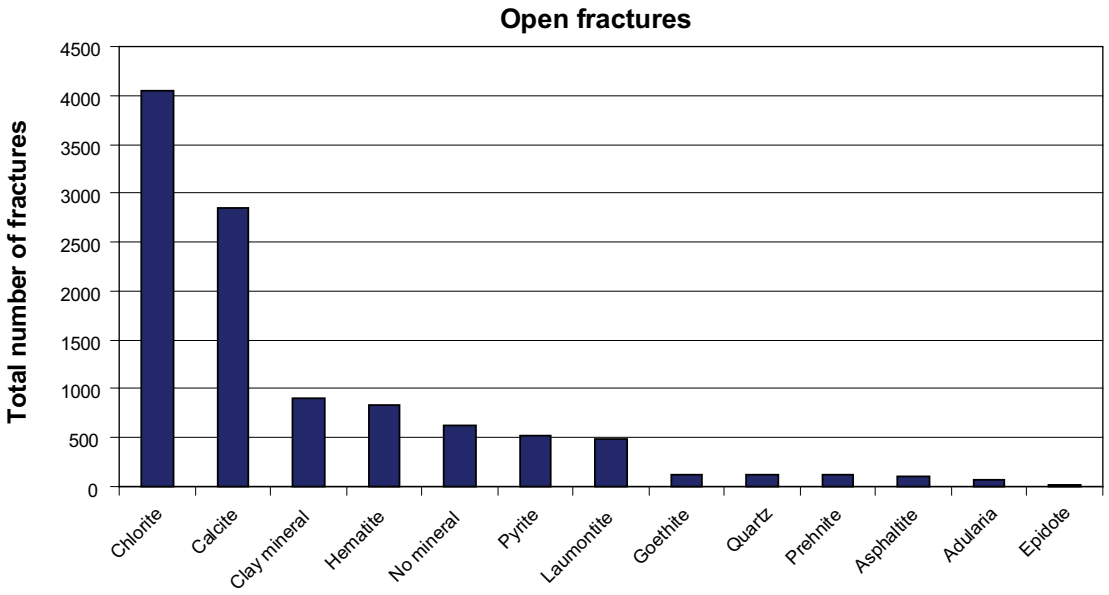


***Figure 2-13.*** *Histogram of fracture minerals in open fractures. Data from KFM01A–08B, total number of open fractures = 5,731.*

**Table 2-11. Relative abundance of fracture minerals in open fractures. The percentage value represent in how many of the sealed fractures a specific mineral has been identified. Data from KFM01A–08B.**

| Mineral | % |
|---|---|
| Chlorite | 71 |
| Calcite | 50 |
| Clay mineral | 16 |
| Hematite | 15 |
| No mineral | 11 |
| Pyrite | 9 |
| Laumontite | 9 |
| Goethite | 2 |
| Quartz | 2 |
| Prehnite | 2 |
| Asphaltite | 2 |
| Adularia | 1 |
| Epidote | 0.2 |

In fractures with an aperture larger than 1 mm. clay minerals are more common relative to chlorite and calcite than in less open fractures (Figure 2-14 and Table 2-12).

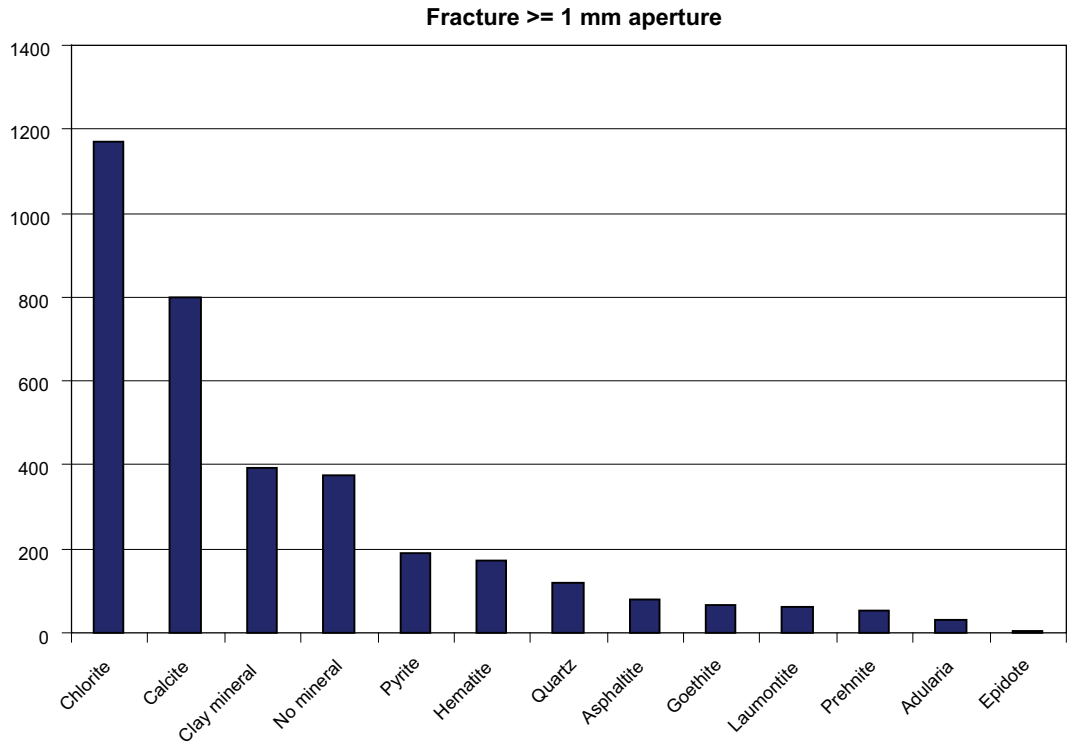


***Figure 2-14.*** *Number of open fractures with an aperture > 1 mm and their mineralogy. Data from KFM01A–08B, total number of fractures = 3,513.*

**Table 2-12. Relative abundance of fracture minerals in open fractures with an aperture > 1 mm. The percentage value represent in how many of the sealed fractures a specific mineral has been identified. Data from KFM01A–08B.**

| Mineral | % |
|---|---|
| Chlorite | 62 |
| Calcite | 42 |
| Clay minerals | 21 |
| No mineral | 19 |
| Pyrite | 10 |
| Hematite | 9 |
| Quartz | 6 |
| Asphaltite | 4 |
| Goethite | 4 |
| Laumontite | 3 |
| Prehnite | 3 |
| Adularia | 2 |
| Epidote | 0.2 |

*Variation in fracture mineralogy in open fractures with depth*

The mineralogy of the open fractures shows, except for the upper 100 m, relatively small variation with depth (Figure 2-13). The main difference is above 100 m where goethite, asphaltite and clay minerals are much more common while chlorite and hematite are less abundant. Pyrite is more abundant in the upper 300 m while the “no mineral” fractures become less abundant below 500 m. Some of the variation with depth may be the result of intersection with individual fracture zones and with which angle different fracture sets is cut by the boreholes

In the upper 100 m, the variation in fracture mineralogy increases when viewed with a higher vertical resolution (Figure 2-16). This is a result of less available data for the uppermost 100 m and unevenly distributed fracture zones close to the surface, an example is asphaltite which often occurs in zones close to the surface giving the uneven distribution in the histogram. Another example is the elevated amount of fractures with clay minerals between 40 and 60 m in Figure 2-15 which is due to a deformation zone in KFM06B with a high amount of clay minerals /Carlsten et al. 2005/

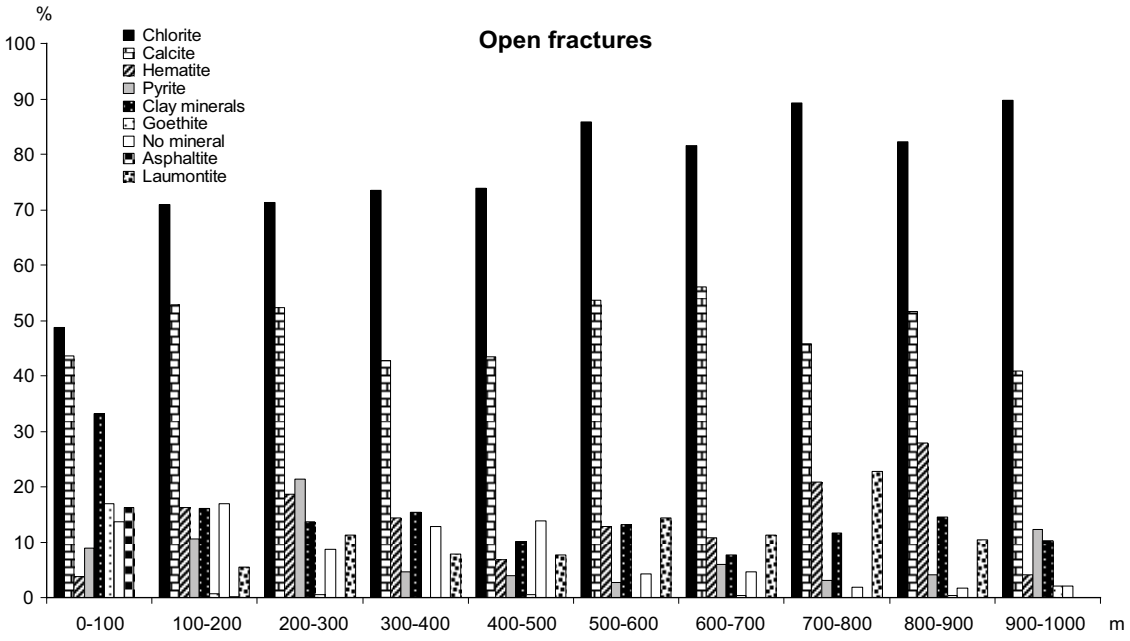


***Figure 2-15.*** *Variation of fracture mineralogy versus depth in open fractures in boreholes. Data from KFM01A–08B, depths have been recalculated to vertical depths.*

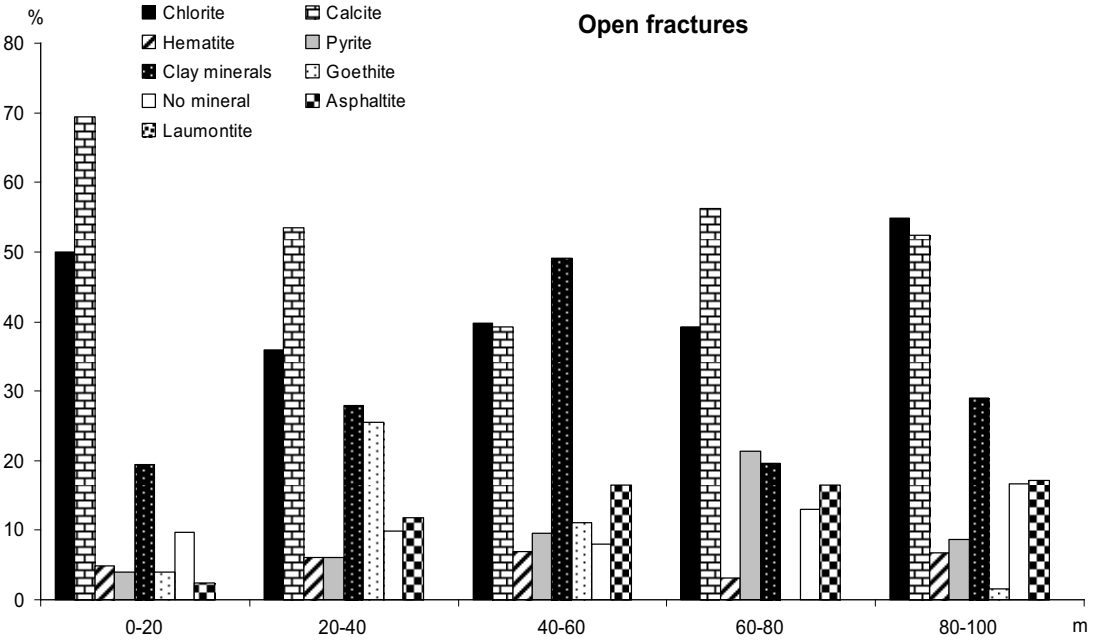


***Figure 2-16.*** *Variation of fracture mineralogy in the upper 100 m of the boreholes. Data from KFM01B, KFM03B, KFM06B and KFM08B, depths have been recalculated to vertical depths.*

The mineralogy of the uppermost 20 m when viewed with a resolution of 5 m (Figure 2-17) (i.e. 5–20 m since no data is available from depths above 5 m) is quite homogenous and no signs of e.g. a redox front can be seen in the Boremap data.

### *2.2.3.3 Crushed zones*

Crushed zones are mapped separately during the drill core mapping and often represent zones with an elevated hydraulic conductivity. The term "crushed zone" correlates to an incohesive fault breccia according to the nomenclature of /Sibson 1977, SKB 2005a/. The fracture mineralogy of these crushed zones is dominated by clay minerals, calcite and chlorite which occur in approximately the same proportions (Figure 2-18 and Table 2-13). Fractures mapped

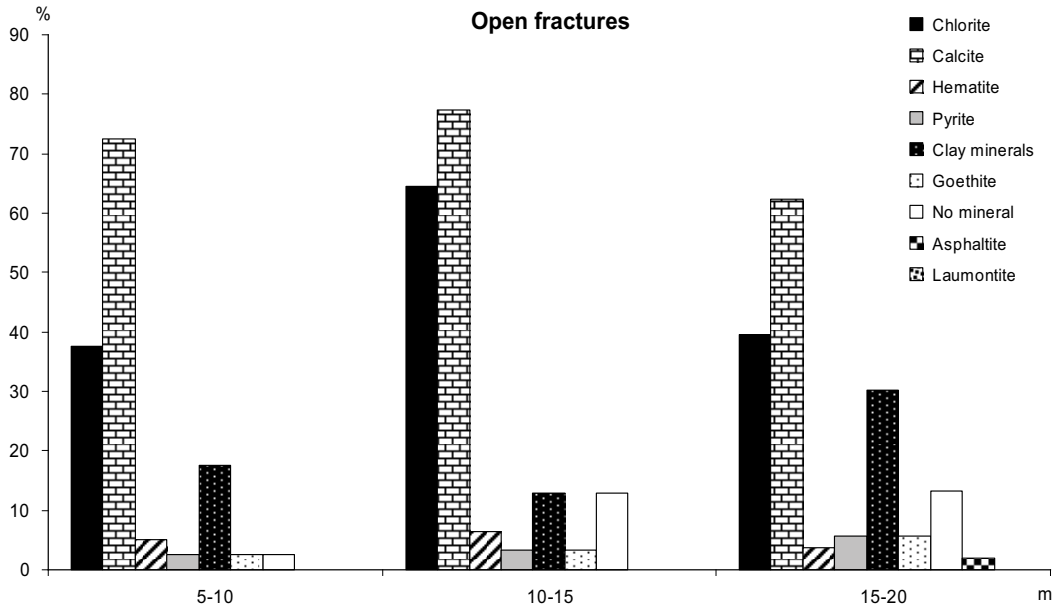


***Figure 2-17.*** *Variation of fracture mineralogy in the upper 20 m of the boreholes. Data from KFM01B, KFM03B, KFM06B and KFM08B, depths have been recalculated to vertical depths. No data is available for the uppermost 5 m.*

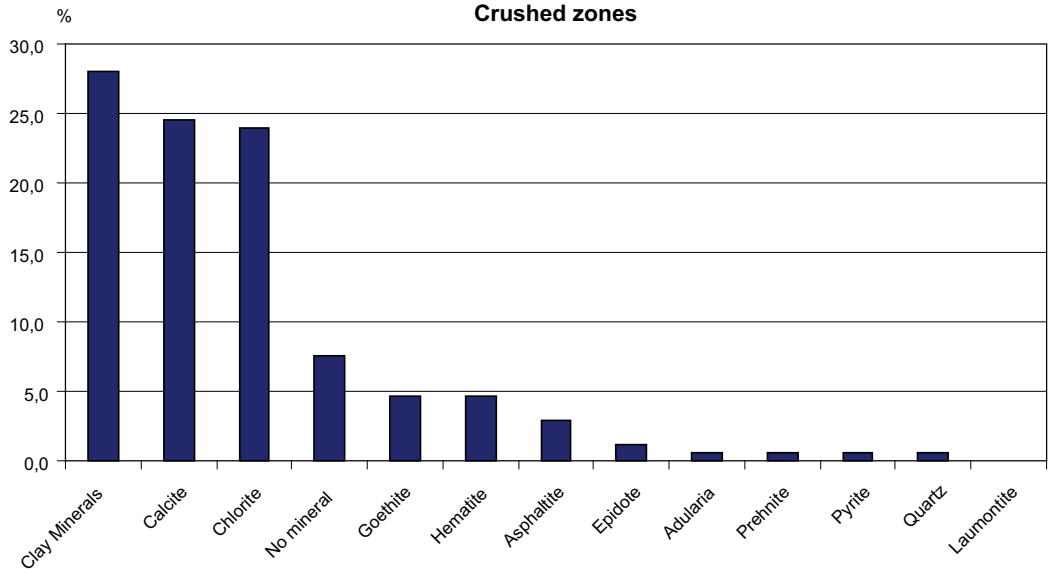


***Figure 2-18.*** *Histogram of fracture minerals in crushed zones. The percentage value represent in how many of the crushed zones each mineral has been identified. Data from KFM01A–08B, total number of crushed zones = 95.*

as “no mineral” (see discussion in Section 2.2.3.1) and the minerals goethite, hematite and epidote are present in between 7 and 3% of the crushed zones while the other minerals only are present in 1% or less of the zones. The smaller amount of pyrite in the crushed zones compared with the fractures may be a result of oxidation caused by circulation of oxidizing fluid which could have been of hydrothermal or low temperature origin.

Since less data is available for the crushed zones than the sealed and open fractures, the trends are less statistically certain. The most obvious difference when mineralogy is plotted versus depth (Figure 2-19) compared to open fractures is the absence of pyrite, the 3% occurrence in the upper 100 m is due to the low total number of crushed zones only 1 mapped occurrence of pyrite. The absence of calcite between 300 and 400 m might be due to the low number of crushed zones mapped in this interval (13).

**Table 2-13. Relative abundance of fracture minerals in crushed zones. The percentage value represent in how many of the crushed zones a specific mineral has been identified. Data from KFM01A–08B.**

| Mineral | % |
|---|---|
| Clay Minerals | 27 |
| Calcite | 23 |
| Chlorite | 23 |
| No mineral | 7 |
| Goethite | 4 |
| Hematite | 4 |
| Asphaltite | 3 |
| Epidote | 1 |
| Adularia | 1 |
| Prehnite | 1 |
| Pyrite | 1 |
| Quartz | 1 |
| Laumontite | < 1 |

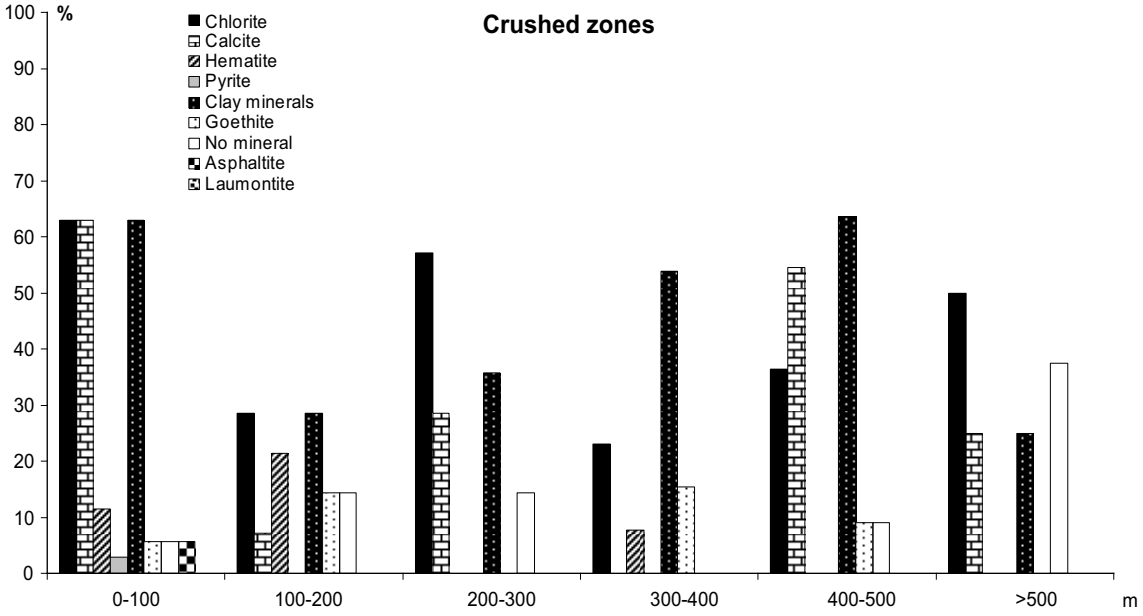


***Figure 2-19.*** *Variation of mineralogy with depth in crushed zones in boreholes KFM01A–08B, depths have been recalculated to vertical depths.*

### 2.2.4 Fracture filling geochemistry

The fracture filling geochemistry data have been compiled from /Sandström and Tullborg 2005/ which includes data from KFM01A–KFM06A. Since the chemistry differs highly between different mineral fillings depending on their mineralogy, no mean value has been calculated. Instead, a short summary of the conclusions of the bulk chemistry of fracture fillings in /Sandström and Tullborg 2005/ is presented below and the chemistry of the analysed fracture fillings can be found in Appendix II.

*K, Rb, Ba, Cs*

These elements are mainly hosted in K-feldspar, mica and clay minerals. K and Ba prefer K-feldspar while Rb and Cs to a higher degree are hosted together with K in clay minerals, especially in illite and mixed layer clays of illite/smectite type. However, the highest Cs content has been found in fractures with the Na-zeolite analcime. Compared to the host rock, Cs is significantly higher in the fracture coatings with values between 2.5 and 32.7 ppm in 17 of 23 samples.

*Na, Ca, Sr*

The main Na minerals are albite and analcime, these minerals are not so common in the fracture fillings and the Na content is often below 1% (0.4–5.1 when albite and/or analcime are present). The dominating Ca mineral is calcite, although several other Ca-bearing minerals like epidote, prehnite and laumontite are common as well. The most likely Sr hosting minerals are laumontite, plagioclase and maybe epidote.

*Fe, Mg, Mn, Ti, V, Sc*

Fe and Mg are mainly hosted in chlorite/corrensite, the Fe/Mg ratio in the chlorite differs highly between different fracture generations where the oldest often are the most Fe-rich. Mn is mainly found in chlorite and clay minerals. Ti, V and Sc generally show a positive correlation with Fe except for some prehnite and pyrite rich samples that show very low Ti, Sc and V content. The $Fe_2O_3$ content in fracture fillings containing chlorite/corrensite is commonly between 5 and 18% (Figure 2-20).

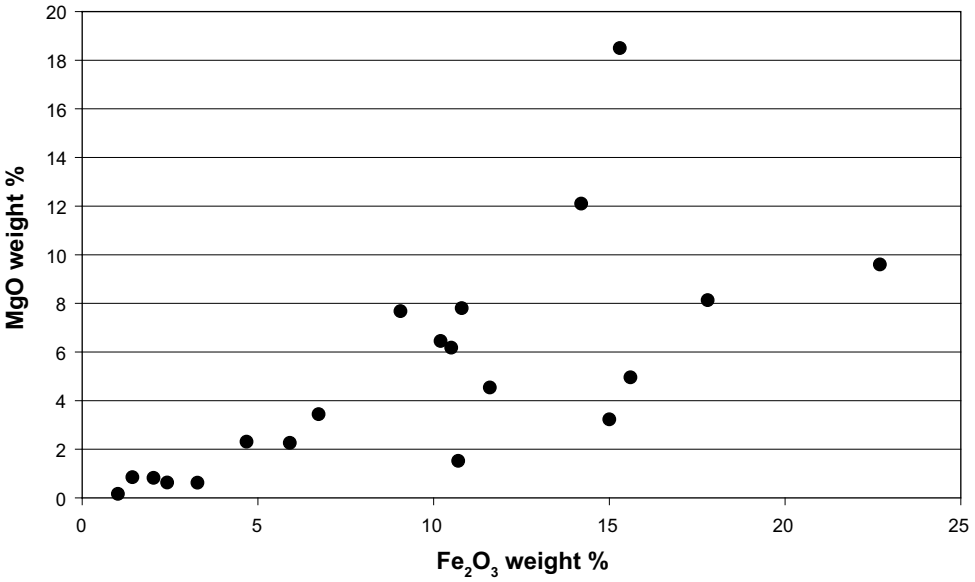


***Figure 2-20.*** *$Fe_2O_3$ versus MgO for bulk samples of fracture fillings. From /Sandström and Tullborg 2005/.*

*U, Th*

Elevated U-content has been found in two fracture fillings from KFM03A at 643.80 m and 644.17 m with 2,310 and 2,200 ppm respectively. Generally, however, the Uranium content is low and varies between 0.46 and 70 ppm. The Thorium content varies between 0.2 and 14.7 ppm in all analysed fracture fillings. The Th/U ratio is below 1 in all samples except one which indicate an enrichment of U in the fracture fillings compared to the host rock (Th/U usually > 2 /Petersson et al. 2004b/. High U content has been found in groundwater samples from different borehole sections, they are shown together with corresponding fracture coating samples in Table 2-14. A correlation between U content in the water samples and corresponding fracture fillings is indicated (cf Figure 2-21).

**Table 2-14. Data of U and Th content in fracture fillings and ground water samples at corresponding borehole lengths. Data from /Sandström and Tullborg 2005, SICADA/.**

| Drill core | Fracture filling | | | Ground water | | | | | |
|---|---|---|---|---|---|---|---|---|---|
| | Depth (m) | U (ppm) | Th (ppm) | SECUP | SECLOW | SECMID | U (ppb) | Th (ppb) | Sampling date |
| KFM01A | 127.4 | 6.7 | 1.5 | 110.10 | 120.77 | 115.44 | 1.5 | < 0.2 | 2003-02-24 |
| KFM01A | 179.35 | 12.1 | 2.9 | 176.80 | 183.90 | 180.35 | 14.9 | 0.6 | 2003-03-31 |
| KFM02A | 118.25 | 4.5 | 2.4 | 106.50 | 126.50 | 116.50 | 5.4 | 0.0 | 2003-11-18 |
| KFM02A | 423.65 | 39.7 | 10.8 | 413.50 | 433.50 | 423.50 | 13.9 | < 0.2 | 2004-02-23 |
| KFM02A | 516.09 | 20.9 | 7.2 | 509.00 | 516.08 | 512.54 | 88.6 | < 0.2 | 2003-10-20 |
| KFM03A | 644.17 | 2,200.0 | 11.4 | 639.00 | 646.12 | 642.56 | 46.1 | < 0.2 | 2004-02-23 |
| KFM06A | 357.81 | 14.9 | < 0.1 | 353.50 | 360.62 | 357.06 | 9.6 | < 0.4 | 2005-03-07 |
| KFM07A | 896.68 | 2.9 | < 0.1 | 848.00 | 1,001.55 | 924.77 | 0.3 | < 0.4 | 2005-03-24 |
| KFM08A | 686.67 | 164 | < 0.1 | 683.50 | 687.14 | 690.79 | 8.9 | < 0.2 | 2005-10-17 |

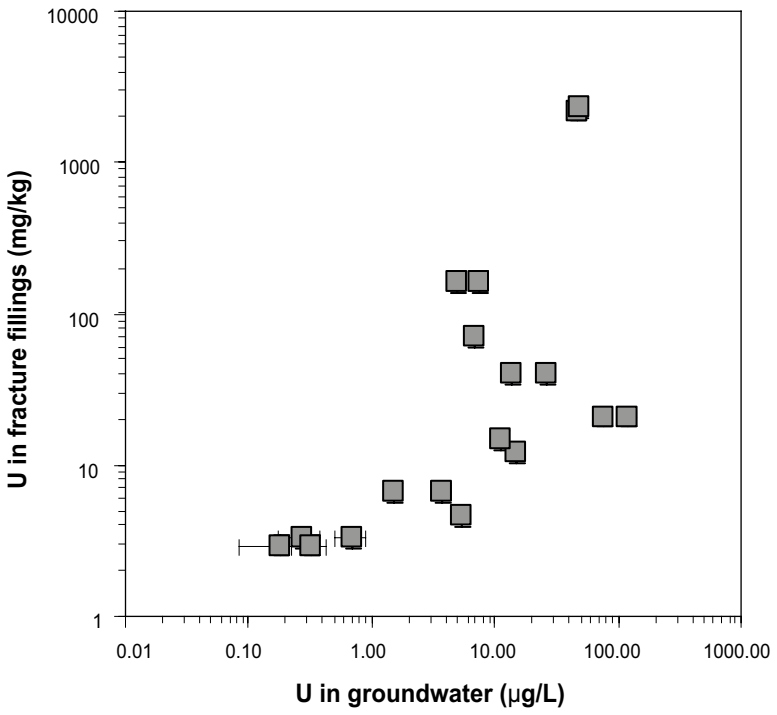


***Figure 2-21.*** *Uranium content in fracture fillings (ppm) versus uranium in water (ppb) samples. The fracture filling samples are from the corresponding drill core length. The precision of both water and fracture analyses is c 15%.*

*REEs*

Compared to the host rock, there are fracture fillings both enriched and depleted in REEs. Although, the most evident trend is enrichment in the light REEs while the heavy REE concentrations are relatively unchanged. All fracture fillings show a more or less pronounced negative Eu anomaly (Figure 2-22). Both negative and positive Ce anomalies are found in a few samples, probably related to (hydrothermal?) oxidation in these fractures. The highest HREEs content is found in the two samples with elevated U concentrations.

### 2.2.4.1 Geochemistry of selected fracture minerals

The geochemistry of selected fracture minerals from the Forsmark site is based on in situ SEM-EDS analyses of pure mineral phases in thin section /Sandström et al. 2004, Sandström and Tullborg 2005/. Since most fractures are a mixture of different mineral phases, the geochemical composition below is to be considered as "end-members" of the different fracture fillings. Trace element analyses of calcite have been carried out by ICP-MS while trace element composition of other minerals has been estimated from ICP-MS data from bulk fracture filling chemistry /Sandström and Tullborg 2005/.

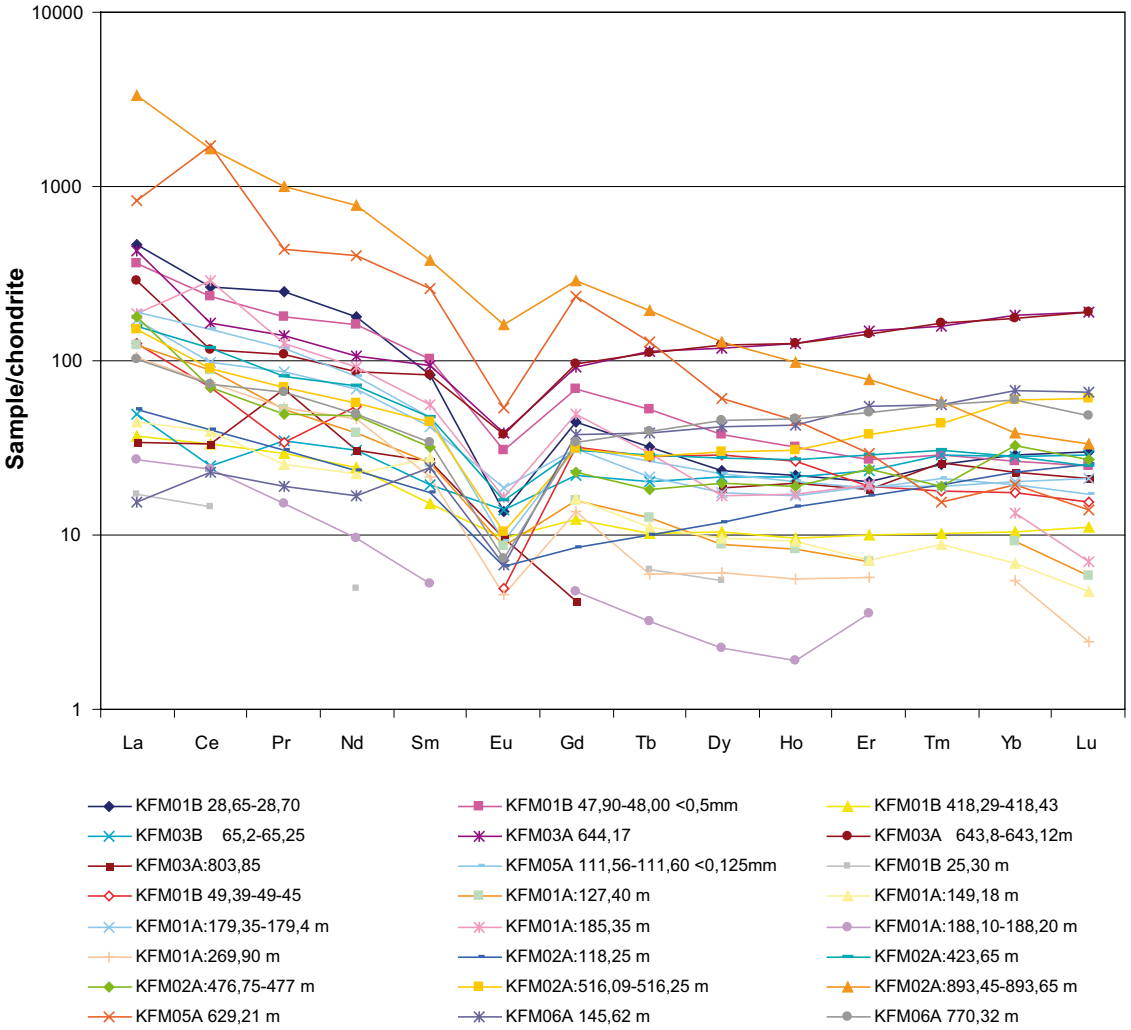


***Figure 2-22.*** *Chondrite normalized REE-pattern for fracture filling material from drill cores KFM01A–KFM06A. Data from /Sandström and Tullborg 2005/. Normalization factors from /Evansen et al. 1978 /.*

*Chlorite/corrensite*

Chlorite and corrensite are the most important $Fe^{2+}$ bearing fracture mineral at the Forsmark site. The FeO content in chlorite/corrensite is normally between 20 and 30% and the MgO content varies between 3 and 24%. The CaO content is normally between 0.2 and 0.9% due to the corrensite component.

*Calcite*

The calcite is a pure $CaCO_3$ with low contents of FeO, MgO and MnO, in most calcite the total amounts of trace components are < 1%. The Sr content varies between different generations of calcite, but the most abundant calcite, especially in open fractures, has generally low Sr content between ~ 20 and 54 ppm. Both U and Th content are low, usually below 0.2 ppm. No other carbonates than calcite have been identified in the fractures at the Forsmark site.

*Epidote*

Epidote has a $Fe_2O_3$ content between 9 and 15% and a MnO content between 0.1 and 0.8%, the CaO content is c 23%.

*Laumontite*

Laumontite has a CaO content between 10 and 13% and FeO content below 0.5%. Although laumontite occurs together with small grains of hematite in Forsmark, a bulk sample of such a fracture filling does not have a higher $Fe_2O_3$ than 1%.The Sr content in the same fracture filling consisting of laumontite, quartz and small amounts of hematite is 338 ppm.

*Asphaltite*

Asphaltite consists of a mixture of hydrocarbons and is often associated with sulphides. The S content is therefore high in the analysed samples and varies between 1,220 and 25,600 ppm. No elevated U or Th content has been detected in the asphaltite /Sandström et al. 2006/.

*Sulphides*

The sulphide minerals in fractures at the Forsmark site are totally dominated by pyrite which makes up more than 99% of all sulphides. Other sulphides present only as trace amounts are galena, sphalerite and chalcopyrite.

### 2.2.5 Redox – Fracture fillings

Mössbauer analyses have been carried out on five samples of fracture filling material, mostly consisting of chlorite (/corrensite) and minor amount of epidote and hematite (Table 2-15) /Sandström and Tullborg 2005/. The oxidation factor for chlorite varies between 0.12 and 0.33 in the samples consisting of only chlorite. The total oxidation factor could only be calculated in two samples due to the small amount of oxides in the samples, the $Fe^{3+}/Fe_{tot}$ ratio in these samples are 0.35 and 0.67, and both these samples contain hematite. Important to note is that even in a fracture containing hematite, $Fe^{2+}$ makes up more than 30% of the total Fe content.

The so far analysed fractures all contain chlorite, an estimation of the redox conditions in fractures with other mineralogy must therefore be estimated. Fractures filled with silicate minerals that exclusively incorporate $Fe^{3+}$, like epidote and prehnite, would give an elevated oxidation factor. Laumontite filled fractures commonly also contain hematite /Sandström and Tullborg 2005/, so a high oxidation factor can be expected for these fractures as well.

In hydraulically conductive zones, clay minerals, chlorite and calcite dominate (Section 2.2.3.3). The $Fe_{tot}$ content in fractures with chlorite/corrensite is commonly between ~ 3 and 13% (calculated from $Fe_2O_3$ content in bulk fracture fillings) (Section 2.2.4), if an oxidation factor of 0.3 is assumed, a $Fe^{2+}$ content of ~ 2–9% in fractures and zones with chlorite/corrensite is suggested.

**Table 2-15. Mössbauer analyses of fracture filling material, data from /Sandström and Tullborg 2005/. *For the calculation of mean values and standard deviation, the silicate oxidation factor has been used instead of the total oxidation factor when only trace amounts of oxides were found in the samples. Oxidation factor (silicate) = $Fe^{3+}_{silicate}$/($Fe^{3+}_{silicate}$+ $Fe^{2+}_{silicate}$), Oxidation factor (total) = $Fe^{3+}_{total}$/($Fe^{3+}_{total}$+ $Fe^{2+}_{total}$), Oxidation factor (oxide) = $Fe^{3+}_{oxide}$/($Fe^{3+}_{oxide}$ + $Fe^{2+}_{oxide}$).**

| Sample | Fe-mineral | Oxidation factor (silicate) | Oxidation factor (total) | Oxidation factor (oxide) |
|---|---|---|---|---|
| KFM02A 118.25–118.70 m | Chlorite | 0.33 | 0.35 | 1 |
| KFM02A 903.65–903.70 m | Chlorite | 0.28 | | Trace magnetite |
| KFM03A 451.85–451.90 m | Chlorite. epidote | 0.30 | | Trace magnetite |
| KFM03A 803.85–804.05 m | Chlorite | 0.12 | | Trace FeOOH? |
| KFM04A 192.00–192.10 m | Chlorite. epidote. hematite | 0.42 | 0.67 | 1 |
| Mean* ± Std | | | 0.34 ± 0.20 | |

# 3 Oskarshamn

## 3.1 Rock mass

The Oskarshamn site investigation carried out in the Simpevarp area is subdivided into the Simpevarp and the Laxemar subareas.

The Simpevarp subarea (Figure 3-1) is dominated by *Ävrö granite* (rock code 501044), *quartz monzodiorite* (rock code 501036) and *fine-grained dioritoid* (rock code 501030). Subordinate rock types are *fine- to medium-grained granite* (rock code 511058), *pegmatite* (rock code 501061), *diorite to gabbro* (rock code 501033), *medium- to coarse-grained granite* (rock code 521058), *and fine-grained mafic rock* (rock code 505102) /Wahlgren et al. 2004/.

The Laxemar subarea (Figure 3-1) is also dominated by *Ävrö granite* (covers about 80% of the surface, rock code 501044) and *quartz monzodiorite,* which dominates in the southern and south-western part of the Laxemar subarea and neighbouring surroundings (covers about 14% of the surface, rock code 501036). Together these two rock types cover about 94% of the bedrock surface in the Laxemar subarea. Subordinate rock types are *fine-grained dioritoid* (rock code 501030), *fine- to medium-grained granite* (rock code 511058), *diorite to gabbro* (rock code 501033), *medium- to coarse-grained granite* (rock code 521058), *fine-grained mafic rock* (rock code 505102), and *pegmatite* (rock code 501061) /Persson Nilsson et al. 2004/.

The rock codes are the standard rock codes used by the Geological Survey of Sweden (SGU) during bedrock mapping. Descriptions of the major rock types and the subordinate rock types are presented in the following sections.

### 3.1.1 Description of rock types

The following section is a description of the rock characteristics compiled from /Wahlgren et al. 2004, 2005, 2006, SKB 2005c, 2006/ when nothing else is stated. The bedrock in the Simpevarp area is dominated by 1.8 Ga intrusive igneous rocks belonging to the Transscandinavian Igneous Belt (TIB). A characteristic feature is magma mingling and mixing relationships between the different rock types. The rocks are mostly well preserved and more or less undeformed, but a weak foliation is locally developed. However, low-grade ductile shear zones do occur.

The various rock types in the Simpevarp and Laxemar subareas display similar and overlapping compositional variations. Apart from the composition, the most important criteria employed in distinguishing between different rock types are texture and grain size.

The major rock types in the area display a compositional alkali-calcic trend characteristic for granite-syenitoid-dioritoid-gabbroid rocks in the Transscandinavian Igneous Belt.

The mineralogical composition of the major and subordinate rock types is based on point counting. All rock types except the Ävrö granite is presented collectively for the Simpevarp and Laxemar subareas. Due to heterogeneity of the Ävrö granite between the subareas, the Ävrö granite mineral data is presented separately for the Simpevarp and Laxemar subareas. The mineral data is from bore holes and field samples from /Wahlgren et al. 2004, 2005, 2006, Drake and Tullborg 2006ab/. Where only trace amounts of minor minerals have been noted, the numeric value of 0.1% has been assigned since it is below the detection limit when 500 points have been used during the point counting, except for the point-counting in /Drake and Tullborg 2006ab/, where 1,000–1,600 points were counted. This value has then been used in the calculations of mean and standard deviation and it is therefore a small systematic error in the values of the minor mineral content.

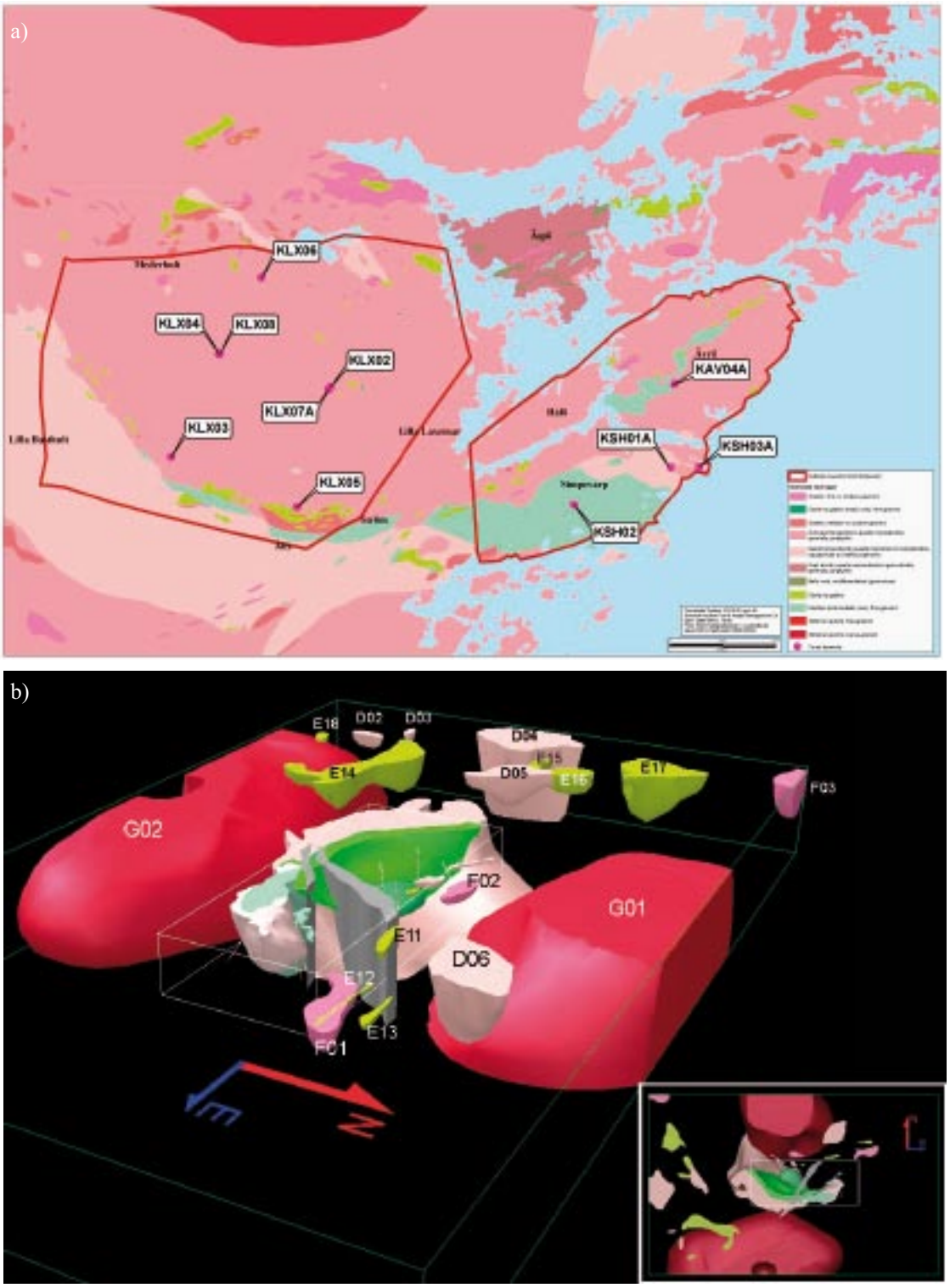


***Figure 3-1(a–b).*** *a) Bedrock geology map of the Simpevarp area (including the Simpevarp and Laxemar subareas) with the surface projections of the boreholes dealt with in this report /SKB GIS 2006/. b) Regional rock domain model with the local scale model domain inserted. The Ävrö granite (RSMA01) is transparent. View from the northeast. From /SKB 2006/.*

The pyrite content is commonly not counted separately during the point counting but falls under the opaque mineral group. However, in the studies of /Drake and Tullborg 2006ab/ the pyrite content has been counted separately and is presented below for a limited number of samples from the major rock types. The mean pyrite content for these samples is below 0.1% and the highest pyrite content in all of these samples is 0.26%. A maximum mean pyrite content based on the S content in the rock has been calculated to ~ 0.136 wt% for quartz monzodiorite, ~ 0.021 wt% for Ävrö granite from both Laxemar and Simpevarp subareas and ~ 0.018 wt% for fine-grained dioritoid (Section 3.1.2.1). However, the main opaque mineral is magnetite which sometimes is replaced partially by hematite. Small amount of ilmenite has also been observed (most common in fine-grained dioritoid and quartz monzodiorite of the major rock types). The calcite content in the rock is low, generally below 0.3%, according to point-counting. The mean apatite content is commonly 0–0.2% and is left out in the compilation below.

Estimated grain size of biotite and pyrite in Ävrö granite, quartz monzodiorite and fine-grained dioritoid from drill cores KSH01A, KSH03A+B and KLX04 is listed below.

Short descriptions of the texture and mineralogy of the rock types in the Simpevarp area are listed below, divided into major and subordinate rock types. The mineralogy of hydrothermally altered, red-stained rock which occurs adjacent to many fractures is also shown in this section (data is only available from Ävrö granite, quartz monzodiorite and fine-grained dioritoid) /Drake and Tullborg 2006ab/. The wall rock alteration has resulted in that the biotite has been completely replaced by chlorite, plagioclase has been saussuritized, i.e. replaced by albite, K-feldspar, prehnite, sericite, epidote and hematite, and partial or complete replacement of magnetite by hematite.

## Major rock types

***Ävrö Granite (granite to quartz monzodiorite) – rock code 501044***

The Ävrö granite (Figure 3-1) comprises a suite of commonly medium-grained, porphyritic rocks that vary in composition from quartz monzodiorite to granite, including granodioritic, tonalitic, quartz dioritic and quartz monzonitic varieties. This large compositional variation is evident in the very varying mineralogical composition, listed below. In the Simpevarp subarea the Ävrö granite is generally less quartz rich (granodioritic to quartz monzodioritic in composition). In the Laxemar subarea and the Ävrö granite can be subdivided into two populations, one richer in quartz (granodioritic to granitic – central part of the area) and one with a lower quartz content (quartz monzodioritic – peripheral parts of the area) that is similar to the quartz monzodiorite that dominates south of the Ävrö granite. The mean opaque content is between 1.0 and 1.5 vol%. The highest pyrite content in the Ävrö granite is 0.2 vol% and the mean content is below 0.05 vol%.

| **Biotite** | **Mean minimum** | **Mean maximum** | **Mean** |
|---|---|---|---|
| Ävrö granite | 0.02 $mm^2$ | 0.24 $mm^2$ | 0.10 $mm^2$ |
| Quartz monzodiorite | 0.02 $mm^2$ | 0.24 $mm^2$ | 0.10 $mm^2$ |
| Fine-grained dioritoid | 0.02 $mm^2$ | 0.24 $mm^2$* | 0.10 $mm^2$ |
| *=occasionally up to 1 $mm^2$ | | | |
| **Pyrite** | **Mean minimum** | **Mean maximum** | **Mean** |
| Ävrö granite | 0.0001 $mm^2$ | 0.0060 $mm^2$ | 0.00125 $mm^2$ |
| Quartz monzodiorite | 0.0001 $mm^2$ | 0.0120 $mm^2$ | 0.00250 $mm^2$ |
| Fine-grained dioritoid | 0.0001 $mm^2$ | 0.0025 $mm^2$ | 0.00100 $mm^2$ |

*Simpevarp – Ävrö granite*

Data from KSH01A, KSH03A and field samples /Wahlgren et al. 2004, 2005, Drake and Tullborg 2006a/.

*Mineralogical composition Ävrö granite Simpevarp (vol%):*

| Mineral | Range | Mean | Std | |
|---|---|---|---|---|
| Quartz | 5.0–33.3 | 16.8 | 6.5 | N=27 |
| K-feldspar | 2.6–32.0 | 16.2 | 8.4 | |
| Plagioclase | 29.2–63.0 | 48.0 | 7.9 | |
| Chlorite | 0–14.2 | 2.3 | 4.3 | |
| Biotite | 0.4–22.0 | 9.6 | 6.4 | |
| Opaque | 0.2–2.0 | 1.2 | 0.5 | |
| –Pyrite[1] | 0–0.06 | 0.02 | 0.03 | |
| Epidote | 0.2–10.3 | 3.5 | 2.7 | |
| Titanite | 0–3.2 | 1.0 | 0.8 | |
| Hornblende | 0–11.0 | 1.0 | 2.6 | |
| Prehnite | 0–0.5 | 0.1 | 0.1 | |
| Calcite | 0–0.6 | 0.2 | 0.2 | |

[1] = *"N=4"*.

Red-stained Ävrö granite adjacent to fractures from KSH03A, Simpevarp subarea /Drake and Tullborg 2006a/.

*Mineralogical composition, red-stained Ävrö granite, Simpevarp (vol%):*

| Mineral | Range | Mean | Std | |
|---|---|---|---|---|
| Quartz | 13.3–20.0 | 17.0 | 2.8 | N=4 |
| K-feldspar | 7.5–31.5 | 19.4 | 11.4 | |
| Sauss.Plag. | 42.8–50.9 | 45.2 | 3.9 | |
| Chlorite | 4.9–12.4 | 8.5 | 3.9 | |
| Biotite | 0–0.6 | 0.1 | 0.0 | |
| Opaque | 0.3–2.3 | 1.0 | 0.9 | |
| –Pyrite | <0.1 | | | |
| Epidote | 1.1–9.4 | 5.7 | 3.4 | |
| Titanite | 0.6–1.9 | 1.4 | 0.6 | |
| Hornblende | 0.1 | 0.1 | 0.0 | |
| Prehnite | 0.1–2.0 | 1.1 | 1.1 | |

*Laxemar – Ävrö granite*

Based on data from bore holes KLX03, KLX04, KLX06, KLX07A+B and field samples /Wahlgren et al. 2004, 2005, 2006, Drake and Tullborg 2006b/.

*Mineralogical composition Ävrö granite, Laxemar (vol%):*

| Mineral | Range | Mean | Std | |
|---|---|---|---|---|
| Quartz | 8.4–32.4 | 19.8 | 6.7 | N=65 |
| K-feldspar | 3.0–38.2 | 18.9 | 8.3 | |
| Plagioclase | 25.6–63.4 | 45.4 | 9.0 | |
| Chlorite | 0–3.7 | 0.2 | 0.6 | |
| Biotite | 2.4–24.8 | 9.9 | 3.7 | |
| Opaque | 0–2.8 | 1.0 | 0.6 | |
| –Pyrite[1] | 0–0.2 | 0.04 | 0.09 | |
| Epidote | 0–10.2 | 1.7 | 1.7 | |
| Titanite | 0–3.2 | 0.9 | 0.6 | |
| Hornblende | 0–10.0 | 1.6 | 2.6 | |
| Prehnite | 0–0.5 | 0.1 | 0.2 | |
| Calcite | 0–3.4 | 0.2 | 0.5 | |

[1]= ”N=5”.

Red-stained Ävrö granite adjacent to fractures, data from KLX04, Laxemar subarea /Drake and Tullborg 2006b/.

*Mineralogical composition Red-stained Ävrö granite, Laxemar (vol%):*

| Mineral | Range | Mean | Std | |
|---|---|---|---|---|
| Quartz | 5.8–30.1 | 18.7 | 9.1 | N=6 |
| K-feldspar | 11.5–30.2 | 20.8 | 8.0 | |
| Sauss.Plag. | 36.7–56.1 | 44.6 | 7.3 | |
| Chlorite | 3.7–17.6 | 7.5 | 5.3 | |
| Biotite | 0–3.1 | 0.7 | 1.3 | |
| Opaque | 0.4–2.6 | 1.5 | 0.8 | |
| –Pyrite | 0.0–0.19 | 0.03 | 0.08 | |
| Epidote | 0.5–3.8 | 1.9 | 1.3 | |
| Titanite | 0.7–1.7 | 1.1 | 0.4 | |
| Hornblende | 0–6.0 | 1.0 | 2.4 | |
| Prehnite | 0.3–2.3 | 1.2 | 0.8 | |

***Quartz monzodiorite – rock code 501036***

The quartz monzodiorite is a grey to reddish grey, medium-grained, equigranular to weakly porphyritic rock with relatively restricted compositional range. The quartz monzodiorite in southern and south-western Laxemar has a slightly higher quartz content compared with the quartz monzodiorite in the Simpevarp subarea. The highest pyrite content is 0.26 vol% and the mean pyrite content is below 0.1 vol%. The rock is dominated by plagioclase (mean content is 43.3 vol%). Contents of biotite, K-feldspar, amphibole and quartz are all in the interval between 9–15 vol% and the amount of epidote and chlorite is between 2 and 3 vol% each. The opaque content is quite high (mean value is 1.4 vol%). The pyrite content is below 0.1 vol%. Data from KSH01A+B, KSH03A+B, KLX03, KLX04 and field samples from the Simpevarp and Laxemar subareas /Drake and Tullborg 2004, Wahlgren et al. 2004, 2005, 2006/.

*Mineralogical composition, quartz monzodiorite (vol%):*

| Mineral | Range | Mean | Std | |
|---|---|---|---|---|
| Quartz | 5–21.0 | 12.2 | 3.7 | N=29 |
| K-feldspar | 20.3–38.2 | 9.4 | 6.3 | |
| Plagioclase | 19.4–53.2 | 43.3 | 6.4 | |
| Chlorite | 0–17.2 | 2.2 | 5.0 | |
| Biotite | 0.3–49.0 | 14.8 | 9.8 | |
| Opaque | 0.2–3.7 | 1.4 | 0.9 | |
| –Pyrite[1] | 0–0.26 | 0.06 | 0.11 | |
| Epidote | 0–14.8 | 2.5 | 3.9 | |
| Titanite | 0–3.2 | 0.7 | 0.8 | |
| Amphibole[2] | 0–41.0 | 11.2 | 9.1 | |
| Pyroxene[2] | 0–8.2 | 1.3 | 2.5 | |
| Prehnite | 0–3.3 | 0.3 | 0.8 | |
| Calcite | 0–2.2 | 0.2 | 0.5 | |

[1]= “N=6”, [2]= “N=23”.

Red-stained quartz monzodiorite adjacent to fractures, data from KSH03A+B /Drake and Tullborg 2006a/.

*Mineralogical composition, red-stained quartz monzodiorite (vol%):*

| Mineral | Range | Mean | Std | |
|---|---|---|---|---|
| Quartz | 3.1–15.9 | 10.3 | 4.9 | N=6 |
| K-feldspar | 1.4–13.3 | 6.1 | 4.5 | |
| Sauss.Plag. | 47.0–54.5 | 51.1 | 2.5 | |
| Chlorite | 9.1–17.7 | 12.5 | 3.8 | |
| Biotite | 0.1–1.8 | 0.6 | 0.6 | |
| Opaque | 1.6–3.6 | 2.2 | 0.8 | |
| –Pyrite | <0.1 | | | |
| Epidote | 1.0–3.2 | 1.6 | 0.8 | |
| Titanite | 0–0.9 | 0.4 | 0.3 | |
| Hornblende[1] | 6.7–18.3 | 12.2 | 5.4 | |
| Prehnite | 0.6–6.3 | 2.8 | 2.0 | |

[1]=including additional augite.

***Fine-grained dioritoid – rock code 501030***

The fine-grained dioritoid is a unequigranular rock with up to 3 mm large megacrysts of hornblende and plagioclase (locally pyroxene and biotite occur as megacrysts). Most of the hornblende megacrysts are believed to be secondary after pyroxene. This rock is a major rock type in the Simpevarp subarea (central and southern part of the Simpevarp peninsula and central Ävrö Island) and a subordinate rock type in the Laxemar subarea, where it occurs as minor bodies in the southern part of the subarea, particularly along the contact zone between the Ävrö granite and the quartz monzodiorite (Figure 3-1). The rock is dominated by plagioclase (mean content is 47.7 vol%). K-feldspar and quartz is generally between 9–15 vol% each and the amount of amphibole, pyroxene and epidote is between 2 and 5 vol%. The pyrite content is below 0.1 vol%. Data from KSH01A, KSH02 and field samples from Simpevarp subarea /Wahlgren et al. 2004, Drake and Tullborg 2006a/.

*Mineralogical composition, fine-grained dioritoid (vol%):*

| Mineral | Range | Mean | Std | |
|---|---|---|---|---|
| Quartz | 0.8–25.4 | 9.5 | 6.4 | N=25 |
| K-feldspar | 0.4–22.8 | 11.1 | 6.7 | |
| Plagioclase | 12–65.6 | 47.7 | 12.0 | |
| Chlorite | 0–16.0 | 1.7 | 4.5 | |
| Biotite | 0–43.8 | 15.2 | 9.8 | |
| Opaque | 0.1–3.4 | 1.2 | 0.8 | |
| –Pyrite[1] | <0.1 | | | |
| Epidote | 0–10.0 | 2.1 | 2.8 | |
| Titanite | 0–1.8 | 0.5 | 0.6 | |
| Amphibole[2] | 0–20 | 4.8 | 6.1 | |
| Pyroxene[2] | 0–22 | 3.7 | 5.5 | |
| Prehnite | 0–0.8 | 0.1 | 0.2 | |
| Olivine | 0–1.4 | 0.1 | 0.3 | |
| Calcite | 0–2.0 | 0.3 | 0.5 | |

[1]= “N=2”, [2]= “N=23”.

Red-stained fine-grained dioritoid adjacent to fractures from KSH01A /Drake and Tullborg 2006a/.

*Mineralogical composition, red-stained fine-grained dioritoid (vol%):*

| Mineral | Range | Mean | Std | |
|---|---|---|---|---|
| Quartz | 14.0–28.6 | 21.3 | 10.3 | N=2 |
| K-feldspar | 11.2–14.7 | 13.0 | 2.4 | |
| Sauss.Plag. | 38.2–49.0 | 43.6 | 7.6 | |
| Chlorite | 14.4–13.4 | 13.9 | 0.7 | |
| Biotite | 1.0–1.4 | 1.2 | 0.3 | |
| Opaque* | 0.3–1.2 | 0.8 | 0.7 | |
| –Pyrite | < 0.1 | | | |
| Epidote | 0.3–0.8 | 0.6 | 0.3 | |
| Titanite | < 0.1 | < 0.1 | < 0.1 | |
| Amph+Px[1] | 0.7–6.5 | 3.6 | 4.1 | |
| Prehnite | 1.2–2.7 | 2.0 | 1.1 | |

[1]=including hornblende, actinolite and augite.

## Subordinate rock types

### *Fine- to medium-grained granite - rock code 511058*

Fine- to medium-grained granite is a common subordinate rock type in the Laxemar and Simpevarp subareas. It occurs as dykes of various thickness (generally 0.1–1 m), but also as veins and minor, irregular bodies in the other rock types. U-Pb zircon dating indicates that the fine- to medium-grained granite is coeval with the country rocks and belongs to the same magmatic generation /Wahlgren et al. 2005/. The rock is dominated by plagioclase, K-feldspar and quartz, with biotite, epidote, chlorite and titanite as minor constitutes. The opaque content is quite low. Data from KSH03A, KLX06 and surface samples from the Simpevarp and Laxemar subareas /Wahlgren et al. 2004, 2005, 2006/.

*Mineralogical composition, fine- to medium grained granite (vol%):*

| Mineral | Range | Mean | Std | |
|---|---|---|---|---|
| Quartz | 22.2-33.0 | 25.5 | 3.8 | N=8 |
| K-feldspar | 26-39.8 | 31.9 | 4.0 | |
| Plagioclase | 25.8-42.8 | 32.5 | 5.8 | |
| Chlorite | 0-3.8 | 1.5 | 1.6 | |
| Biotite | 0-10.8 | 3.9 | 3.9 | |
| Opaque | 0-1.4 | 0.7 | 0.5 | |
| Epidote | 0-5.2 | | 2.0 | 1.9 |
| Titanite | 0-2.0 | 1.0 | 0.8 | |
| Amphibole | 0-0.4 | 0.1 | 0.1 | |
| Muscovite | 0-4.0 | 0.8 | 1.3 | |
| Calcite | 0-0.2 | 0.1 | 0.1 | |

***Medium- to coarse-grained granite – rock code 501058***

Scattered minor bodies of red to greyish red, medium- to coarse-grained granite occur in the Laxemar and Simpevarp subareas. It occurs as mixed and mingled, diffusely delimited small occurrences in the Ävrö granite. Two surface samples from the Laxemar subarea /Wahlgren et al. 2005/ have been analysed. This rock type has higher plagioclase content and lower K-feldspar content than the fine- to medium-grained granite.

*Mineralogical composition, medium- to coarse-grained granite (vol%):*

| Mineral | Range | Mean | Std | |
|---|---|---|---|---|
| Quartz | 26.2–27.8 | 27.0 | 1.1 | N=2 |
| K-feldspar | 16.6–26.4 | 21.5 | 6.9 | |
| Plagioclase | 38.4–47.8 | 43.1 | 6.6 | |
| Chlorite | 0–0.2 | 0.1 | 0.1 | |
| Biotite | 6.2 | 6.2 | 0 | |
| Opaque | 0.2–1.0 | 0.6 | 0.6 | |
| Epidote | 0–1.4 | | 0.7 | 1.0 |
| Titanite | 0.2 | 0.2 | 0 | |
| Muscovite | 0.4 | 0.4 | 0 | |
| Prehnite | 0–0.2 | 0.1 | 0.1 | |

***Diorite to gabbro – rock code 501033***

Diorite-gabbro occurs as scattered minor bodies and enclaves, particularly in the Ävrö granite in the Laxemar subarea and its immediate surroundings. The most prominent occurrence of diorite to gabbro is the concentration along the contact zone between the Ävrö granite and the quartz monzodiorite in the southern part of the Laxemar subarea. Data from surface samples from the Laxemar and Simpevarp subareas /Wahlgren et al. 2004, 2005/.

*Mineralogical composition, diorite to gabbro (vol%):*

| Mineral | Range | Mean | Std | |
|---|---|---|---|---|
| Quartz | 0–4.8 | 2.8 | 1.9 | N=5 |
| K-feldspar | 0–1.2 | 0.5 | 0.5 | |
| Plagioclase | 42.2–55.6 | 47.6 | 5.1 | |
| Chlorite | <0.1 | | | |
| Biotite | 4.8–20.6 | 12.7 | 6.1 | |
| Opaque | 2.6–9.2 | 5.2 | 2.4 | |
| Epidote | 0–3.2 | | 1.3 | 1.3 |
| Titanite | 0–3.8 | 1.6 | 1.7 | |
| Amphibole | 8.2–36.0 | 25.2 | 11.2 | |
| Pyroxene | 0–11.2 | 2.3 | 5.0 | |
| Calcite | 0–0.4 | 0.3 | 0.2 | |

***Pegmatite – rock code 501066***

Pegmatite frequently occurs as less than 0.3 m thick dykes.

*Mineralogical composition (N=0)*

No data available

***Fine-grained mafic rock – rock code 505102***

Locally, a fine-grained mafic rock (diorite to gabbro) occurs as sheets, dykes or minor bodies. Data from KSH02 /Wahlgren et al. 2004/. The only analysed sample of this rock type has a high content of biotite, plagioclase, amphibole, titanite and opaques.

*Mineralogical composition, fine-grained mafic rock (vol%):*

| Mineral | Range | |
|---|---|---|
| Quartz | 5.6 | N=1 |
| K-feldspar | 2.0 | |
| Plagioclase | 29.8 | |
| Biotite | 34.8 | |
| Opaque | 4.0 | |
| Epidote | 3.8 | |
| Titanite | 7.2 | |
| Amphibole | 12.8 | |

### 3.1.2 Geochemistry

The geochemistry of the three dominating rock types (Ävrö granite, quartz monzodiorite and fine-grained dioritoid) in the Simpevarp area is described below. Since Ävrö granite vary somewhat in composition between the Simpevarp and Laxemar subareas geochemistry of Ävrö granite from these two subareas are described separately. The geochemistry of quartz monzodiorite and fine-grained dioritoid are presented collectively for the two subareas. The geochemistry of hydrothermally altered, red-stained rock found adjacent to fractures is described separately for each of the major rock types.

### *3.1.2.1 Ävrö granite (rock code 501044)*

The geochemistry of the most abundant rock type in the candidate area, the Ävrö granite (rock code 501044), is characterized by a quite high $SiO_2$ content (61–64 wt%). The $SiO_2$ content is somewhat higher (64 wt%) in the Laxemar subarea than in the Simpevarp subarea (61 wt%) due to higher quartz content in the Laxemar samples (which are mainly from the granite-dominated part of the subarea). The geochemistry of fresh and red-stained rock type 501044 is summarized in Tables 3-1, 3-2, 3-3 and 3-4. The high Ba content is commonly indications of high alkali feldspar content and low mica content in the rock. The Cs content is mainly related the content of biotite. The quite high CaO and Sr contents are due to the relatively high plagioclase content and partly due to the quite high epidote content. The rock type has very low concentrations of almost all trace elements except the REEs. The U and Th content are both normal. The rock has only been analysed for S in a few samples and the mean value from these samples is about 115 ppm. Stoichiometric recalculation of the S content to pyrite gives a maximum mean pyrite content of ~ 0.021 wt%. Chondrite-normalized REE pattern show enrichment in the light REEs relative to the heavy REEs which is typical for granitic rocks (Figures 3-2 and 3-3). Most of the samples do not show any Eu or Ce anomalies.

In the red-stained, hydrothermally altered Ävrö granite adjacent to fractures the $K_2O$, $Na_2O$ and Rb values are higher and CaO, $Al_2O_3$ and Sr values are lower than in the fresh rock due to replacement of plagioclase by K-feldspar and albite in the red-stained rock. The Cs content is lower in the red-stained rock due to replacement of biotite by chlorite. The higher LOI values of the red-stained rock compared to the fresh rock is due to the formation of secondary water-bearing minerals like chlorite, sericite, epidote and prehnite. The $Fe_2O_3$ content in the red-stained rock is however about the same in the red-stained rock and in the fresh rock. The U content is generally somewhat higher and the Th content is generally somewhat lower in the red-stained rock compared to the fresh rock. The S content is generally lower in the red-stained rock compared to the fresh rock due to oxidation of primary pyrite. However, the S content is enriched in some red-stained samples due to formation of pyrite in the rock after the red-staining event /Drake and Tullborg 2006ab/. The content of the REEs remains constant in the red-stained rock compared to the fresh rock.

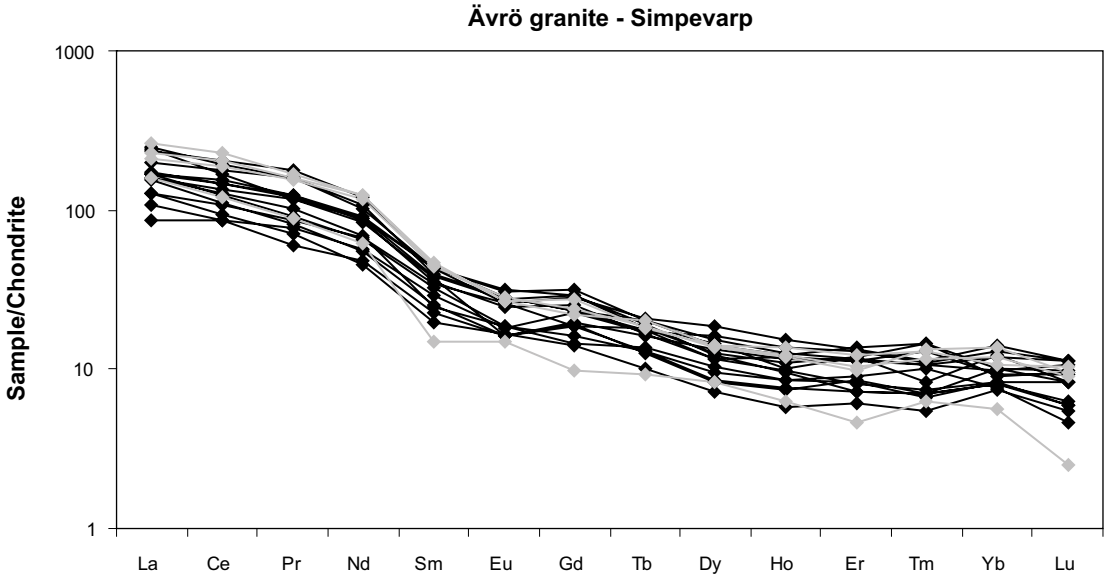


***Figure 3-2.*** *Chondrite normalized REE-pattern for Ävrö granite (black) and red-stained Ävrö granite (grey) from Simpevarp subarea. Data from KSH01A, KSH03A+B and field samples /Wahlgren et al. 2004, Drake and Tullborg 2006a/. Chondrite values from /Evansen et al. 1978/. (N=19, samples with values below detection limit for some elements are excluded).*

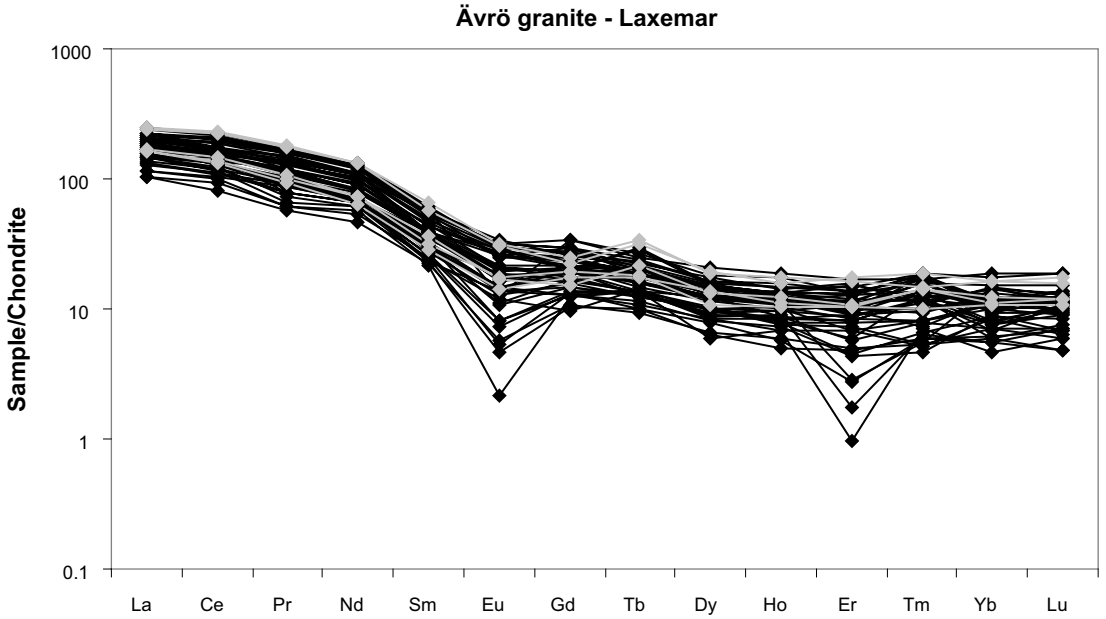


***Figure 3-3.*** *Chondrite normalized REE-pattern for Ävrö granite (black) and red-stained Ävrö granite (grey) Laxemar subarea. Data from KLX03, KLX04, KLX06, KLX07A+B, KLX08 and field samples /Wahlgren et al. 2005, Drake and Tullborg 2006b, Wahlgren et al. 2006/. Chondrite values from /Evansen et al. 1978/. (N=52, samples with values below detection limit for some elements are excluded).*

**Table 3-1. Whole-rock geochemistry of Ävrö granite – rock code 501044 from Simpevarp subarea. Mean and standard deviation values have been calculated based on data from KSH01A, KSH03A and field samples /Wahlgren et al. 2004, Drake and Tullborg 2006a/. N=20 (except N=4 for Cs, F and S and N=15 for REEs).**

| Element | Mean | Std | Element | Mean | Std | Element | Mean | Std | Element | Mean | Std |
|---|---|---|---|---|---|---|---|---|---|---|---|
| **$SiO_2$(wt%)** | 62.37 | 5.02 | **Ba (ppm)** | 1,197.80 | 366.16 | **Sc(ppm)** | 9.29 | 6.86 | **La(ppm)** | 41.15 | 11.63 |
| **$Al_2O_3$** | 16.44 | 1.52 | **Be** | 2.75 | 0.39 | **Sn** | 1.58 | 2.25 | **Ce** | 87.77 | 23.96 |
| **CaO** | 3.88 | 1.50 | **Co** | 9.58 | 9.14 | **Sr** | 964.35 | 326.25 | **Pr** | 10.71 | 3.36 |
| **$Fe_2O_3$** | 4.93 | 1.82 | **Cr** | 81.02 | 149.96 | **Ta** | 1.17 | 0.29 | **Nd** | 37.10 | 10.61 |
| **$K_2O$** | 3.54 | 0.54 | **Cs** | 1.10 | 0.42 | **Th** | 8.90 | 4.17 | **Sm** | 5.27 | 1.28 |
| **MgO** | 2.42 | 1.94 | **Cu** | 28.10 | 34.56 | **U** | 4.38 | 1.96 | **Eu** | 1.33 | 0.34 |
| **MnO** | 0.09 | 0.03 | **Ga** | 44.04 | 26.95 | **V** | 76.32 | 35.48 | **Gd** | 4.52 | 1.12 |
| **$Na_2O$** | 4.14 | 0.59 | **Hf** | 4.51 | 1.03 | **W** | 0.23 | 0.50 | **Tb** | 0.61 | 0.12 |
| **$P_2O_5$** | 0.29 | 0.12 | **Mo** | < 2 | n.a. | **Y** | 21.72 | 6.38 | **Dy** | 3.12 | 0.81 |
| **$TiO_2$** | 0.70 | 0.22 | **Nb** | 11.37 | 2.08 | **Zn** | 80.42 | 21.77 | **Ho** | 0.59 | 0.15 |
| **TOTAL** | 98.80 | 0.80 | **Ni** | 17.64 | 29.28 | **Zr** | 214.02 | 55.20 | **Er** | 1.68 | 0.41 |
| **LOI** | 1.08 | 0.46 | **Rb** | 95.39 | 16.80 | | | | **Tm** | 0.25 | 0.07 |
| **F** | 0.11 | 0.03 | **S** | 114.53 | 78.95 | | | | Yb | 1.63 | 0.35 |
| | | | | | | | | | **Lu** | 0.21 | 0.06 |

**Table 3-2. Whole-rock geochemistry of red-stained Ävrö granite – rock code 501044 from Simpevarp subarea. Mean and standard deviation values have been calculated based on data from KSH03A /Drake and Tullborg 2006a/. N=4.**

| Element | Mean | Std | Element | Mean | Std | Element | Mean | Std | Element | Mean | Std |
|---|---|---|---|---|---|---|---|---|---|---|---|
| $SiO_2$(wt%) | 61.93 | 3.21 | Ba (ppm) | 1,622.50 | 602.52 | Sc(ppm) | 8.46 | 1.46 | La(ppm) | 52.63 | 10.86 |
| $Al_2O_3$ | 16.43 | 0.69 | Be | 2.22 | 0.27 | Sn | 2.24 | 0.97 | Ce | 117.93 | 29.04 |
| CaO | 3.31 | 1.25 | Co | 9.01 | 1.76 | Sr | 957.75 | 387.44 | Pr | 13.74 | 3.44 |
| $Fe_2O_3$ | 4.96 | 0.86 | Cr | 114.53 | 19.11 | Ta | 1.13 | 0.22 | Nd | 50.08 | 14.21 |
| $K_2O$ | 4.26 | 0.58 | Cs | 1.00 | 0.20 | Th | 8.08 | 2.89 | Sm | 5.82 | 2.36 |
| MgO | 2.03 | 0.31 | Cu | 12.37 | 13.62 | U | 5.07 | 1.82 | Eu | 1.41 | 0.36 |
| MnO | 0.08 | 0.01 | Ga | 12.84 | 2.20 | V | 69.98 | 15.84 | Gd | 4.26 | 1.57 |
| $Na_2O$ | 4.21 | 0.31 | Hf | 5.14 | 0.75 | W | 1.44 | 1.67 | Tb | 0.62 | 0.19 |
| $P_2O_5$ | 0.31 | 0.07 | Mo | < 2 | n.a. | Y | 23.45 | 4.91 | Dy | 3.18 | 0.73 |
| $TiO_2$ | 0.74 | 0.15 | Nb | 9.65 | 3.05 | Zn | 68.65 | 13.36 | Ho | 0.63 | 0.19 |
| TOTAL | 98.23 | 1.05 | Ni | 12.08 | 2.93 | Zr | 235.00 | 40.23 | Er | 1.54 | 0.54 |
| LOI | 1.70 | 0.22 | Rb | 108.20 | 10.53 | | | | Tm | 0.28 | 0.08 |
| F | 0.17 | 0.09 | S | 85.80 | 90.15 | | | | Yb | 1.75 | 0.58 |
| | | | | | | | | | Lu | 52.63 | 10.86 |

**Table 3-3. Whole-rock geochemistry Ävrö granite – rock code 501044 from Laxemar subarea. Mean and standard deviation values have been calculated based on data from KLX03, KLX04, KLX06, KLX07A+B and field samples /Wahlgren et al. 2004, 2005, 2006, Drake and Tullborg 2006b/. N=52 (except N=5 for Cs, F and S).**

| Element | Mean | Std | Element | Mean | Std | Element | Mean | Std | Element | Mean | Std |
|---|---|---|---|---|---|---|---|---|---|---|---|
| $SiO_2$(wt%) | 64.88 | 4.26 | Ba (ppm) | 1,371.02 | 354.72 | Sc(ppm) | 6.83 | 2.38 | La(ppm) | 41.81 | 9.59 |
| $Al_2O_3$ | 15.98 | 1.31 | Be | 2.61 | 0.46 | Sn | 4.09 | 4.58 | Ce | 92.14 | 23.86 |
| CaO | 3.26 | 0.96 | Co | 6.85 | 3.34 | Sr | 933.79 | 311.98 | Pr | 10.66 | 3.29 |
| $Fe_2O_3$ | 4.43 | 1.11 | Cr | 31.87 | 15.31 | Ta | 0.96 | 0.27 | Nd | 40.21 | 12.10 |
| $K_2O$ | 3.87 | 0.48 | Cs | 2.51 | 0.30 | Th | 8.83 | 4.66 | Sm | 5.79 | 1.91 |
| MgO | 1.68 | 0.57 | Cu | 29.05 | 29.16 | U | 3.45 | 1.43 | Eu | 1.07 | 0.52 |
| MnO | 0.07 | 0.02 | Ga | 33.63 | 23.25 | V | 61.02 | 20.28 | Gd | 3.90 | 1.34 |
| $Na_2O$ | 3.98 | 0.42 | Hf | 4.84 | 1.20 | W | 0.72 | 0.53 | Tb | 0.61 | 0.20 |
| $P_2O_5$ | 0.25 | 0.09 | Mo | < 2 | n.a. | Y | 19.58 | 4.83 | Dy | 2.96 | 0.94 |
| $TiO_2$ | 0.62 | 0.18 | Nb | 9.37 | 2.35 | Zn | 77.68 | 35.41 | Ho | 0.59 | 0.19 |
| TOTAL | 99.02 | 1.06 | Ni | 19.62 | 7.45 | Zr | 221.50 | 51.87 | Er | 1.48 | 0.64 |
| LOI | 0.68 | 0.18 | Rb | 94.74 | 20.03 | | | | Tm | 0.29 | 0.11 |
| F | 0.16 | 0.06 | S | 114.26 | 129.63 | | | | Yb | 1.63 | 0.56 |
| | | | | | | | | | Lu | 0.25 | 0.08 |

**Table 3-4. Whole-rock geochemistry of red-stained Ävrö granite – rock code 501044 from Laxemar subarea. Mean and standard deviation values have been calculated based on data from KLX04 /Drake and Tullborg 2006b/. N=6.**

| Element | Mean | Std | Element | Mean | Std | Element | Mean | Std | Element | Mean | Std |
|---|---|---|---|---|---|---|---|---|---|---|---|
| $SiO_2$(wt%) | 65.00 | 4.78 | Ba (ppm) | 1,201.67 | 190.10 | Sc(ppm) | 6.64 | 2.54 | La(ppm) | 46.15 | 10.98 |
| $Al_2O_3$ | 15.70 | 1.28 | Be | 2.81 | 0.35 | Sn | 2.47 | 0.55 | Ce | 105.35 | 30.28 |
| CaO | 2.49 | 0.80 | Co | 9.00 | 2.60 | Sr | 769.50 | 222.31 | Pr | 12.05 | 3.95 |
| $Fe_2O_3$ | 3.99 | 1.21 | Cr | 60.22 | 8.14 | Ta | 1.11 | 0.29 | Nd | 42.28 | 15.56 |
| $K_2O$ | 3.99 | 0.47 | Cs | 2.06 | 0.47 | Th | 16.23 | 2.68 | Sm | 6.35 | 2.42 |
| MgO | 1.74 | 0.67 | Cu | 18.39 | 9.27 | U | 5.71 | 1.78 | Eu | 1.19 | 0.47 |
| MnO | 0.08 | 0.02 | Ga | 27.33 | 3.25 | V | 60.22 | 25.40 | Gd | 3.75 | 1.02 |
| $Na_2O$ | 4.27 | 0.64 | Hf | 6.63 | 0.64 | W | 2.91 | 0.98 | Tb | 0.87 | 0.27 |
| $P_2O_5$ | 0.25 | 0.11 | Mo | < 2 | n.a. | Y | 20.10 | 5.29 | Dy | 3.70 | 0.94 |
| $TiO_2$ | 0.60 | 0.23 | Nb | 11.46 | 3.16 | Zn | 73.80 | 24.28 | Ho | 0.73 | 0.16 |
| TOTAL | 98.12 | 0.56 | Ni | 19.00 | 4.22 | Zr | 229.17 | 36.27 | Er | 2.11 | 0.54 |
| LOI | 1.48 | 0.38 | Rb | 120.67 | 18.00 | | | | Tm | 0.36 | 0.07 |
| F | 0.15 | 0.06 | S | 72.48 | 68.09 | | | | Yb | 2.13 | 0.47 |
| | | | | | | | | | Lu | 0.33 | 0.08 |

### *3.1.2.2 Quartz monzodiorite (rock code 501036)*

The quartz monzodiorite (rock code 501036) has a more homogeneous chemical composition than the Ävrö granite. The geochemistry fresh and red-stained quartz monzodiorite is summarized in Table 3-5 and 3-6, respectively. The quartz monzodiorite has a lower content of e.g. $SiO_2$, $K_2O$ and Ba and a higher content of e.g. $Fe_2O_3$, MgO, MnO, $TiO_2$, Sc and V than the Ävrö granite due to lower contents of quartz and K-feldspar and higher contents of biotite, hornblende and magnetite in the quartz monzodiorite. In the Chondrite normalized REE diagram (Figure 3-4), it can be seen that the REE trends are very similar to the Ävrö granite, although the mean content of the light REEs is a bit lower and the mean content of the heavy REEs is a bit higher in the quartz monzodiorite. The S content is higher and the U and Th contents are slightly higher in the quartz monzodiorite than in the Ävrö granite, although the S contents vary widely between the samples and the S content has only been measured in a few samples. Stoichiometric recalculation of the S content to pyrite gives a maximum mean pyrite content of ~ 0.136 wt%. The Cr content is higher in quartz monzodiorite than in Ävrö granite due to higher magnetite content in the quartz monzodiorite.

In the red-stained quartz monzodiorite the $K_2O$, $Na_2O$ and Rb values are higher and CaO, $Al_2O_3$ and Sr values are lower than in the fresh rock due to replacement of plagioclase by K-feldspar and albite. The Cs content is lower in the red-stained rock due to replacement of biotite by chlorite. The higher LOI values of the red-stained rock compared to the fresh rock is due to the formation of secondary water-bearing minerals like chlorite, sericite, epidote and prehnite. The $Fe_2O_3$ content in the red-stained rock is however about the same in the red-stained rock as in the fresh rock nearby. The S content is generally lower in the red-stained rock compared to the fresh rock due to oxidation of primary pyrite. However, the S content is enriched in some red-stained samples due to formation of pyrite in the rock after the red-staining event /Drake and Tullborg 2006ab/. The content of the REEs remains constant in the red-stained rock compared to the fresh rock.

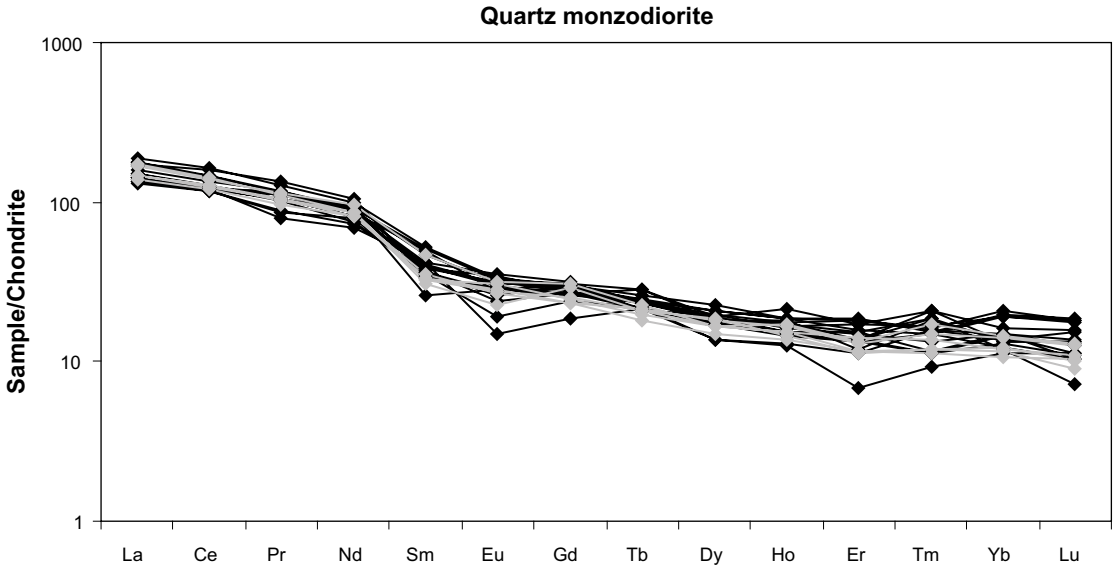


***Figure 3-4.*** *Chondrite normalized REE-pattern for quartz monzodiorite (black) and red-stained quartz monzodiorite (red). Data from KSH01A+B, KSH03A+B, KLX03, KLX04 and field samples from the Simpevarp and Laxemar subareas /Drake and Tullborg 2006a, Wahlgren et al. 2004, 2005, 2006/. Chondrite values from /Evansen et al. 1978/. (N=23, samples with values below detection limit for some elements are excluded).*

**Table 3-5. Whole-rock geochemistry of quartz monzodiorite – rock code 501036. Mean and standard deviation values have been calculated based on data from KSH01A+B, KSH03A+B, KLX03, KLX04 and field samples from the Simpevarp and Laxemar subareas /Drake and Tullborg 2006a, Wahlgren et al. 2004, 2005, 2006/ N=*22,* except N=5 for Cs, F and S.**

| Element | Mean | Std | Element | Mean | Std | Element | Mean | Std | Element | Mean | Std |
|---|---|---|---|---|---|---|---|---|---|---|---|
| $SiO_2$(wt%) | 56.64 | 2.93 | Ba (ppm) | 1,041.64 | 169.16 | Sc(ppm) | 18.49 | 3.50 | La(ppm) | 37.18 | 4.50 |
| $Al_2O_3$ | 16.38 | 0.63 | Be | 2.24 | 0.24 | Sn | 1.95 | 0.66 | Ce | 82.83 | 10.34 |
| CaO | 5.64 | 0.94 | Co | 16.00 | 4.29 | Sr | 733.95 | 151.93 | Pr | 8.65 | 3.83 |
| $Fe_2O_3$ | 8.15 | 1.19 | Cr | 85.96 | 51.81 | Ta | 0.83 | 0.23 | Nd | 39.60 | 4.84 |
| $K_2O$ | 3.10 | 0.61 | Cs | 1.96 | 0.64 | Th | 5.90 | 2.26 | Sm | 5.83 | 1.17 |
| MgO | 3.44 | 0.83 | Cu | 38.58 | 23.44 | U | 2.22 | 0.92 | Eu | 1.45 | 0.48 |
| MnO | 0.14 | 0.02 | Ga | 37.97 | 36.90 | V | 136.12 | 33.63 | Gd | 4.96 | 1.64 |
| $Na_2O$ | 3.38 | 0.20 | Hf | 5.00 | 1.73 | W | 0.66 | 0.60 | Tb | 0.73 | 0.32 |
| $P_2O_5$ | 0.38 | 0.07 | Mo | < 2 | n.a. | Y | 31.05 | 2.59 | Dy | 4.36 | 0.87 |
| $TiO_2$ | 1.06 | 0.13 | Nb | 10.36 | 1.60 | Zn | 94.78 | 20.50 | Ho | 0.86 | 0.21 |
| TOTAL | 98.31 | 1.31 | Ni | 24.33 | 10.23 | Zr | 232.88 | 73.66 | Er | 1.91 | 1.07 |
| LOI | 1.11 | 0.57 | Rb | 84.08 | 24.86 | | | | Tm | 0.33 | 0.15 |
| F | 0.12 | 0.01 | S | 726.23 | 366.64 | | | | Yb | 2.24 | 0.67 |
| | | | | | | | | | Lu | 0.31 | 0.11 |

**Table 3-6. Whole-rock geochemistry of red-stained quartz monzodiorite – rock code 501036. Mean and standard deviation values have been calculated based on data from KSH03A+B /Drake and Tullborg 2006a/ (*N=8*).**

| Element | Mean | Std | Element | Mean | Std | Element | Mean | Std | Element | Mean | Std |
|---|---|---|---|---|---|---|---|---|---|---|---|
| $SiO_2$(wt%) | 54.33 | 3.77 | Ba (ppm) | 1,085.50 | 199.89 | Sc(ppm) | 20.82 | 2.82 | La(ppm) | 37.53 | 3.48 |
| $Al_2O_3$ | 15.95 | 0.55 | Be | 1.76 | 0.20 | Sn | 0.44 | 0.83 | Ce | 82.87 | 6.19 |
| CaO | 5.39 | 1.71 | Co | 14.78 | 2.97 | Sr | 447.17 | 100.89 | Pr | 10.15 | 0.71 |
| $Fe_2O_3$ | 8.76 | 1.37 | Cr | 113.38 | 14.12 | Ta | 0.65 | 0.16 | Nd | 40.88 | 2.75 |
| $K_2O$ | 3.52 | 0.46 | Cs | 1.33 | 0.79 | Th | 3.22 | 1.19 | Sm | 5.42 | 0.91 |
| MgO | 3.91 | 0.73 | Cu | 26.05 | 7.60 | U | 1.86 | 0.49 | Eu | 1.62 | 0.19 |
| MnO | 0.15 | 0.02 | Ga | 12.78 | 1.00 | V | 142.22 | 28.58 | Gd | 5.31 | 0.64 |
| $Na_2O$ | 3.85 | 0.24 | Hf | 4.48 | 0.86 | W | 0.74 | 0.27 | Tb | 0.77 | 0.06 |
| $P_2O_5$ | 0.43 | 0.10 | Mo | < 2 | n.a. | Y | 31.25 | 2.13 | Dy | 4.31 | 0.32 |
| $TiO_2$ | 1.15 | 0.15 | Nb | 8.74 | 1.80 | Zn | 79.00 | 17.24 | Ho | 0.88 | 0.07 |
| TOTAL | 97.42 | 0.66 | Ni | 15.53 | 5.62 | Zr | 202.67 | 52.56 | Er | 2.08 | 0.19 |
| LOI | 2.22 | 0.56 | Rb | 93.42 | 26.01 | | | | Tm | 0.35 | 0.06 |
| F | 0.13 | 0.04 | S | 498.27 | 464.62 | | | | Yb | 2.08 | 0.25 |
| | | | | | | | | | Lu | 0.28 | 0.04 |

### *3.1.2.3 Fine-grained dioritoid (rock code 501030)*

The fine-grained dioritoid (rock code 501030) is also more homogeneous in composition than the Ävrö granite. The geochemistry of fresh and red-stained fine-grained dioritoid is summarized in Tables 3-7 and 3-8, respectively. Most of the major elements in the fine-grained dioritoid show similar contents as in the quartz monzodiorite. Exceptions are e.g. the slightly higher $SiO_2$ contents and the slightly lower $Fe_2O_3$ and MgO contents in the fine-grained dioritoid, which is partly due to the higher plagioclase and K-feldspar content and lower amphibole and magnetite content in the dioritoid. The content of S (only measured in two samples) is lower in the fine-grained dioritoid than in Ävrö granite and quartz monzodiorite. Stoichiometric recalculation of the S content to pyrite gives a maximum mean pyrite content of ~ 0.018 wt% for fine-grained dioritoid. The U and Th contents are higher than in the quartz monzodiorite and about the same as in Ävrö granite. In the Chondrite normalized REE diagram (Figure 3-5), it can be seen that the REE trends are largely similar to the quartz monzodiorite samples.

In the red-stained fine-grained dioritoid adjacent to fractures the CaO, $Al_2O_3$ and Sr values are lower than in the fresh rock due to replacement of plagioclase by K-feldspar and albite. The Cs content is lower in the red-stained rock due to replacement of biotite by chlorite. The higher LOI values of the red-stained rock compared to the fresh rock is due to the formation of secondary water-bearing minerals like chlorite, sericite, epidote and prehnite. The $Fe_2O_3$ content in the red-stained rock is however about the same in the red-stained rock as in the fresh rock. The S content is generally lower in the red-stained rock compared to the fresh rock due to oxidation of primary pyrite. The content of the REEs remains constant in the red-stained rock compared to the fresh rock.

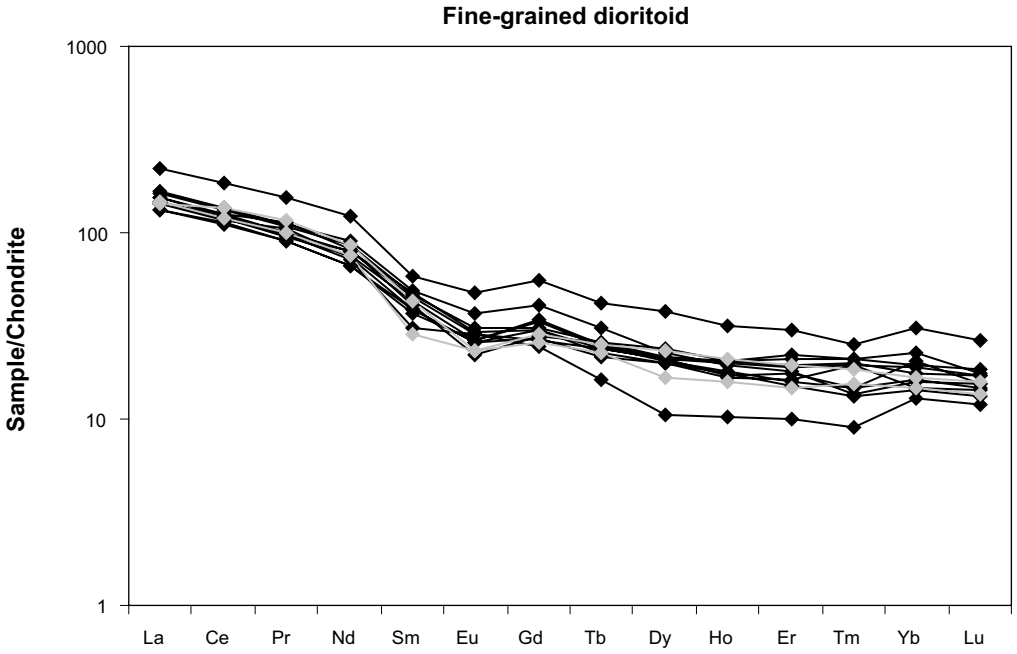


***Figure 3-5.*** *Chondrite normalized REE-pattern for fine-grained dioritoid (black) and red-stained fine-grained dioritoid (red). Data from KSH01A, KSH02 and field samples from Simpevarp subarea /Wahlgren et al. 2004, Drake and Tullborg 2006a/. Chondrite values from /Evansen et al. 1978/. (N=13, samples with values below detection limit for some elements are excluded).*

**Table 3-7. Whole-rock geochemistry of fine-grained dioritoid – rock code 501030. Mean and standard deviation values have been calculated based on data from KSH01A, KSH02 and field samples from Simpevarp subarea /Wahlgren et al. 2004, Drake and Tullborg 2006a/. N=17, except N=2 for Cs, F and S.**

| Element | Mean | Std | Element | Mean | Std | Element | Mean | Std | Element | Mean | Std |
|---|---|---|---|---|---|---|---|---|---|---|---|
| $SiO_2$(wt%) | 59.02 | 2.18 | Ba (ppm) | 955.65 | 308.78 | Sc(ppm) | 16.66 | 3.71 | La(ppm) | 36.94 | 5.55 |
| $Al_2O_3$ | 16.16 | 0.42 | Be | 2.33 | 0.28 | Sn | 2.86 | 2.22 | Ce | 80.28 | 11.70 |
| CaO | 5.16 | 0.95 | Co | 12.90 | 6.00 | Sr | 591.00 | 134.99 | Pr | 6.93 | 4.71 |
| $Fe_2O_3$ | 7.28 | 1.10 | Cr | 46.30 | 48.03 | Ta | 1.21 | 0.31 | Nd | 36.82 | 6.81 |
| $K_2O$ | 3.43 | 0.54 | Cs | 2.03 | 0.08 | Th | 7.59 | 3.05 | Sm | 6.14 | 1.46 |
| MgO | 2.88 | 0.67 | Cu | 23.03 | 14.62 | U | 3.24 | 1.22 | Eu | 1.32 | 0.67 |
| MnO | 0.12 | 0.01 | Ga | 44.35 | 18.65 | V | 120.27 | 28.81 | Gd | 5.59 | 2.50 |
| $Na_2O$ | 3.25 | 0.24 | Hf | 5.90 | 1.16 | W | 0.98 | 0.85 | Tb | 0.71 | 0.41 |
| $P_2O_5$ | 0.32 | 0.06 | Mo | < 2 | n.a. | Y | 34.82 | 6.29 | Dy | 5.16 | 1.50 |
| $TiO_2$ | 1.01 | 0.14 | Nb | 11.63 | 2.46 | Zn | 88.16 | 17.23 | Ho | 0.99 | 0.29 |
| TOTAL | 98.64 | 1.33 | Ni | 14.86 | 8.69 | Zr | 259.47 | 45.69 | Er | 2.03 | 1.61 |
| LOI | 1.00 | 0.79 | Rb | 104.45 | 18.77 | | | | Tm | 0.33 | 0.20 |
| F | 0.13 | 0.01 | S | 98.20 | 13.86 | | | | Yb | 2.69 | 0.93 |
| | | | | | | | | | Lu | 0.38 | 0.12 |

**Table 3-8. Whole-rock geochemistry of red-stained fine-grained dioritoid – rock code 501030. Mean and standard deviation values have been calculated based on data from KSH01A /Drake and Tullborg 2006a/ (*N*=2).**

| Element | Mean | Std | Element | Mean | Std | Element | Mean | Std | Element | Mean | Std |
|---|---|---|---|---|---|---|---|---|---|---|---|
| $SiO_2$(wt%) | 59.85 | 1.20 | Ba (ppm) | 572.50 | 61.52 | Sc(ppm) | 17.95 | 0.64 | La(ppm) | 35.85 | 0.64 |
| $Al_2O_3$ | 15.25 | 0.21 | Be | 2.00 | 0.29 | Sn | 2.01 | 2.01 | Ce | 81.30 | 6.22 |
| CaO | 4.35 | 1.29 | Co | 12.45 | 1.63 | Sr | 235.50 | 2.12 | Pr | 10.48 | 1.17 |
| $Fe_2O_3$ | 7.32 | 0.10 | Cr | 125.50 | 10.61 | Ta | 0.85 | 0.16 | Nd | 37.85 | 3.32 |
| $K_2O$ | 3.40 | 0.21 | Cs | 0.97 | 0.03 | Th | 6.75 | 1.26 | Sm | 5.53 | 1.52 |
| MgO | 2.69 | 0.13 | Cu | 22.30 | 8.63 | U | 3.04 | 0.54 | Eu | 1.35 | 0.01 |
| MnO | 0.11 | 0 | Ga | 11.10 | 0.57 | V | 111.00 | 11.31 | Gd | 5.55 | 0.37 |
| $Na_2O$ | 3.56 | 0.13 | Hf | 6.33 | 1.09 | W | 0.77 | 0.17 | Tb | 0.90 | 0.07 |
| $P_2O_5$ | 0.28 | 0.01 | Mo | < 2 | n.a. | Y | 36.45 | 6.15 | Dy | 5.09 | 1.24 |
| $TiO_2$ | 0.98 | 0 | Nb | 9.19 | 1.29 | Zn | 69.70 | 14.28 | Ho | 1.04 | 0.20 |
| TOTAL | 97.80 | 0.14 | Ni | 2.83 | 0.01 | Zr | 269.50 | 37.48 | Er | 2.82 | 0.54 |
| LOI | 2.15 | 0.21 | Rb | 82.65 | 1.63 | | | | Tm | 0.44 | 0.06 |
| F | 0.13 | 0 | S | 82.50 | 7.21 | | | | Yb | 2.59 | 0.26 |
| | | | | | | | | | Lu | 0.38 | 0.04 |

### 3.1.3 Porosity

Porosity measurements have been carried out on the rock types at Simpevarp and Laxemar within several different programs (e.g. geology, thermal properties and transport). All determinations consider connected porosity and are measured with water saturation technique. However, the methods used in different studies differ in terms of e.g. sample selection, sample size, water saturation time and drying time (detailed description about the methods can be found in method descriptions SKB MD 160.002e, SKB MD 540.001, SKB MD 540.003 and SS EN 1936). The terminology used varies as well and the porosity measured is presented as effective, open or connected, of which the latter is preferred in this compilation. The porosity results from the Geology, Transport and Thermal properties programs are briefly discussed below. A more thorough comparison of the different porosity measurements will be carried out during 2006 (pers. comm. E. Gustavsson).

*Geology program*

The porosity of surface samples and drill core samples from the Simpevarp and Laxemar subareas has been measured as a part of the Geology program and are presented in /SKB 2006/. The porosity of surface samples and borehole samples differ somewhat, partly due to influence on the borehole samples by the drilling and by the influence of weathering of the surface samples. The highest porosity values (mean values generally above 0.4%, Table 3-9) are found in Ävrö granite, quartz monzodiorite, fine-grained granite and medium- to coarse-grained granite. Fine-grained dioritoid and diorite to gabbro generally show lower porosity values (below 0.4%).

**Table 3-9. Connected porosity measured by water saturation technique from the *Geology program*. Data from surface samples ([1]) and drill core samples ([2]) from Simpevarp and Laxemar subareas /Mattsson et al. 2004, SKB 2006/. Range of the values is not presented in the reports.**

| Rock type | | Mean | Std | No |
|---|---|---|---|---|
| 501044 | Ävrö granite – Laxemar[1,2]/Simpevarp[1] | 0.44 | 0.19 | 79 |
| 501036 | Quartz monzodiorite – Simpevarp[2] | 0.44 | 0.14 | 13 |
| 501036 | Quartz monzodiorite – Laxemar[1] | 0.54 | 0.11 | 12 |
| 501030 | Fine-grained dioritoid[1,2] | 0.33 | 0.08 | 9 |
| 51033 | Diorite to gabbro – Laxemar[1,2] | 0.19 | 0.14 | 11 |
| 501058 | Fine-grained granite[1] | 0.55 | 0.10 | 7 |
| 501058 | Medium- to coarse-grained granite[1] | 0.58 | 0.07 | 7 |

*Transport program*

Samples from boreholes KLX02 and KLX04 from /Börjesson and Gustavsson 2005/ are presented in Table 3-10. The presented data are only from relatively unaltered samples with a length of 3 cm. A smaller number of samples of other sizes have also been measured within the Transport program but these results are not included in this compilation. The porosity values from the Transport program are lower than from the Geology program, partly due to the different techniques used and partly due to the lack of surface samples in the Transport program data. The values from the Transport program show that Ävrö granite and fine-grained granite and granite (rock code 501058) have higher values than quartz monzodiorite, fine-grained dioritoid and fine-grained diorite to gabbro.

*Thermal properties program*

In the thermal properties program porosity measurements have been carried out on drill core samples from KSH01A, KSH02, KAV04A, KLX02, KLX03, KLX04, KLX05 and KLX06 /Savukoski 2004ab, Savukoski and Carlsson 2004, Liedberg 2005, Savukoski 2005ab/. These analyses have been carried out on drill core samples with a length of about 2.5 cm using water saturation technique. Altered, heavily fractured and red-stained samples (especially samples from KLX04) are left out in the compilation in this report (Table 3-11). The results from the Thermal properties program are slightly higher than the results from the transport program. The relative difference in porosity between the major rock types do however correspond very well to the results from the Transport program with higher porosity in the Ävrö granite compared to quartz monzodiorite and fine-grained dioritoid. The two porosity values for diorite to gabbro are however exceptionally high.

**Table 3-10. Connected porosity measured by water saturation technique from the Transport program. Data from relatively unaltered drill core samples (KLX02 and KLX04) of 3 cm length from Laxemar subarea /Börjesson and Gustavsson 2005/.**

| Rock type | | Range | Mean | Std | No |
|---|---|---|---|---|---|
| 501044 | Ävrö granite | 0.13–0.46 | 0.28 | 0.09 | 33 |
| 501036 | Quartz monzodiorite | 0.09–0.21 | 0.13 | 0.05 | 6 |
| 501030 | Fine-grained dioritoid | 0.06–0.39 | 0.14 | 0.14 | 5 |
| 505102 | Fine-grained mafi rock | 0.15–0.21 | 0.17 | 0.03 | 3 |
| 501058 | Fine-grained granite | 0.22 | 0.22 | 0 | 3 |
| 501058 | Granite | 0.38 | n.a. | n.a. | 1 |

**Table 3-11. Connected porosity measured by water saturation technique from the Thermal properties program. Data is from relatively unaltered drill core samples (KSH01A, KSH02, KAV04A, KLX02, KLX03, KLX05 and KLX06) of 2.5 cm length from Simpevarp and Laxemar subareas /Savukoski, 2004ab, Savukoski and Carlsson 2004, Liedberg 2005, Savukoski 2005ab/.**

| Rock type | | Range | Mean | Std | No |
|---|---|---|---|---|---|
| 501044 | Ävrö granite | 0.2–0.6 | 0.42 | 0.14 | 35 |
| 501036 | Quartz monzodiorite | 0.2–0.4 | 0.25 | 0.07 | 20 |
| 501030 | Fine-grained dioritoid | 0.1–0.4 | 0.22 | 0.08 | 20 |
| 501033 | Diorite to gabbro | 1.0–1.1 | * | * | 2 |
| 501058 | Fine-grained granite[1] | | 0.55 | 0.10 | 7 |
| 501058 | Medium- to coarse-grained granite[1] | | 0.58 | 0.07 | 7 |

In conclusion: Ävrö granite and granite (rock code 501058: fine- to medium-grained and medium- to coarse-grained) where present, generally have higher porosity than quartz monzodiorite and fine-grained dioritoid which commonly have higher values than diorite to gabbro and fine-grained mafic rock (rock codes 505102 and 501033, except in analyses of 501033 from the Thermal properties program). Since no surface samples are used in the Transport program and Thermal properties program analyses the results from these programs are recommended to be used rather then the data from the Geology program.

The porosity is generally higher in red-stained rock adjacent to fractures compared to unaltered rock and the increase is commonly about 20% but can be more than 100% /Drake and Tullborg 2006b/. The higher porosity in the red-stained rock is due to the higher amount of micro-fractures, grain boundary porosity and intragranular porosity as a result of hydrothermal alteration.

### 3.1.4 Density

Ävrö granite (2,716 ± 40 kg $m^{-3}$, Table 3-12) generally has slightly lower density than quartz monzodiorite (Laxemar: 2,767 ± 19 kg $m^{-3}$, Simpevarp: 2,837 ± 57 kg $m^{-3}$) and fine-grained dioritoid (2,786 ± 20 kg $m^{-3}$) /SKB 2006/. Fine-grained granite (2,625 ± 12 kg $m^{-3}$) and medium- to coarse-grained granite (2,647 ± 17 kg $m^{-3}$) have even lower density than Ävrö granite /Mattsson et al. 2004/. The rock type with the highest density in the Simpevarp and Laxemar subareas are diorite to gabbro (2,960 ± 43 kg $m^{-3}$) /SKB 2006/. In the red-stained rock adjacent to fractures the decrease in density is generally about 0.01–0.02 kg $m^{-3}$ (at most 0.07 kg $m^{-3}$) compared to unaltered rock /Drake and Tullborg 2006b/.

**Table 3-12. Density (kg/$m^3$) of rock types from Simpevarp and Laxemar subareas /SKB 2006/[1] and /Mattsson et al. 2004/[2].**

| Rock type | | Mean | Std | No |
|---|---|---|---|---|
| 501044 | Ävrö granite[1] | 2,716 | 40 | 81 |
| 501036 | Quartz monzodiorite – Simpevarp[1] | 2,837 | 57 | 13 |
| 501036 | Quartz monzodiorite – Laxemar[1] | 2,767 | 19 | 12 |
| 501030 | Fine-grained dioritoid[1] | 2,786 | 20 | 9 |
| 501033 | Diorite to gabbro[1] | 2,960 | 43 | 11 |
| 501058 | Fine- to medium-grained granite[2] | 2,625 | 12 | 7 |
| 501058 | Medium- to coarse-grained granite[2] | 2,647 | 17 | 8 |

### 3.1.5 Redox – Whole rock

Mössbauer analyses of relatively unaltered as well as red-stained rock have been carried out on Ävrö granite, quartz monzodiorite and fine-grained dioritoid from boreholes KSH01A, KSH03A+B and KLX04 (Table 3-13) /Drake and Tullborg 2006ab/. A generally small increase of $Fe^{3+}/Fe_{tot}$ in the red-stained rock compared to the unaltered rock is shown. The mean $Fe^{3+}/Fe_{tot}$ content is 2.9% higher in the red-stained rock (mean $Fe^{3+}/Fe_{tot}$ content = 43.0%) compared with the relatively unaltered rock (mean $Fe^{3+}/Fe_{tot}$ content = 40.7%). This increase is related to the partial or complete replacement of magnetite by hematite and subordinately the replacement of biotite by chlorite and the general increase of epidote in the red-stained rock compared to the unaltered rock. The $Fe^{3+}/Fe_{tot}$ content in the oxide phase is almost always higher in the red-stained rock than in the unaltered rock due to partial replacement of magnetite by hematite, which is in agreement with lower susceptibility of red-stained rock compared to unaltered rock /Mattson and Thunehed 2004/. However, since most of the Fe in the rock is contained in the silicate phase which have fairly unchanged $Fe^{3+}/Fe_{tot}$ contents, the total change in $Fe^{3+}/Fe_{tot}$ contents between the red-stained rock and the unaltered rock is not as high as susceptibility measurements suggest.

The most important $Fe^{2+}$ bearing minerals (low $Fe^{3+}/Fe_{tot}$–ratio) in the rocks in the Simpevarp area are chlorite, biotite, magnetite and subordinately hornblende and augite. Most important $Fe^{3+}$ bearing minerals are magnetite ($Fe^{3+}/Fe_{tot}$ = 0.667), hematite ($Fe^{3+}/Fe_{tot}$ = 1) and epidote ($Fe^{3+}/Fe_{tot}$ ≈1). Pyrite is also an important $Fe^{2+}$ bearing mineral but it is only found in very small amounts in the rock (below 0.26 vol%, mean value is below 0.1 vol%).

The total $Fe^{2+}$ content is higher and the $Fe^{3+}/Fe_{tot}$-ratio is lower in quartz monzodiorite and fine-grained dioritoid compared to Ävrö granite. This mainly due to the higher amount of ferromagnesian silicates and the lower amount of epidote in the quartz monzodiorite and fine-grained dioritoid compared to the Ävrö granite. It should also be noted that the Ävrö granite samples with a more quartz monzodioritic composition have lower $Fe^{3+}/Fe_{tot}$ ratios and higher $Fe^{2+}$ contents than the Ävrö granite samples with a more granodioritic/granitic composition. The Ävrö granite also show a much larger variation in $Fe^{3+}/Fe_{tot}$ compared to quartz monzodiorite and fine-grained dioritoid (although the Ävrö granite samples are more numerous).

Fine-grained dioritoid samples (N=2) are from KSH01A. Quartz monzodiorite samples (N=10) are from KSH03A+B. Ävrö granite samples (N=19) are from KSH03A and KLX04. Pyrite is commonly present in very small amounts in the samples (generally below 0.26 vol. %, mean value is below 0.1 vol. %) and is not included in Table 3-13. However, both point-counting and whole rock chemical analyses show that pyrite and sulphur is generally depleted in the red-stained rock compared to the reference rock (exceptions occur).

## 3.2 Fracture mineralogy

### 3.2.1 Description of sampled boreholes and fracture zones

Fracture data is obtained during the Boremap mapping of the drill cores /Ehrenborg and Stejskal 2004abcd, 2005, Ehrenborg and Dahlin 2005abcd, 2006 and in manuscript/. The data is exported to the SKB database SICADA. The quantitative statistical analyses of fracture data in this report are based on this data extracted from SICADA and analysed using Microsoft Excel. The more qualitative fracture mineral data, chemical analyses and Mössbauer analyses have been obtained from the detailed fracture mineralogy studies /Tullborg 1995, Drake and Tullborg 2004, 2005, 2006c and in manuscript/. The fracture data used in this report are from boreholes KSH01A+B, KSH02, KSH03A+B, KAV04A+B from Simpevarp subarea, KLX02–06, KLX07A+B and KLX08 from Laxemar subarea (Figure 3-1 and Table 3-14). It should be noted that only one of the boreholes from the Laxemar subarea in this report include core from the upper 100 m, in contrast to the boreholes from the Simpevarp subarea which all include the upper 100 m. This makes the Laxemar fracture data from the upper 0–100 m included in this report less statistically representative. However, drilling of cored boreholes including the uppermost 100 m is currently in progress in the Laxemar subarea.

**Table 3-13. Schematic summary of the changes in $Fe^{3+}/Fe_{tot}$-ratios and related mineralogy in the different rock types. Values in brackets are average values. Data from KSH01A, KSH03A+B and KLX04 /Drake and Tullborg 2006ab/.**

| Sample† | Silicates Biotite (vol. %) | Chlorite (vol. %) | Epidote (vol. %) | $Fe^{3+}/Fe_{tot}$ silicate(%) | Oxides Oxides [a] (vol %) | Magnetite (vol %)[b] | Hematite (vol %) [b] | Mt+Hem (vol %) [b] | $Fe^{3+}/Fe_{tot}$ oxide (%) | Total $Fe^{3+}/Fe_{tot}$ total (%) | $Fe_{tot}$ (wt%)[c] | $Fe^{2+}{}_{tot}$ (wt.%) | $Fe^{3+}{}_{tot}$ (wt%) |
|---|---|---|---|---|---|---|---|---|---|---|---|---|---|
| **Dioritoid** | 6.7–15.4 (11.1) | 0.8–6.7 | 0.1–0.2 | 20–22.6 | 0.6–0.7 | 60–72.7 | 10–18.2 | 9.1–30 | 62–65 | 26–31 | 5.10–5.52 | 3.77–3.81 | 1.33–1.71 |
| **Unaltered[d]** | | (3.8) | (0.15) | (21.3) | (0.65) | (66.4) | (14.1) | (19.5) | (63.5) | (28.5) | (5.31) | (3.79) | (1.52) |
| **Dioritoid** | 1–1.4 | 13.4–14.4 | 0.3–0.8 | 12–23 | 0.3–1.2 | 16.7–25 | 0–25 | 50–83.3 | 69.4* | 28* | 5.07* | 3.65* | 1.42* |
| **red-stained** | (1.2) | (13.9) | (0.6) | (17.5) | (0.72) | (20.8) | (12.5) | (66.7) | | | | | |
| **QMD** | 0.3–11.8 | 0.9–17.2 | 0.1–1.4 | 15–25 | 0.3–3.2 | 2–100 | 0–9.8 | 0–88.2 | 62–100 | 32–42 | 4.65–7.00 | 2.93–4.69 | 1.73–2.85 |
| **Unaltered[d]** | (4.4) | (10.4) | (0.5) | (21.6) | (1.8) | (72.8) | (2.9) | (24.3) | (74.2) | (35.9) | (6.20) | (3.97) | (2.22) |
| **QMD** | 0.1–1.8 | 9.1–17.7 | 1–3.2 | 16.5–31 | 0.6–3.6 | 0–80 | 7.1–32.3 | 0–92.9 | 72–100 | 30.4–46.6 | 4.62–7.20 | 3.22–4.62 | 1.41–3.25 |
| **red-stained** | (0.6) | (12.5) | (1.6) | (23.5) | (1.9) | (22.8) | (15.8) | (61.5) | (85.2) | (38.8) | (6.12) | (3.72) | (2.40) |
| **Ävrö granite** | 0.6–12 | 0.6–11.5 | 0.2–10.3 | 19–44 | 0.6–1.8 | 0–100 | 0–31.8 | 0–90.9 | 65–89 | 36.0–53.5 | 2.06–3.90 | 1.12–2.23 | 0.8–1.71 |
| **Unaltered[d]** | (5.2) | (4.8) | (3.6) | (32.9) | (1.3) | (45.7) | (7.4) | (46.4) | (75.6) | (44.9) | (3.07) | (1.70) | (1.36) |
| **Ävrö granite red-stained** | 0–3.1 | 3.8–17.6 | 0.5–9.4 | 20–52 | 0.3–2.7 | 0–100 | 10–76.9 | 0–83.3 | 66–100 | 32.0–57.8 | 2.11–4.04 | 1.03–2.54 | 0.78–2.21 |
| | (0.4) | (8.4) | (3.4) | (33.0) | (1.3) | (26.3) | (28.5) | (43.8) | (84.2) | (47.8) | (3.06) | (1.60) | (1.46) |

Dioritoid = Fine-grained dioritoid (rock type 501030)

QMD = Quartz monzodiorite (rock type 501036)

Ävrö granite = rock type 501044

Mt+Hem = magnetite partially replaced by hematite

* = Based on one sample

[a] = Magnetite and hematite (ilmenite is excluded),

[b] = % of counted oxide vs. total counts of magnetite, hematite and magnetite+hematite,

[c] = $Fe_2O_3$ multiplied by 0.6995.

[d] = Includes partially altered but not red-stained samples.

**Table 3-14. Summary of the length of mapped core and orientation of the boreholes used in this report. The cored boreholes KAV04A, KSH01A, KSH03A, KLX07A, KLX03, KLX04, KLX05, KLX06 and KLX08 start at ~ 100 m below the bedrock surface while the boreholes KAV04B, KSH01B, KSH03B and KLX07B are drilled from the bedrock surface to obtain information of the upper 100 m of the bedrock. The cored borehole KSH02 starts at ~ 20 m below the bedrock surface (980 m of core). The cored borehole KLX02 starts at ~ 200 m depth and reaches 1,700 m depth. The Boremap-mapping of this hole only incorporates the section from 200 m down to 1,000 m.**

| Borehole | Mapped core (m) | Borehole orientation |
|---|---|---|
| Simpevarp subarea | | |
| KAV04A | 900 | 87/–86° |
| KAV04B | 90 | 134/–90° |
| KSH01A | 900 | 174/–85° |
| KSH01B | 93 | 178/–88° |
| KSH02 | 975 | 331/–86° |
| KSH03A+B | 895 | 125/–64° |
| KSH03B | 100 | 128/–59º |
| Laxemar subarea | | |
| KLX02 | 800 | 358/–85° |
| KLX03 | 900 | 199/–75° |
| KLX04 | 890 | 0/–85° |
| KLX05 | 890 | 189/–65° |
| KLX06 | 865 | 329/–65° |
| KLX07A | 735 | 174/–65º |
| KLX07B | 190 | 174/–85º |
| KLX08 | 890 | 199/–60º |

The confidence of the Boremap data is classified as certain, probable or possible during the drill core mapping. In the data used in this report, 73% of the fractures have been classified as certain, 23% as probable and 4% as possible. Data of all confidence levels has been used in this report and there is therefore a small error in the result due to the low confidence in the fractures mapped as possible. It should be noted that the certain, probable and possible classification has nothing to do with whether a fracture is open or sealed.

In this report the fracture data is divided into Simpevarp (KAV04A+B, KSH01A+B, KSH02, KSH03A+B) and Laxemar (KLX03–06, KLX07A+B, KLX08). KLX02 is presented separately since it is drilled with conventional drilling techniques, which cause more rotation and grinding of the core and more flushing of fracture minerals in open fractures than for the triple-tube drilling technique used for the other boreholes. The differences between KLX02 and the other drill cores are for instance indicated by the high amount of open fractures in KLX02 compared to the other drill cores in this report, and it can be suspected that many of these have been opened during drilling. However, in the chapter of crushed zones (Section 3.2.3.3), data from KLX02 is included in the Laxemar data since the crushed zones are not interpreted to be drilling induced.

### 3.2.2 Variation of fractures with depth

The total number of fractures per 100 m drilled borehole (open, partly open and sealed) is shown in Figure 3-6, 3-7, 3-8, 3-9 and Table 3-15. The irregularity in this fracture frequency trend is at least partly a result of that the boreholes are oriented towards different deformation zones which will be intersected at different depths. In both Simpevarp and Laxemar there is a diffuse trend of decreasing fracture frequencies from 300 m and to 1,000 m (900 m in Laxemar due to a fracture zone in KLX04 at 900–1,000 m).

In Simpevarp, deformation zones are very abundant in the interval 200–300 m (KSH01A, KSH02, KSH03A), abundant in the intervals 100–200 (KSH01A, KSH03A), 400–600 m (KSH01A, KSH02) and exist to a smaller degree in the interval 700–900 m (KSH01, KSH02). The intersection of deformation zones at these depths is highly visible in the fracture frequencies, especially at 200–300 m and 500–600 m (Figure 3-6). The upper 100 m of the boreholes do not cut any major deformation zones in Simpevarp.

Detailed fracture frequency data for each of the boreholes KSH01A+B, KSH02, KSH03A+B, and KLX02 is available in /SKB 2005/ (p 142–146).

In Laxemar deformation zones are abundant in the interval 100–400 m (especially in KLX04, 06, 07A, 08), 600–800 m (especially in KLX04, 06, 07A, 08) and 900–1,000 m (KLX04). The intersection of deformation zones at these depths is highly visible in the fracture frequencies, (Figure 3-7).

In the southern Laxemar subarea, the amount of fractures per hundred meters of drill core is commonly lower than in the whole Laxemar subarea, especially in the uppermost 500 m. The interval 0–100 m is left out of Figure 3-8 due to the low amount of core (4 m) from this interval.

In KLX02 the highest fracture frequencies are found in the interval 800–1,000 m due to intersection of deformation zones (Figure 3-9).

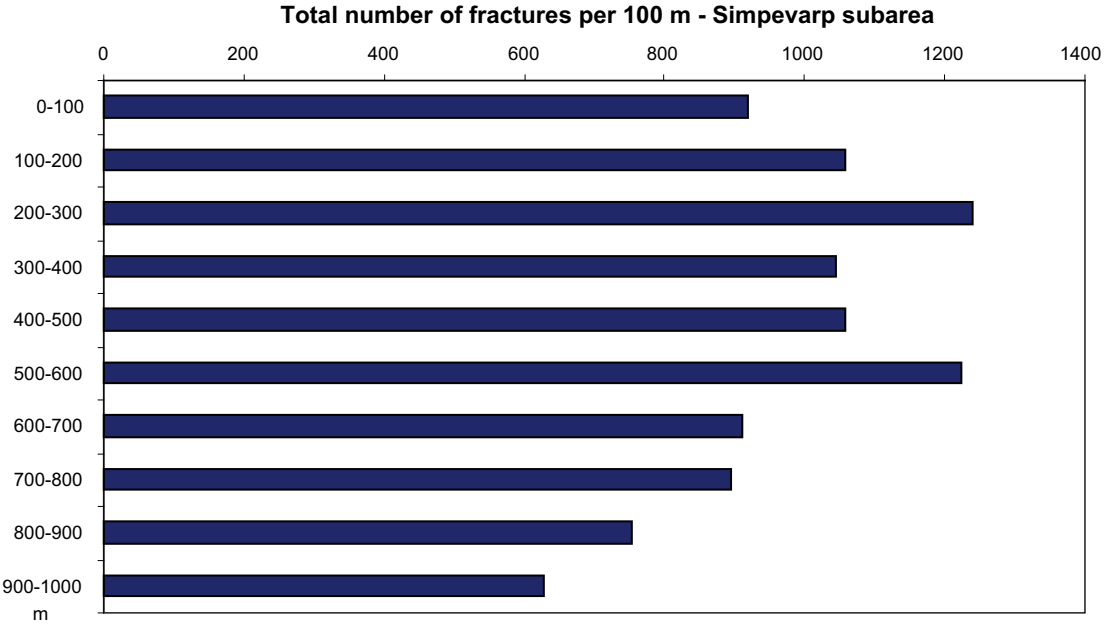


***Figure 3-6.*** *Total number of fractures per 100 m drilled borehole. Data from KSH01A+B, KSH02, KSH03A+B and KAV04A+B.*

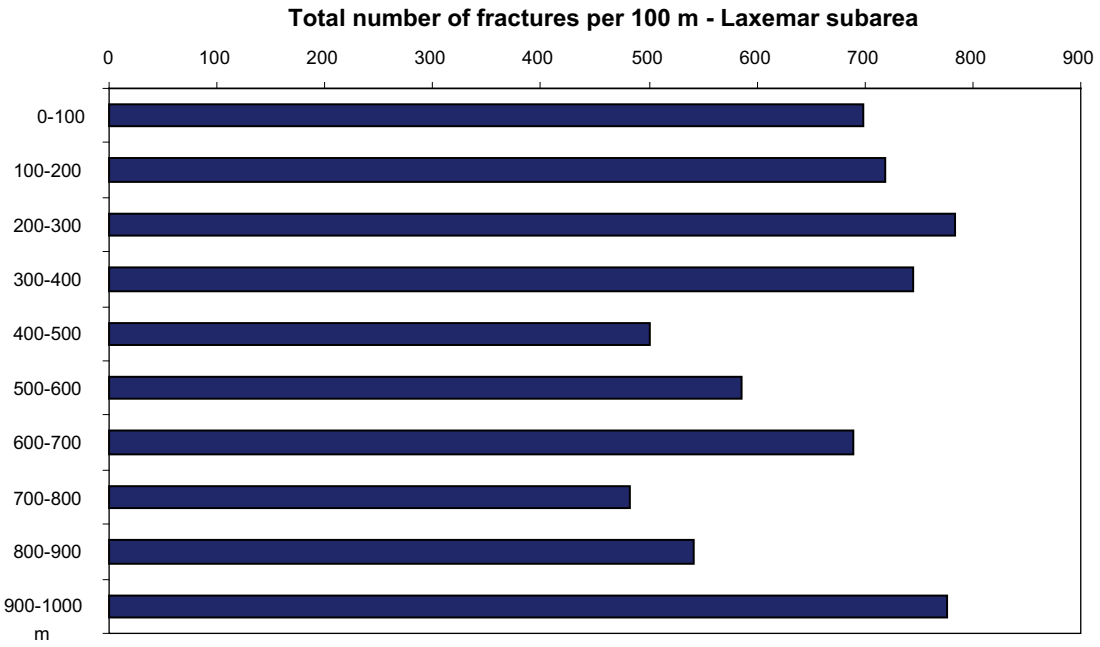


***Figure 3-7.*** *Total number of fractures per 100 m drilled borehole. Data from KLX03A–KLX08A and KLX07B.*

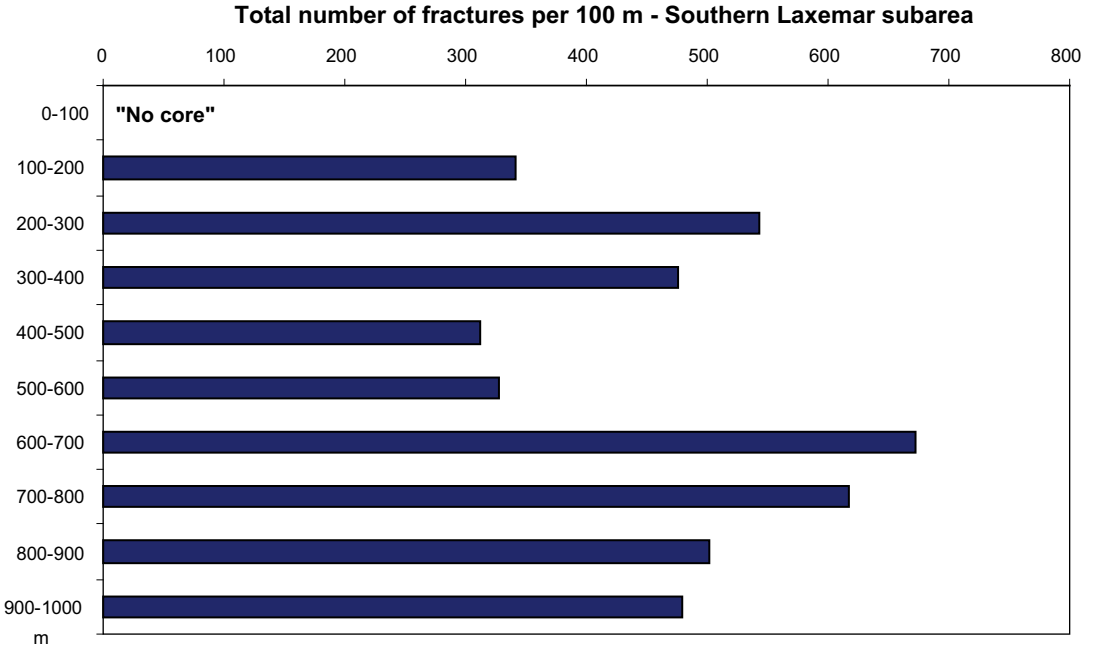


***Figure 3-8.*** *Total number of fractures per 100 m drilled borehole in the southern part of the Laxemar subarea. Data from KLX03 and KLX05.*

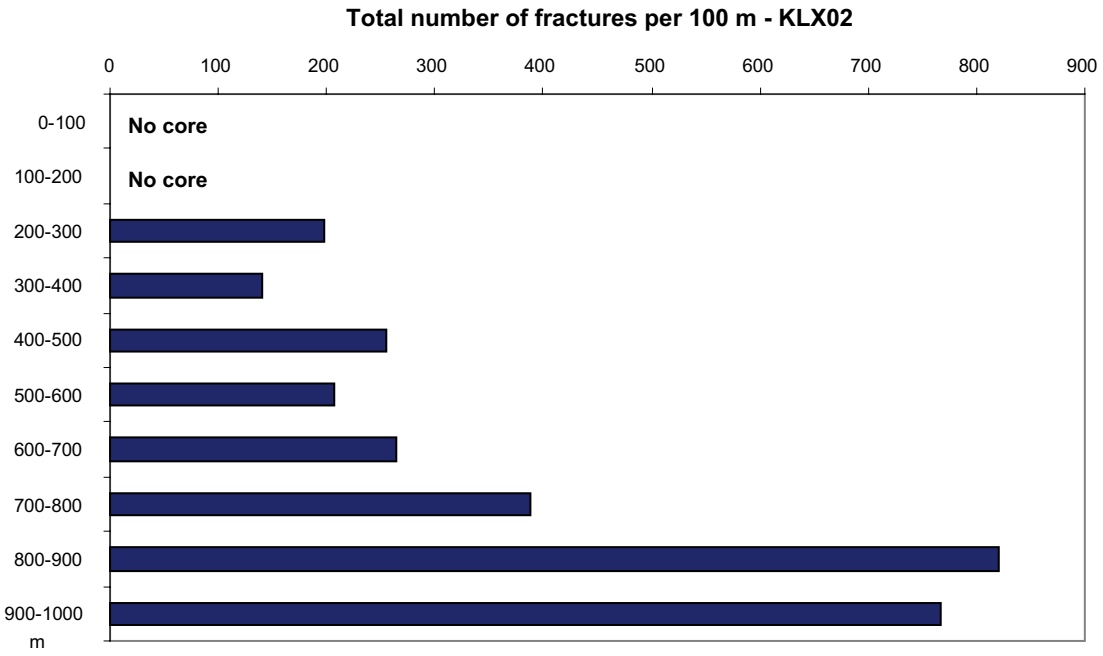


***Figure 3-9.*** *Total number of fractures per 100 m drilled borehole. Data from KLX02.*

**Table 3-14. Total number of fractures per 100 m drilled borehole. Data from KSH01A+B, KSH02, KSH03A+B and KAV04A+B (Simpevarp), KLX03–KLX06, KLX07A+B and KLX08 (Laxemar), KLX03 and KLX05 (Southern Laxemar) and KLX02.**

| m | Fractures/100 m | | | |
|---|---|---|---|---|
| | Simpevarp | Laxemar | Southern Laxemar | KLX02 |
| 0–100 | 918 | 698 | No core | No core |
| 100–200 | 1,057 | 719 | 342 | No core |
| 200–300 | 1,240 | 784 | 543 | 194 |
| 300–400 | 1,046 | 747 | 475 | 140 |
| 400–500 | 1,057 | 502 | 313 | 255 |
| 500–600 | 1,224 | 587 | 328 | 207 |
| 600–700 | 910 | 691 | 672 | 265 |
| 700–800 | 896 | 484 | 617 | 388 |
| 800–900 | 752 | 542 | 502 | 820 |
| 900–1,000 | 628 | 778 | 478 | 767 |
| Total | 37,454 | 31,845 | 7,912 | 3,036 |

The total number of fractures in the available data is 72,235 of which 68% are sealed, 31% are open and 0.03% are partly open.

In the Simpevarp subarea the open fractures are most abundant in the intervals 200–300 m, 500–700 m due to the presence of deformation zones at these depths. The amount of open fracture is low at 0–100 m (200 fractures/100 m) due to the lack of major deformation zones in this interval. The mean value of open fractures per 100 m in Simpevarp is 305 (Figure 3-10 and Table 3-15).

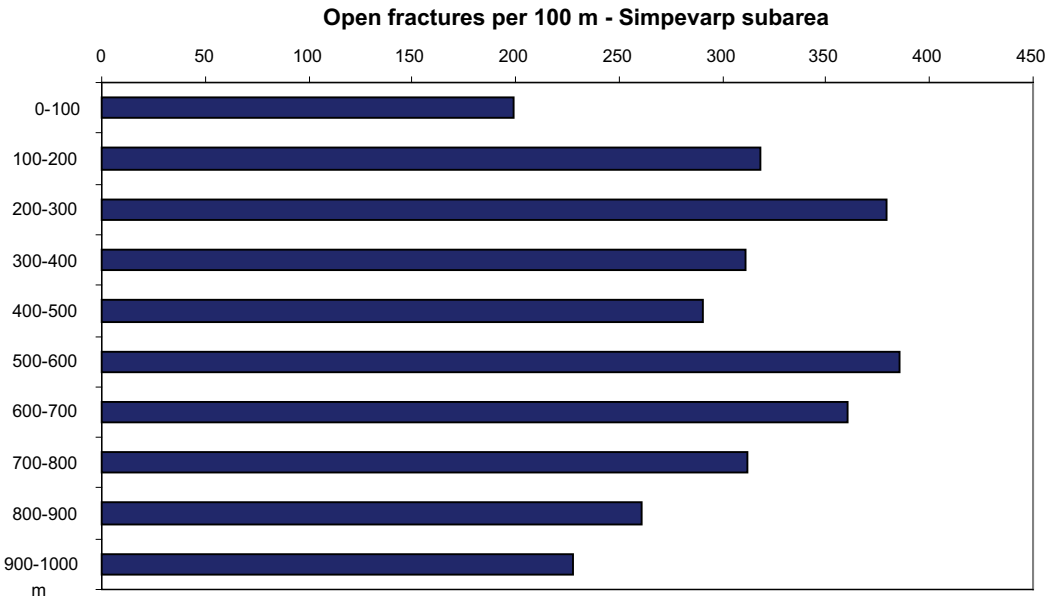


***Figure 3-10.*** *Number of open fractures per 100 m drilled borehole. Data from KSH01A+B, KSH02, KSH03A+B and KAV04A+B.*

In the Laxemar subarea the open fractures are most abundant in the interval 0–100 m (316 fractures/100 m) and 900–1,000 m (409 fractures/100 m). The fracture frequency in the interval 900–1,000 m is mainly based on drill core KLX04. Since this borehole penetrates a deformation zone in this interval the apparent fracture frequency will be unrepresentatively high for these depths. The high amount of open fractures at 900–1,000 m is due to intersection of deformation zones (especially in KLX04). The amount of open fractures/100 m generally decreases with increasing depth, down to 900 m, with the lowest values at intervals 400–500 m (95 fracture/100 m) and 800–900 m (92 fractures/100 m). The mean value of open fractures per 100 m in Laxemar is 206 (Figure 3-11 and Table 3-15). Most data is from the intervals 100–900 m.

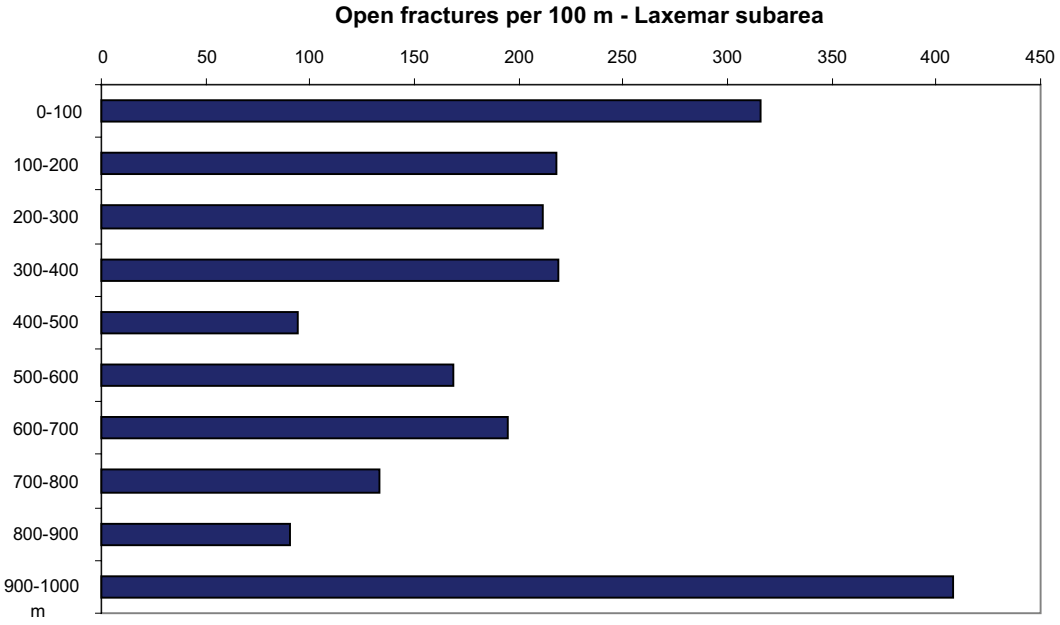


***Figure 3-11.*** *Number of open fractures per 100 m drilled borehole. Data from KLX03–KLX08 and KLX07B.*

In the southern Laxemar subarea, the amount of open fractures is commonly very low (mean value is 57 fractures/m). The highest amount is found in the interval 700–800 m (Figure 3-12). The interval 0–100 m is left out since the amount of core is very small (4 m).

In KLX02 the highest amount of open fractures (> 500 fractures/100 m) is found in the interval 800–1,000 m due to intersection of deformation zones (Figure 3-13). The mean value of open fractures per 100 m in KLX02 is 260 (Table 3-15).

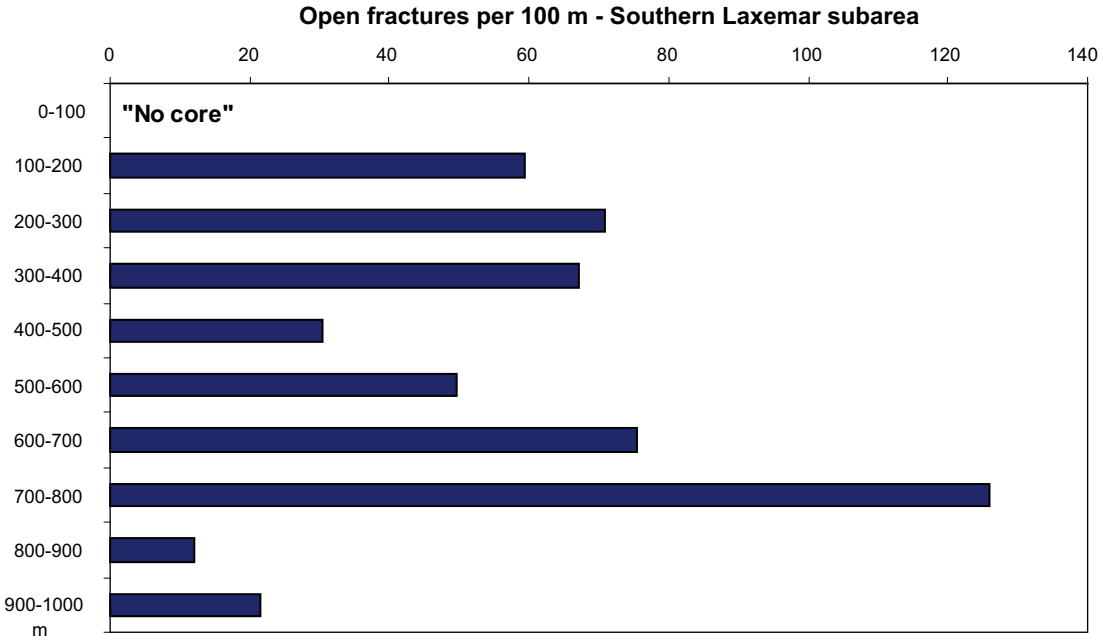


***Figure 3-12.*** *Number of open fractures per 100 m drilled borehole in the southern part of the Laxemar subarea. Data from KLX03 and KLX05.*

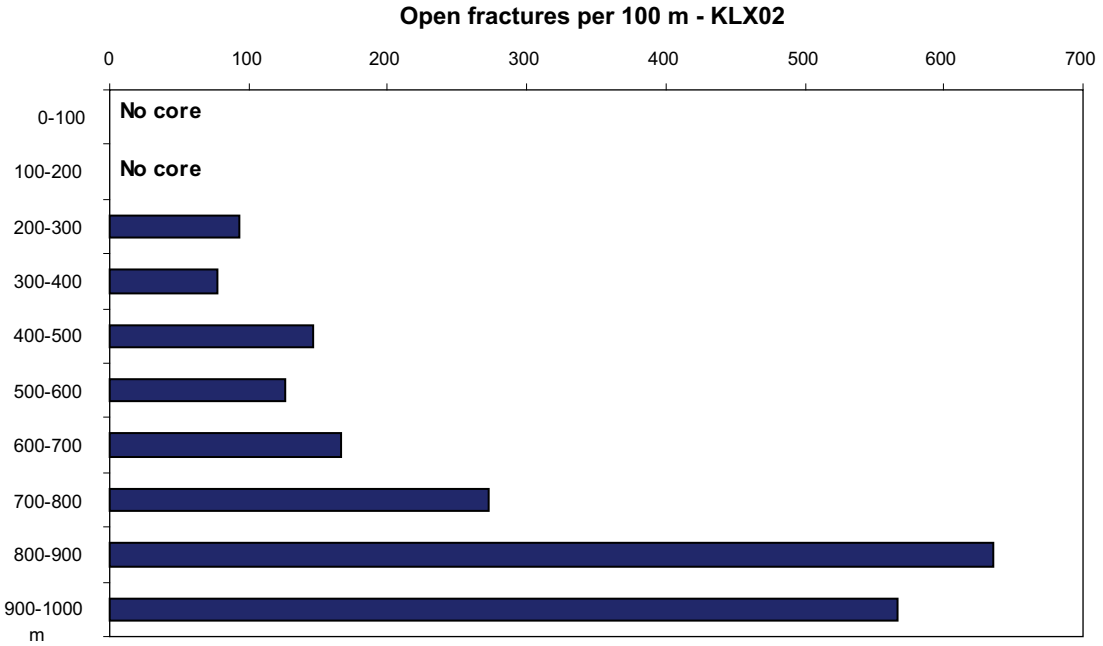


***Figure 3-13.*** *Number of open fractures per 100 m drilled borehole. Data from KLX02.*

**Table 3-15. Number of open fractures per 100 m drilled borehole. Data from KSH01A+B, KSH02, KSH03A+B and KAV04A+B (Simpevarp), KLX03–KLX06, KLX07A+B and KLX08 (Laxemar), KLX03 and KLX05 (Southern Laxemar) and KLX02.**

| m | Fractures/100 m | | | |
|---|---|---|---|---|
| | Simpevarp | Laxemar | Southern Laxemar | KLX02 |
| 0–100 | 199 | 316 | No core | No core |
| 100–200 | 318 | 218 | 60 | No core |
| 200–300 | 380 | 212 | 71 | 92 |
| 300–400 | 311 | 220 | 67 | 78 |
| 400–500 | 291 | 95 | 31 | 146 |
| 500–600 | 386 | 169 | 50 | 126 |
| 600–700 | 361 | 196 | 76 | 167 |
| 700–800 | 312 | 134 | 126 | 272 |
| 800–900 | 261 | 92 | 12 | 636 |
| 900–1,000 | 227 | 409 | 22 | 566 |

### 3.2.3 Abundance of fracture filling minerals

In this report "fracture filling" is used as a collective term for both coating and loose material in open fractures and for all material in sealed fractures. The collective term "fracture filling" for material in open fractures is used since the chemical analyses are usually carried out on both filling and coating material which are difficult to separate during sampling. When the term "coating" is used it refers only to the solid material coated to the fracture surface. Based on drill core samples, thin sections and Boremap data, the typical width of a chlorite coating has been estimated to ~ 0.25 mm. This would give a volume of $0.25\times10^{-3}$ m$^3$ chlorite per m$^2$ chlorite coated fracture surface. The specific gravity for chlorite varies between 2.6 and 3.3 g cm$^{-3}$ /Deer et al. 1992/ which gives a mass between 0.65 and 0.83 kg m$^{-2}$. A minimum estimate of the chlorite content in a chlorite bearing open fracture is a 0.1 mm thick coating covering 5% of the fracture surface. A minimum estimate of chlorite in a chlorite bearing fracture is thus between 0.013 and 0.017 kg m$^{-2}$. A characteristic chlorite coated fracture is showed in Figure 3-14.

The width of a typical calcite fracture varies more than for chlorite, from less than a millimetre up to 5 cm (very rarely). Calcite is generally more irregularly distributed on the fracture surfaces than chlorite (Figure 3-15). Base on drill core samples and Boremap data, a rough estimation of open calcite coated fractures is that the average thickness is ~ 0.5 mm and that the mineral covers ~ 20–30% of the fracture surface. This would give a volume of $0.1\times10^{-3}$ m$^3$

***Figure 3-14.*** *Chlorite coated fracture. Drill core diameter is ~ 50 mm (KSH03A: 452.36 m).*

***Figure 3-15.*** *Calcite coated fracture. Drill core diameter is ~ 50 mm (KLX07A: 346.73–346.82 m).*

to $0.15\times10^{-3}$ $m^3$ calcite per $m^2$ calcite coated fracture surface. Based on the specific gravity of calcite of 2.715 g $cm^{-3}$ /Deer et al. 1992/, this would give a calcite mass of 0.27 to 0.41 kg $m^{-2}$ in calcite coated fractures. A minimum estimate of the calcite content in a calcite bearing open fracture is a 0.1 mm thick coating covering 1% of the fracture surface. A minimum estimate of calcite in a calcite bearing fracture is thus 0.0027 kg $m^{-2}$.

The pyrite content in fractures is difficult to estimate quantitatively since the pyrite content varies widely on the fracture surfaces. There are two varieties of pyrite in the Simpevarp area. The first of these varieties is an early formed hydrothermal pyrite which commonly occurs as anhedral or subhedral crystals. These pyrite crystals are found along with e.g. quartz in sealed fractures. The second pyrite variety is made up of later formed crystals which are anhedral to euhedral when occurring in narrow, sealed fractures and euhedral, cubic when occurring on fracture surfaces. These crystals are commonly unevenly distributed on the fracture surfaces, are less than 0.2 mm in size and are often found along with calcite. A rough estimation of the maximum mean amount of pyrite is based on an surface coverage of 0.5% and a crystal side of 0.2 mm, given the specific gravity of pyrite (4.95–5.03 g $cm^{-3}$ /Deer et al. 1992/), a maximum pyrite content in an average pyrite bearing fracture is estimated to 0.005 kg $m^{-2}$ fracture surface. A minimum estimate of the pyrite content in a pyrite bearing open fracture is a 0.1 mm big crystals covering 0.1% of the surface. A minimum estimate of pyrite in a pyrite bearing fracture is thus between 0.0005 kg $m^{-2}$.

Some of the fracture minerals occur as small grains or in small amount which make them difficult to identify during the drill core mapping. Examples of fracture minerals that are underrepresented in the Boremap data due to difficulty to identify them macroscopically or with hand lens are clay minerals. Another difficulty in the mapping is that the most common fillings in the area often are fine-grained and made up of several minerals. The relative abundance of the minerals will give the filling specific attributes, which vary between different fractures thus making it difficult to characterize and identify the minerals. Prehnite is for example underrepresented in the Boremap data since it resembles to quartz and epidote or a mixture of these minerals. Other minerals that are underrepresented in the Boremap data are adularia and to a lesser degree barite, zeolites (laumontite and harmotome) and apophyllite. On the other hand, hematite, which is a common mineral especially in the Simpevarp subarea, is overrepresented in the Boremap data. This is a result of its ability to colour other minerals when present only as trace amounts. The hematite often occurs as sub-microscopic grains not larger than a few microns and yet colour the fracture filling red (Figure 3-16). Many of the sealed fractures mapped with hematite as the major fracture mineral are probably hematite stained adularia. Adularia is also difficult to identify since it may vary in colour from grey to red.

Histograms of the mineralogy of sealed and open fractures are shown in Figure 3-18 to 3-23. Note that most of the fractures contain more than one mineral and that the sum of all fractures in the histograms therefore is higher than the total number of individual fractures.

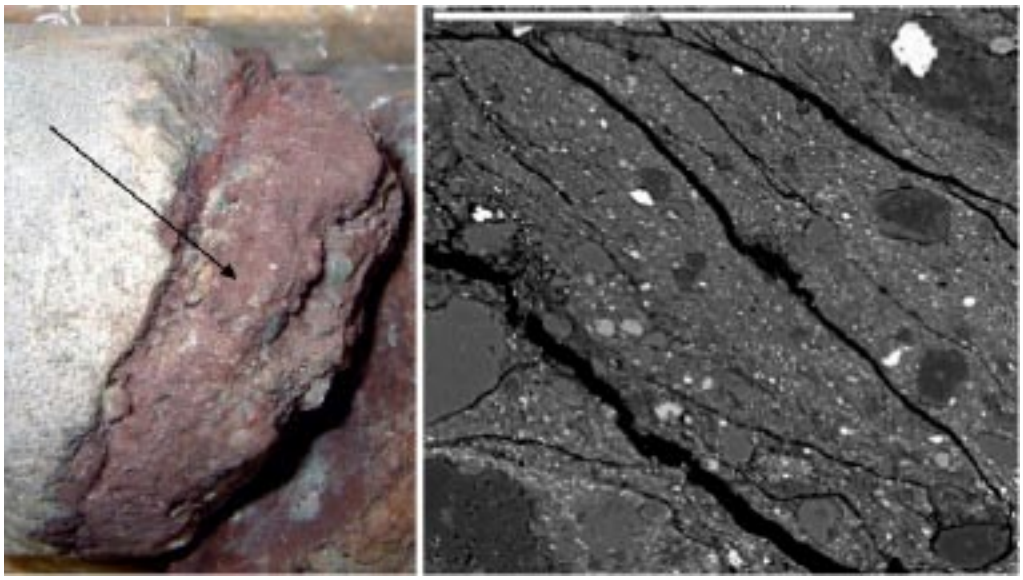

***Figure 3-16.*** *Photograph and back-scattered SEM-image of red-stained gauge/cataclasite (arrow) consisting of chlorite, adularia, clay minerals, hematite and quartz fragments from sample KSH03A 271.53–271.63 m. Drill core diameter is ~ 50 mm (left) and the scale bar in the SEM-image is 200 µm. Note the small amount of hematite grains in the back-scattered SEM-image to the right (bright spots) responsible for the red colour of the gauge/cataclasite.*

#### *3.2.3.1 Sealed fractures*

Sealed fractures are; 25,697 (69%) from Simpevarp, 22,801 (72%) from Laxemar and 851 (28%) from KLX02 of the fractures in the analysed Boremap data. The most abundant fracture minerals are calcite and chlorite which occur in 29–43 and 24–36% respectively of all sealed fractures (Figure 3-18, 3-19, 3-20 and Table 3-16). It should be noted that these values only give the frequency of fractures carrying a specific mineral and not the amount. Calcite occurs as fracture fillings up to some centimetres in width but are commonly between 0.2 and 2 mm. X-ray diffraction analyses show that some fractures mapped as chlorite often consist of chlorite and clay minerals like corrensite (a chlorite-like mixed layer clay with layers of chlorite and smectite or vermiculite), illite and smectite /Drake and Tullborg 2004/. This makes clay minerals underestimated in the mapping (especially in Simpevarp and KLX02). Chlorite occurs mostly as thin fracture coatings although centimetre-wide chlorite coatings are occasionally observed.

Quartz is found in 17–24% of all sealed fractures and epidote in 9-27%. Both of these minerals have been overestimated in Simpevarp and KLX02 at the expense of prehnite and to a lesser degree adularia which are underestimated. Hematite has been mapped in 5–7 of the sealed fractures (1% in KLX02). The quantities of hematite in these fractures are often small, see discussion in Section 3.2.3. 19–21% of the sealed fractures are narrow fractures with altered wall rock and no visible filling (Figure 3-17).

Pyrite is much more abundant in sealed fractures in Laxemar (7%) than in Simpevarp (1%). Laumontite, fluorite, muscovite, gypsum, goethite, chalcopyrite and amphibole are found in 1% or less of all sealed fractures.

***Figure 3-17.*** *Photograph of a typical, hardly visible, sealed fracture with no visible fill but with altered wall rock. Drill core diameter is about 50 mm. These fractures are presented as "no fill – altered walls" in this report.*

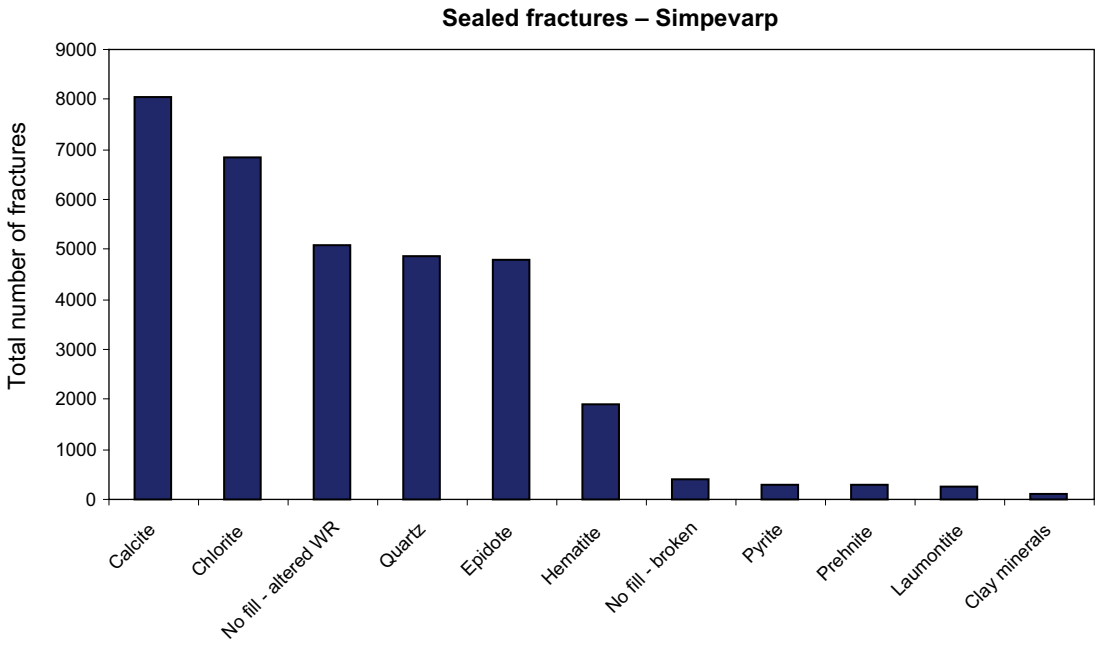


***Figure 3-18.*** *Histogram of fracture minerals in sealed fractures. Data from KSH01A+B, KSH02, KSH03A+B and KAV04A+B, total number of sealed fractures = 25,697.*

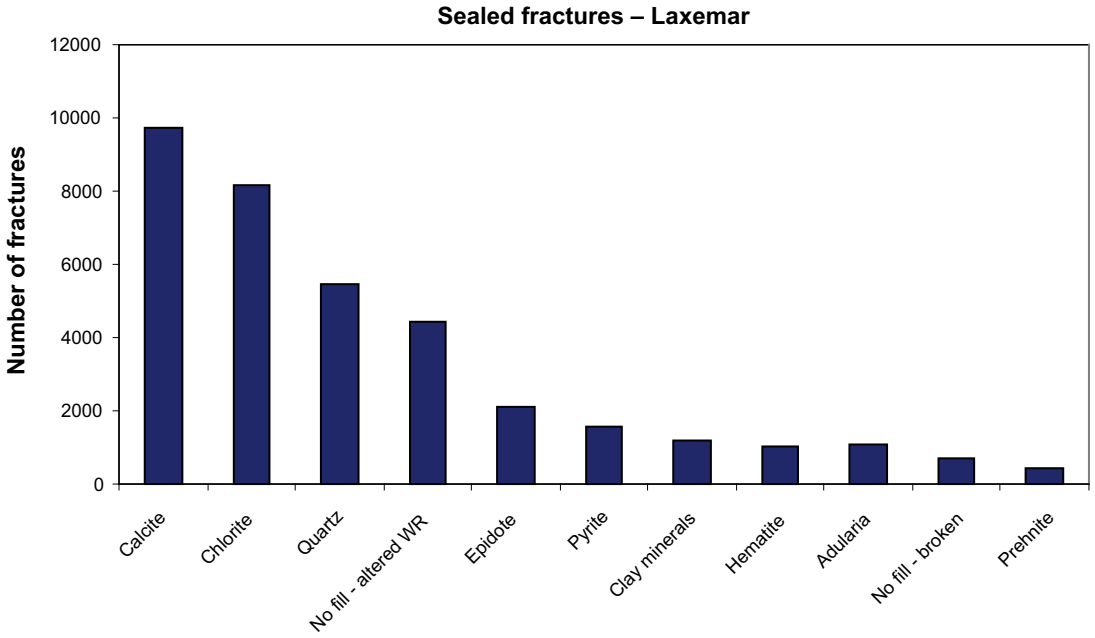


***Figure 3-19.*** *Histogram of fracture minerals in sealed fractures. Data from KLX03A–KLX08A and KLX07B, total number of sealed fractures = 22,801.*

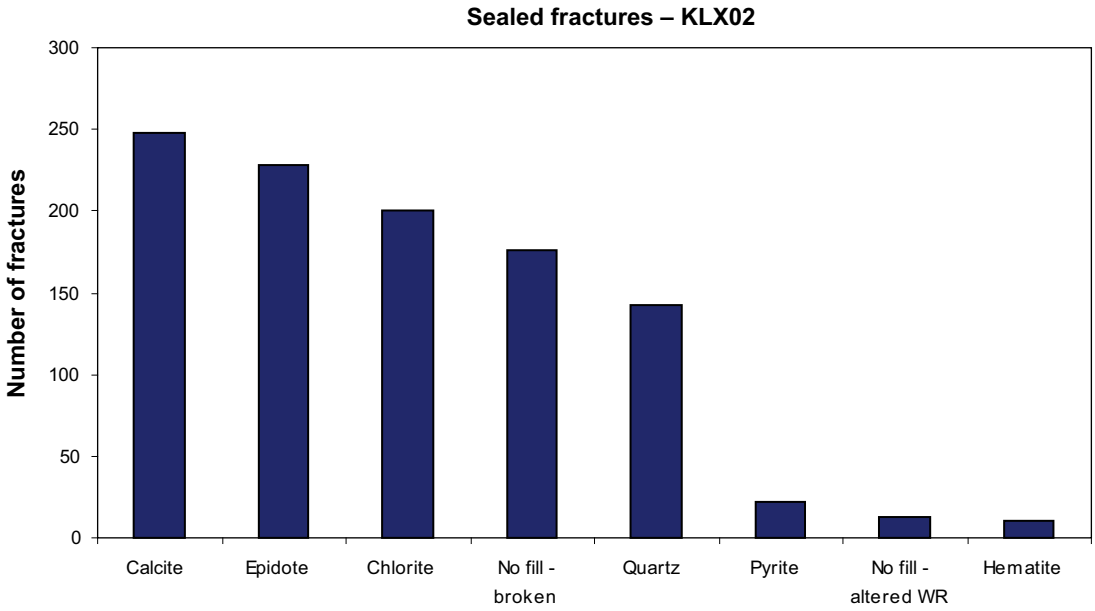


***Figure 3-20.*** *Histogram of fracture minerals in sealed fractures. Data from KLX02, total number of sealed fractures = 851.*

**Table 3-16. Relative abundance of fracture minerals in sealed fractures. The percentage value represent in how many of the sealed fractures a specific mineral has been identified. Data from KSH01A+B, KSH02, KSH03A+B and KAV04A+B (Simpevarp), KLX03–KLX06, KLX07A+B and KLX08 (Laxemar) and KLX02. "All fractures" includes Simpevarp, Laxemar and KLX02.**

| Mineral | Simpevarp % | Laxemar % | KLX02 % | All fractures % |
|---|---|---|---|---|
| Calcite | 31 | 43 | 29 | 36 |
| Chlorite | 27 | 36 | 24 | 31 |
| Quartz | 19 | 24 | 17 | 21 |
| No fill – altered WR | 20 | 19 | 21 | 19 |
| Epidote | 19 | 9 | 27 | 15 |
| Hematite | 7 | 5 | 1 | 6 |
| Pyrite | 1 | 7 | 3 | 4 |
| Clay minerals | 0.4 | 5 | 0.1 | 3 |
| No fill – broken | 2 | 3 | 2 | 3 |
| Adularia | 0.1 | 5 | 0.1 | 2 |
| Prehnite | 1 | 2 | < 0.1 | 1 |
| Laumontite | 1 | 0.7 | < 0.1 | 0.9 |
| Fluorite | 0.2 | 0.6 | < 0.1 | 0.4 |
| Muscovite | < 0.1 | 0.7 | < 0.1 | 0.3 |
| Gypsum | < 0.1 | 0.5 | < 0.1 | 0.2 |
| Goethite | 0.3 | < 0.1 | < 0.1 | 0.1 |
| Chalcopyrite | 0.2 | 0.1 | 0.1 | 0.2 |
| Amphibole | < 0.1 | 0.3 | 0.1 | 0.1 |

#### *3.2.3.2 Open fractures*

11,708 (31%) from Simpevarp, 8,994 (28%) from Laxemar and 2,083 (69%) from KLX02 of the fractures in the analysed Boremap data are open. The open fractures are dominated by chlorite and calcite which occur in 68–74 and 57–71% respectively of all open fractures (Figure 3-21 to 3-23 and Table 3-17). Compared to the sealed fractures, calcite, chlorite, clay minerals, hematite and pyrite are more abundant in the open fractures (except for KLX02 where amount of mapped clay minerals is small). Clay minerals and pyrite are particularly abundant in open fractures in Laxemar (38 and 18%, respectively) and hematite is particularly abundant in open fractures in Simpevarp (25%). 1–3% of the open fractures in Simpevarp and Laxemar have been mapped as empty and these fractures are most certainly drill induced. The amount of empty (broken) is higher in KLX02, which may be due to drilling induced fractures enhanced by the different drilling technique used for this borehole. The amount of adularia (7%) in the mapping data from Laxemar is much higher compared to Simpevarp and KLX02, the amount of adularia is however highly underestimated in Simpevarp and KLX02. Goethite, prehnite, laumontite, muscovite, chalcopyrite, gypsum and fluorite all occur in 1% or less of all open fractures.

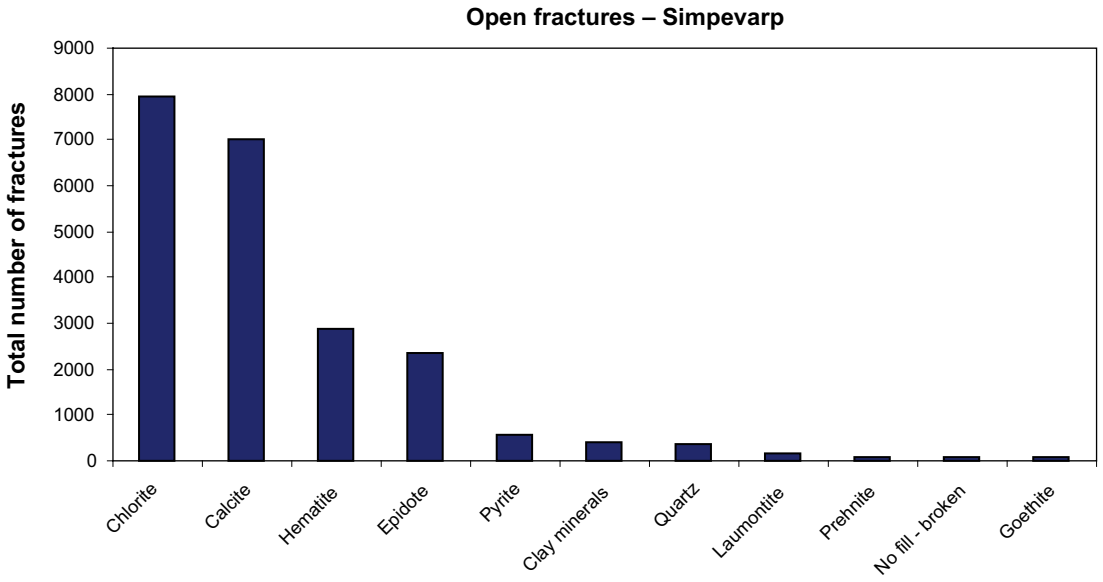


***Figure 3-21.*** *Histogram of fracture minerals in open fractures. Data from KSH01A+B, KSH02, KSH03A+B and KAV04A+B, total number of open fractures = 11,708.*

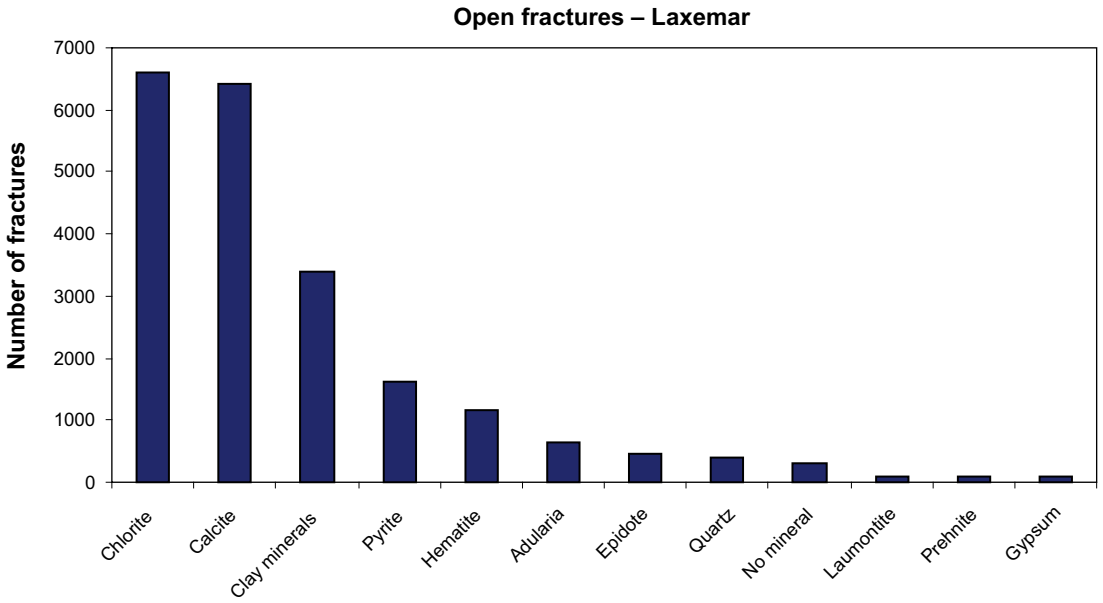


***Figure 3-22.*** *Histogram of fracture minerals in open fractures. Data from KLX03–KLX08A and KLX07B., total number of open fractures = 8,994.*

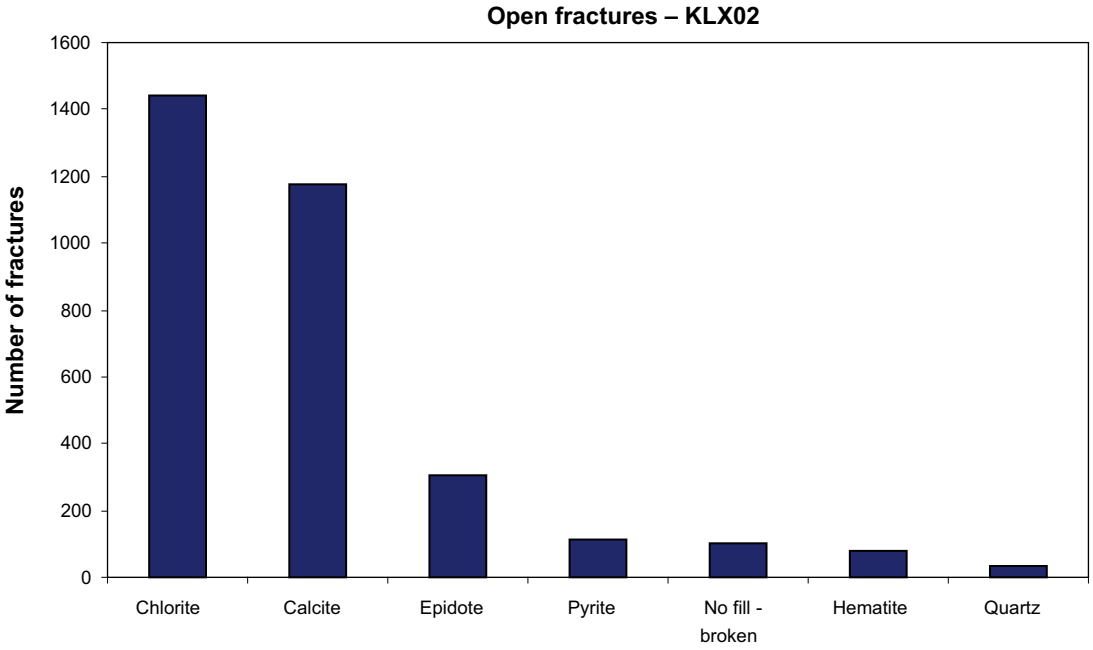


***Figure 3-23.*** *Histogram of fracture minerals in open fractures. Data from KLX02., total number of open fractures = 2,083.*

**Table 3-17. Relative abundance of fracture minerals in open fractures. The percentage value represent in how many of the sealed fractures a specific mineral has been identified. Data from KSH01A+B, KSH02, KSH03A+B and KAV04A+B (Simpevarp), KLX03–KLX06, KLX07A+B and KLX08 (Laxemar) and KLX02. All fractures include Simpevarp, Laxemar and KLX02.**

| Mineral | Simpevarp % | Laxemar % | KLX02 % | All fractures % |
|---|---|---|---|---|
| Chlorite | 68 | 74 | 69 | 70 |
| Calcite | 60 | 71 | 57 | 64 |
| Hematite | 25 | 13 | 4 | 18 |
| Clay minerals | 4 | 38 | < 0.1 | 17 |
| Epidote | 20 | 5 | 15 | 14 |
| Pyrite | 5 | 18 | 5 | 10 |
| Quartz | 3 | 4 | 2 | 4 |
| Adularia | < 0.1 | 7 | 0.1 | 3 |
| No fill – broken | 0.7 | 3 | 5 | 2 |
| Laumontite | 1 | 1 | 0.1 | 1 |
| Prehnite | 0.7 | 1 | < 0.1 | 0.7 |
| Goethite | 0.7 | < 0.1 | < 0.1 | 0.4 |
| Fluorite | 0.2 | 0.6 | < 0.1 | 0.4 |
| Gypsum | < 0.1 | 0.9 | < 0.1 | 0.4 |
| Chalcopyrite | 0.2 | 0.3 | 0.1 | 0.2 |
| Muscovite | < 0.1 | 0.3 | < 0.1 | 0.1 |

In fractures with an aperture larger than 1 mm clay minerals, hematite, pyrite and goethite are more common relative than in open fractures with smaller aperture (Figure 3-24 to 3-26 and Table 3-18), while the amount of e.g. calcite and chlorite is about the same. This trend is similar for Simpevarp, Laxemar and KLX02, except for goethite which was not observed in KLX02.

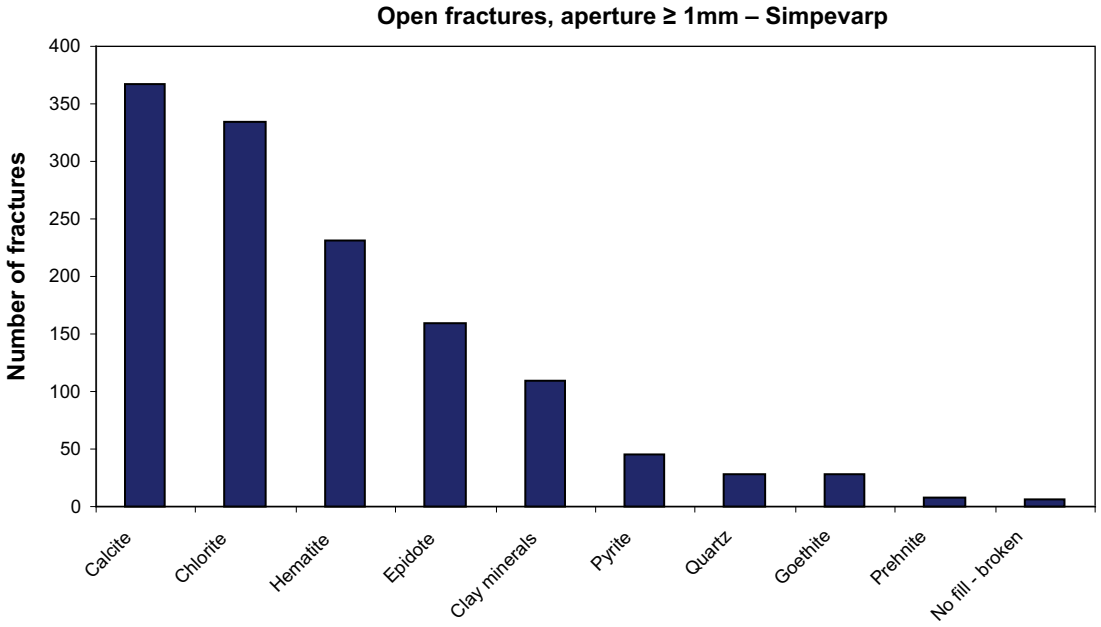


***Figure 3-24.*** *Number of open fractures with an aperture ≥ 1 mm and their mineralogy. Data from KSH01A+B, KSH02, KSH03A+B and KAV04A+B, total number of fractures = 606.*

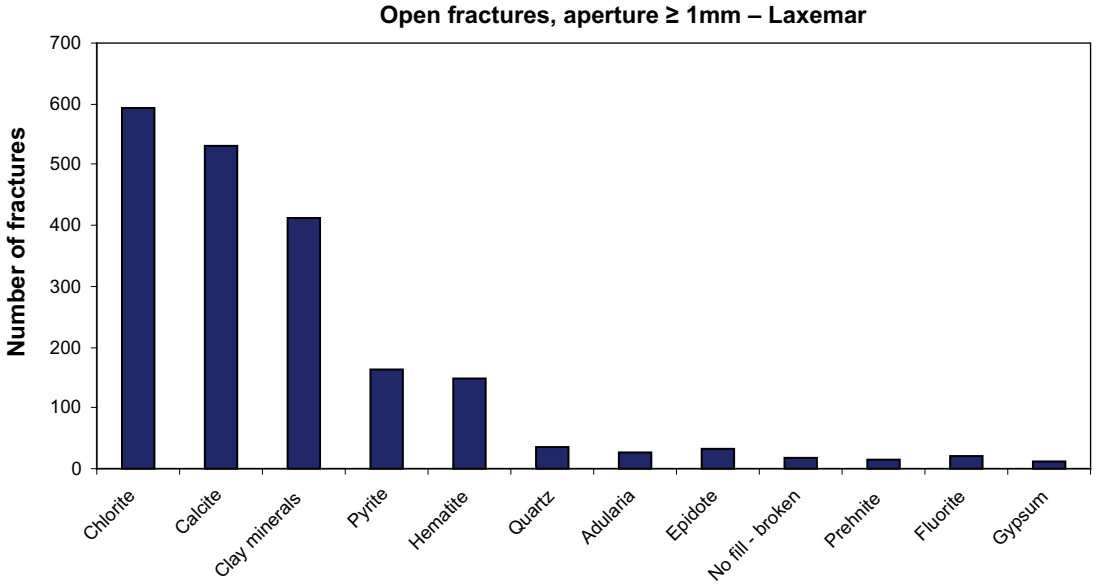


***Figure 3-25.*** *Number of open fractures with an aperture ≥ 1 mm and their mineralogy. Data from KLX03-KLX08A and KLX07B, total number of fractures = 733.*

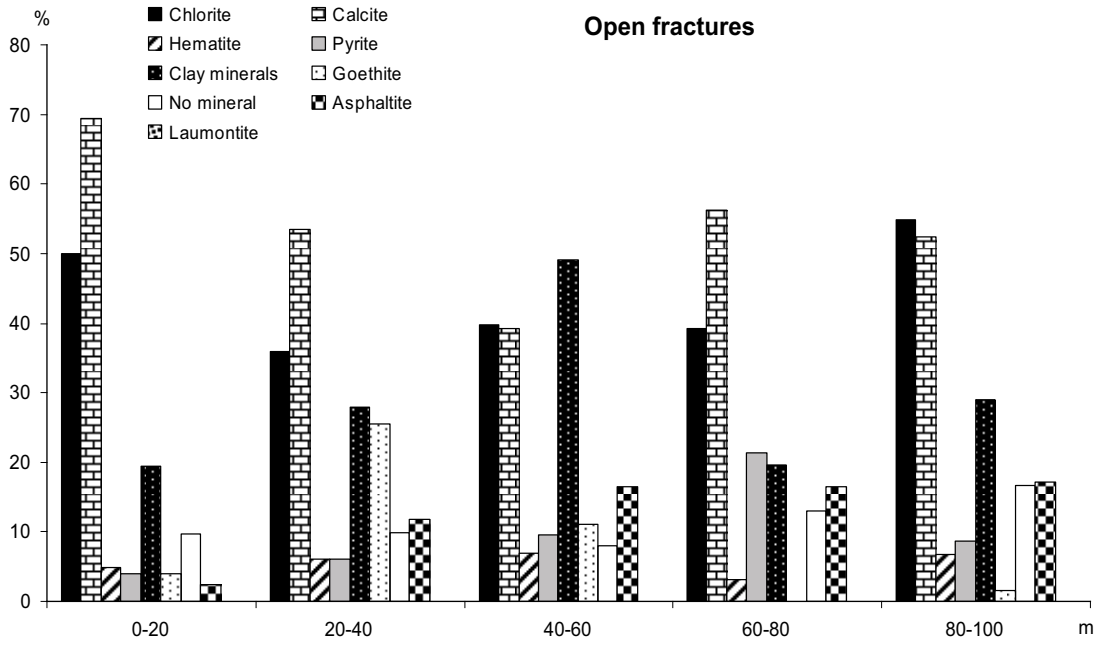


***Figure 3-26.*** *Number of open fractures with an aperture ≥ 1 mm and their mineralogy. Data from KLX02, total number of fractures = 62.*

**Table 3-18. Relative abundance of fracture minerals in open fractures with an aperture ≥ 1 mm. The percentage value represent in how many of the sealed fractures a specific mineral has been identified. Data from KSH01A+B, KSH02, KSH03A+B and KAV04A+B (Simpevarp), KLX03–KLX06, KLX07A+B and KLX08 (Laxemar) and KLX02. All fractures include Simpevarp, Laxemar and KLX02.**

| Mineral | Simpevarp % | Laxemar % | KLX02 % | All fractures % |
|---|---|---|---|---|
| Chlorite | 55 | 81 | 61 | 69 |
| Calcite | 61 | 73 | 82 | 68 |
| Clay minerals | 18 | 56 | 2 | 37 |
| Hematite | 38 | 20 | 3 | 27 |
| Pyrite | 8 | 22 | 24 | 17 |
| Epidote | 26 | 5 | 5 | 14 |
| Quartz | 5 | 5 | 2 | 5 |
| Adularia | < 0.1 | 4 | < 0.1 | 2 |
| Prehnite | 1 | 2 | < 0.1 | 2 |
| No fill – broken | 1 | 2 | < 0.1 | 2 |
| Goethite | 5 | < 0.1 | < 0.1 | 2 |
| Fluorite | 0.5 | 3 | < 0.1 | 2 |
| Gypsum | < 0.1 | 2 | < 0.1 | 0.9 |
| Laumontite | 0.5 | 1 | < 0.1 | 0.7 |
| Chalcopyrite | 0.2 | 0.5 | 2 | 0.4 |

*Variation in fracture mineralogy in open fractures with depth*

The mineralogy of the open fractures shows, except for the upper 100 m, relatively small variation with depth for Simpevarp, Laxemar and KLX02 (Figures 3-27 to 3-29). The main difference is above 100 m where goethite and clay minerals (only in Simpevarp) are more common. Pyrite is most abundant in the intervals 300–400 m and 600–900 m in Simpevarp,

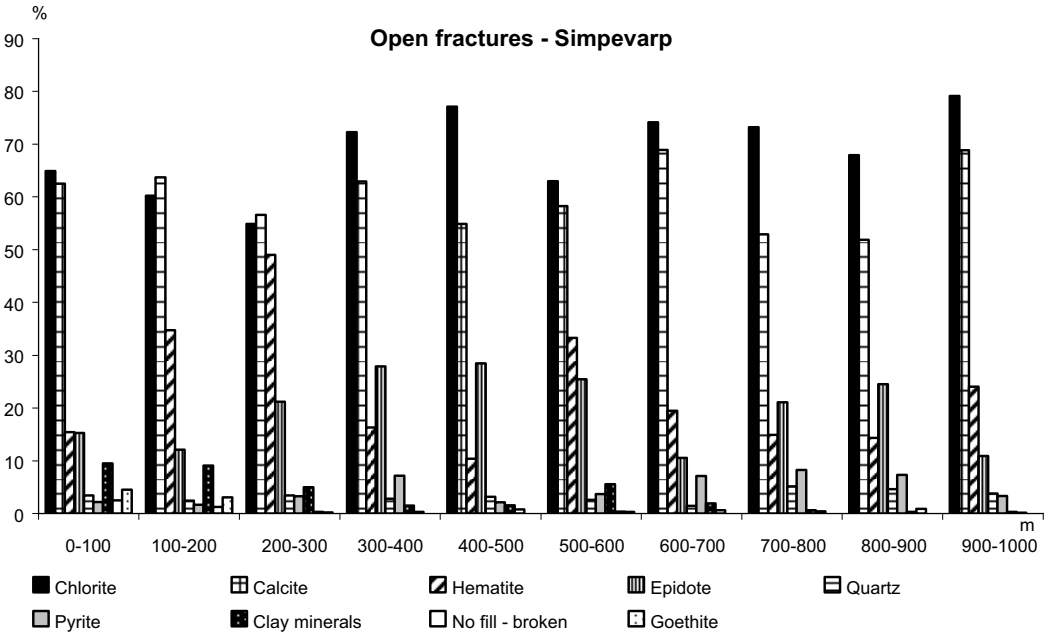


***Figure 3-27.*** *Variation of fracture mineralogy versus depth in open fractures in boreholes. Data from KSH01A+B, KSH02, KSH03A+B and KAV04A+B, depths have been recalculated to vertical depths.*

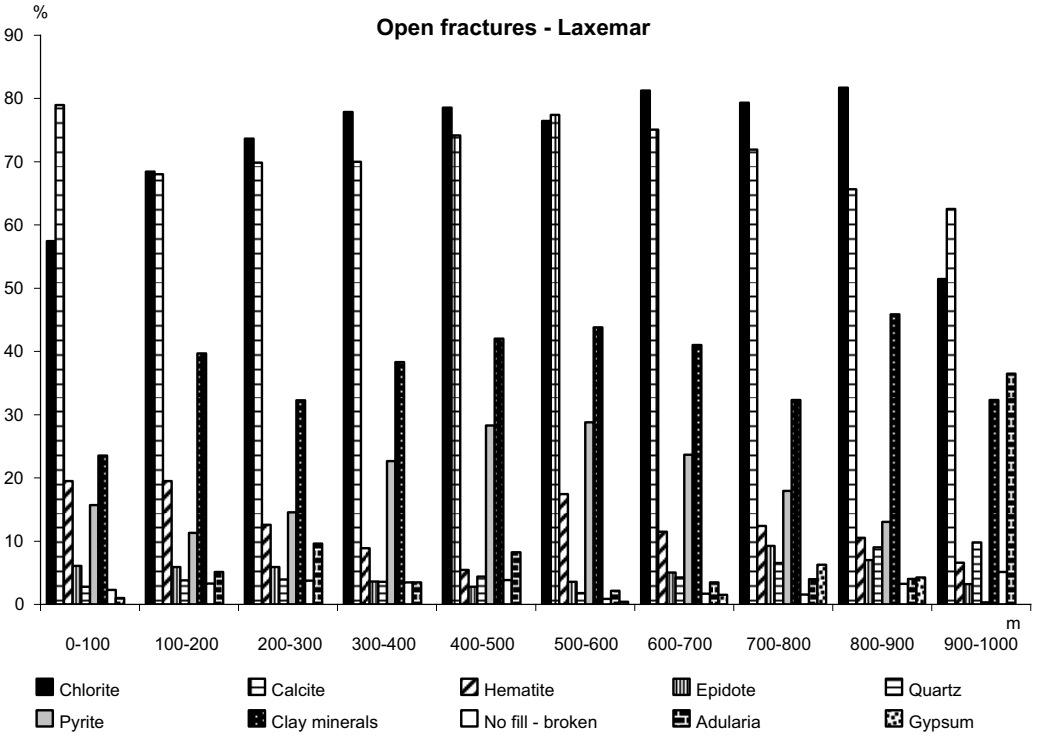


***Figure 3-28.*** *Variation of fracture mineralogy versus depth in open fractures in boreholes. Data from KLX03–KLX08A and KLX07B, depths have been recalculated to vertical depths.*

300–700 m in Laxemar and 300–800 m in KLX02. Some of the variation with depth may be the result of intersection with individual fracture zones and with which angle different fracture sets is cut by the boreholes. The high hematite content in Simpevarp in the intervals 200–300 m and 500–600 m are for instance partly due to the cutting of deformations zones by the borehole at these depths.

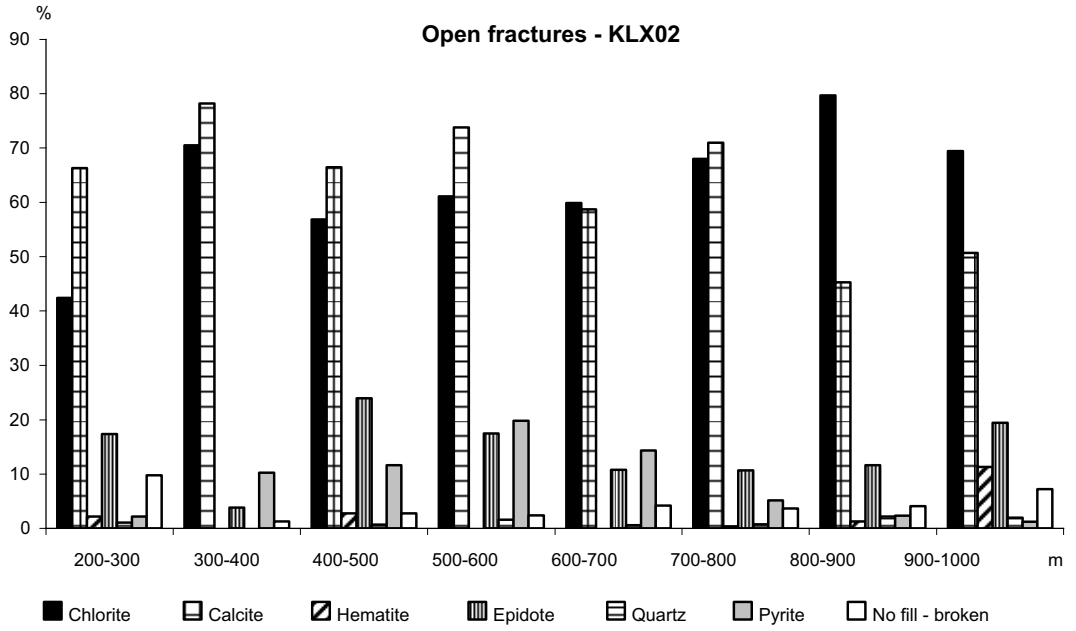


***Figure 3-29.*** *Variation of fracture mineralogy versus depth in open fractures in boreholes. Data from KLX02, depths have been recalculated to vertical depths.*

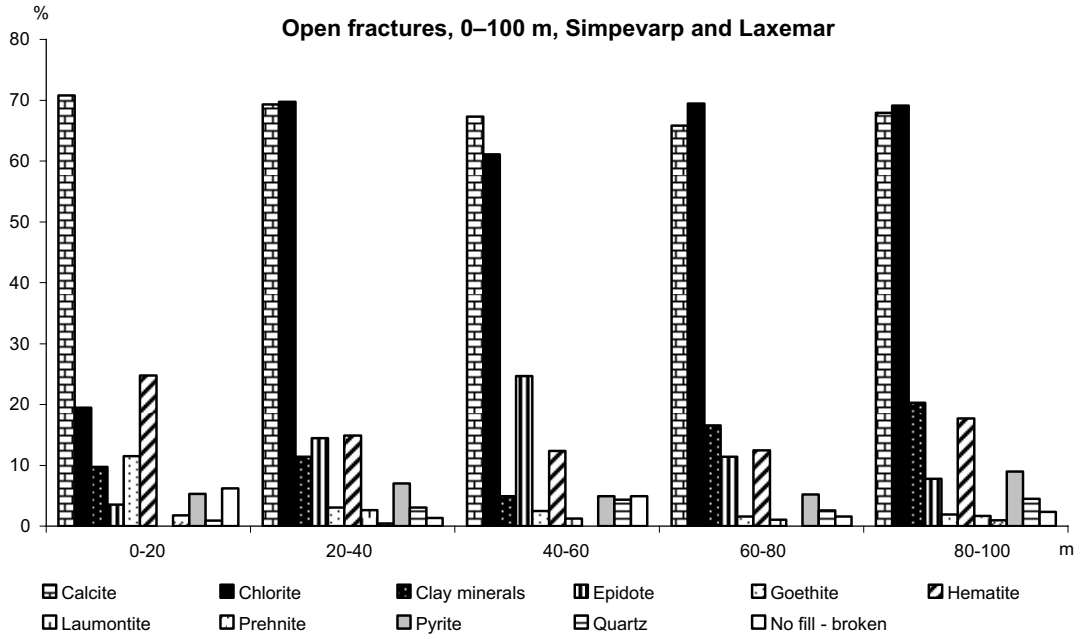


***Figure 3-30.*** *Variation of fracture mineralogy in the upper 100 m of the boreholes. Data from Simpevarp (KSH01B, KSH02, KSH03A+B and KAV04B, number of fracture is 725) and Laxemar (KLX03, KLX05, KLX06, KLX07A+B, KLX08, number of fractures is 395), depths have been recalculated to vertical depths.*

In the upper 100 m, the variation in fracture mineralogy increases when viewed with a higher vertical resolution (Figure 3-30). This is a result of less available data for the uppermost 100 m (especially for Laxemar) and the small amounts of deformation zones in the upper 100 m of the boreholes. Because of the few drill cores from the uppermost 80 m the available data from this depth from Simpevarp (four drill cores) and Laxemar (one drill core) are plotted together in Figure 3-30. The amount of goethite is higher in the uppermost 20 m, while the amount of e.g. chlorite is lower in this interval compared to the interval 20–100 m.

The mineralogy of the uppermost 20 m when viewed with a resolution of 5 m (Figure 3-31) (i.e. 5–20 m since only one open fracture is available from depths above 5 m) is inconclusive although the amount of pyrite increases with depth. Only four fractures are found in the interval 5–10 m which makes the amount of goethite very high since it is found in three of the fractures. The amount of calcite is about the same for the interval 5–20 m.

#### *3.2.3.3 Crushed zones*

Crushed zones are mapped separately during the drill core mapping and often represent zones with an elevated hydraulic conductivity. The term "crushed zone" correlates to an incohesive fault breccia according to the nomenclature of /Sibson 1977/. The fracture mineralogy of these crushed zones in Simpevarp and Laxemar (including KLX02) is dominated by calcite and chlorite, 84–92 and 81–90%, respectively (Figures 3-32 and 3-33 and Table 3-19). Hematite, epidote and clay minerals are also quite common in the crushed zones (about 9–60%). Pyrite, adularia, quartz and laumontite are found in less then 10% of the fracture zones while fluorite, goethite and chalcopyrite are found in less then 1%. Less than 1% of the fractures have been mapped as "no fill – broken". The relatively small amount of pyrite and high amount of hematite might indicate higher infiltration of oxidizing waters in the crushed zones. The pyrite and clay mineral contents are considerably higher in Laxemar (11% and 59%, respectively) compared to Simpevarp (3% and 9%, respectively), while the hematite content is higher in Simpevarp (46%, compared to 27% in Laxemar).

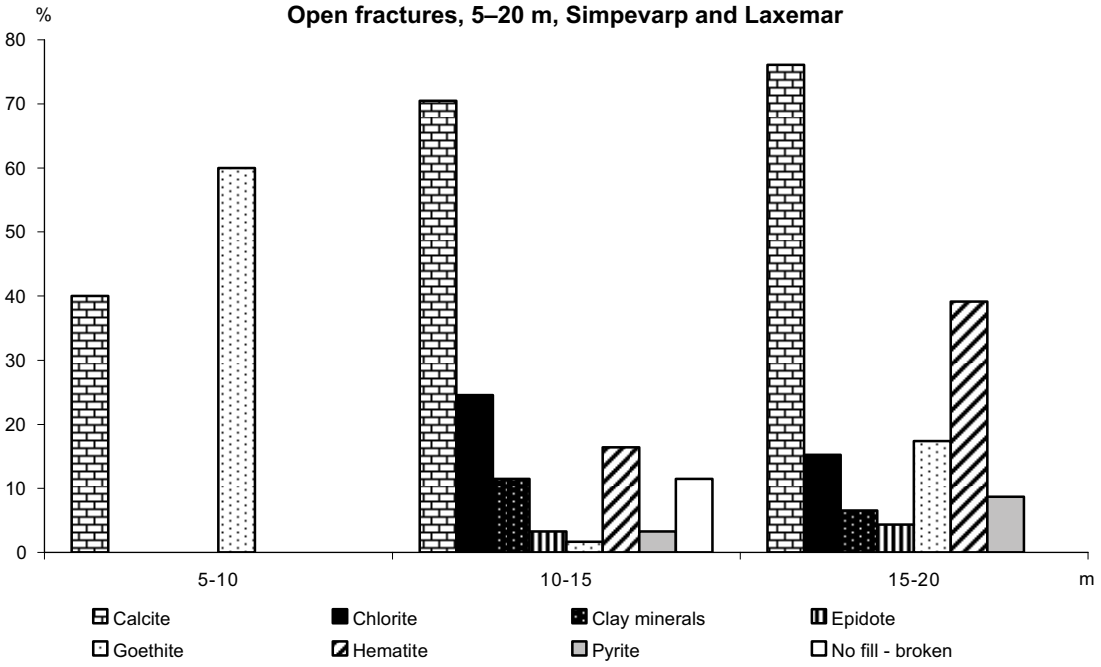


***Figure 3-31.*** *Variation of fracture mineralogy in the interval 5–20 of the boreholes. Data from Simpevarp (KSH01B, KSH03B and KAV04B, number of fractures is 49) and Laxemar (KLX07B, number of fractures is 64), depths have been recalculated to vertical depths.*

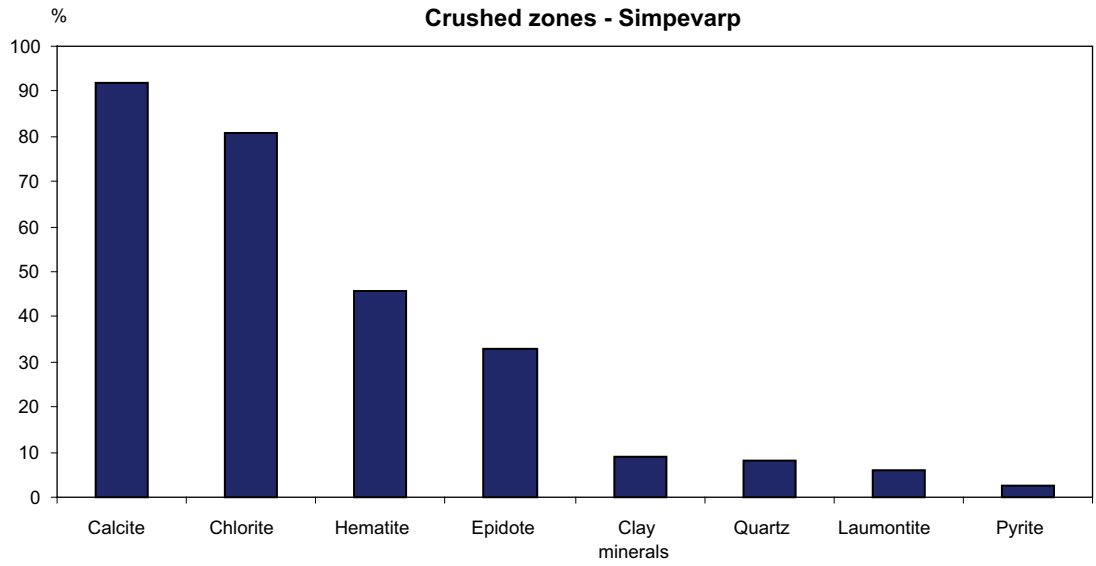


***Figure 3-32.*** *Histogram of fracture minerals in crushed zones from boreholes KSH01A, KSH02, KSH03A+B and KAV04A+B from Simpevarp. The percentage value represent in how many of the crushed zones each mineral has been identified. Total number of crushed zones is 146.*

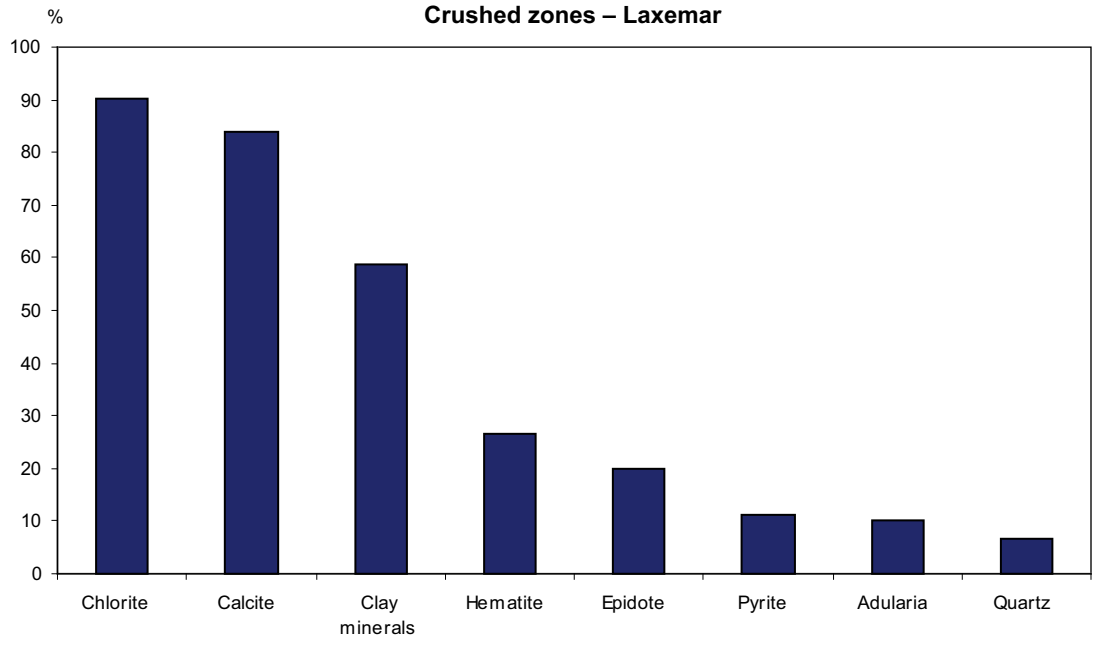


***Figure 3-33.*** *Histogram of fracture minerals in crushed zones from boreholes KLX02–KLX08 from Laxemar. The percentage value represent in how many of the crushed zones each mineral has been identified. Total number of crushed zones is 206.*

Since less data is available for the crushed zones than the sealed and open fractures, the trends are less statistically certain. The most obvious difference when mineralogy is plotted versus depth (Figures 3-34 and 3-35) compared to open fractures is the low amount of pyrite, the high occurrence in the upper 100 m in Laxemar is due to the low total number of crushed zones (5) and core. In Laxemar the lowest number of crush zones (11) apart for the upper 100 m is found in the depth intervals 400–500 m, 700–800 m and 800–900 m. In Simpevarp the lowest number of crush zones (about 5–7) is found in the depth intervals 0–100 m, 300–400 m and 400–500 m.

**Table 3-19. Relative abundance of fracture minerals in crushed zones. The percentage value represent in how many of the crushed zones a specific mineral has been identified. Data from Simpevarp (KSH01A, KSH02, KSH03A+Band KAV04A+B) and Laxemar (KLX02–KLX06, KLX07A+B and KLX08).**

| Mineral | Simpevarp % | Laxemar % | All fractures % |
|---|---|---|---|
| Calcite | 92 | 84 | 87 |
| Chlorite | 81 | 90 | 86 |
| Clay minerals | 9 | 59 | 38 |
| Hematite | 46 | 27 | 35 |
| Epidote | 33 | 20 | 25 |
| Pyrite | 3 | 11 | 8 |
| Quartz | 8 | 7 | 7 |
| Adularia | < 0.1 | 10 | 6 |
| Laumontite | 6 | 2 | 4 |
| Fluorite | < 0.1 | 1 | 0.9 |
| No mineral | 0.7 | 0.5 | 0.6 |
| Goethite | < 0.1 | 0.5 | 0.3 |
| Chalcopyrite | < 0.1 | 0.5 | 0.3 |

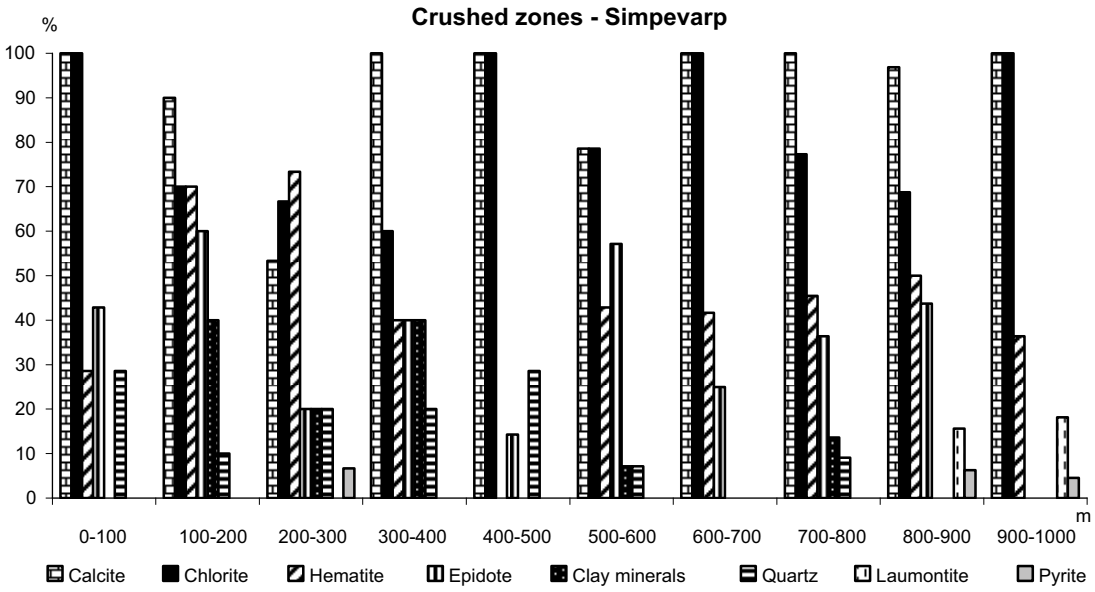


***Figure 3-34.*** *Variation of mineralogy with depth in crushed zones in boreholes KSH01A, KSH02, KSH03A+B and KAV04A+B from Simpevarp. Depths have been recalculated to vertical depths.*

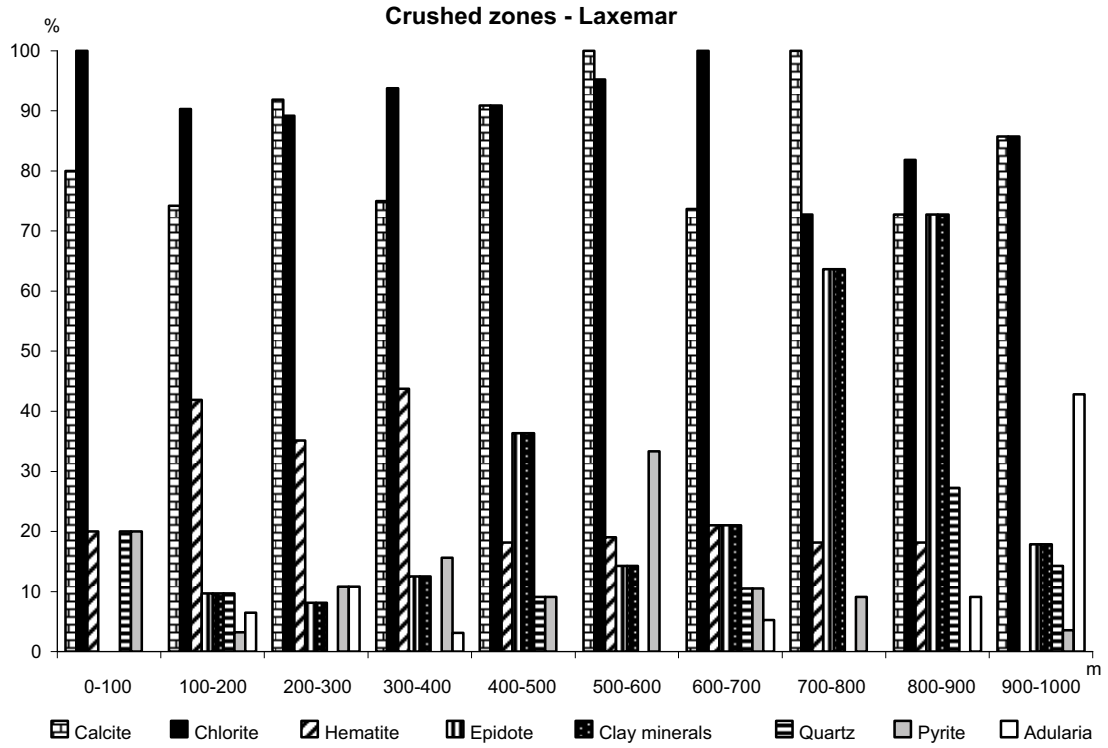


***Figure 3-35.*** *Variation of mineralogy with depth in crushed zones in boreholes KLX02–KLX08 from Laxemar. Depths have been recalculated to vertical depths.*

### 3.2.4 Fracture filling geochemistry

The fracture filling geochemistry data (usually includes both coating and filling material, cf Section 3.2.3) have been compiled from data from both Simpevarp (KSH01A+B, KSH02 and KSH03A) and Laxemar (KLX03, KLX04, KLX06 and KLX07A+B) subareas (data from SICADA). The data is mostly from gouge. Analyses from the different areas are presented collectively since the fracture filling geochemistry are very similar between the two subareas /Drake and Tullborg 2004, 2005, 2006c and in manuscript/ and since the chemistry between different samples differ more than between the samples from the different subareas a collective presentation is more representative then a separate presentation of the data. Since the chemistry differs highly between different fillings depending on their mineralogy, no mean value has been calculated. Instead, a short summary of the conclusions of the bulk chemistry of fracture fillings is presented here, the chemistry of the analysed fracture fillings can be found in Appendix III.

*K, Rb, Ba, Cs*

These elements are mainly hosted in K-feldspar, mica and clay minerals. Ba is also hosted in barite and harmotome. K and Ba prefer K-feldspar while Rb and Cs to a higher degree are hosted together with K in clay minerals, especially in illite and mixed layer clays of illite/smectite type. Compared to the host rock, Cs is significantly higher in the fracture coatings with values between 2.5 and 100 ppm in 13 of 20 samples (mean value of 20 samples is 16.5 compared to about 1–2.5 ppm for the host rock).

*Na, Ca, Sr*

The main Na mineral is albite which is rather uncommon as a fracture mineral in the Oskarshamn region, which is also shown in the lower content of $Na_2O$ in the fracture fillings compared to the host rock. The dominating Ca mineral is calcite, although many other Ca-bearing minerals are common like epidote, prehnite and laumontite. The most likely Sr hosting minerals are laumontite, plagioclase and epidote.

*Fe, Mg, Mn, Ti, Sc, V*

Fe and Mg are mostly hosted in chlorite and clay minerals corrensite and illite and the Fe/Mg-ratio in chlorite differs highly between different fracture generations. Mn is mainly found in chlorite and clay minerals. Ti, V and Sc generally show a positive correlation with Fe. The total Fe given as $Fe_2O_3$ content in fracture fillings containing chlorite/corrensite is between 2 and 15% (one sample has a $Fe_2O_3$ content of 21.5%, Figure 3-36). The amount of $Fe_2O_3$, MgO, MnO and V is generally higher or slightly higher in the fracture fillings than in the host rock, while the amount $TiO_2$ is about the same or slightly lower in the fracture fillings compared to the host rock.

*U, Th*

The U and Th-contents are below 23 ppm and 20 ppm, respectively in the analysed fracture fillings from both Simpevarp and Laxemar, and the U values are generally higher than in the host rock but the spread in U and Th values are much larger in the fracture fillings than in the host rock. Mean values of U and Th in the fracture fillings are 9.35 ppm and 7.98 ppm, respectively. The U/Th ratio is commonly higher in the fracture fillings than in the host rock which infers an enrichment of U compared to Th in the fracture fillings.

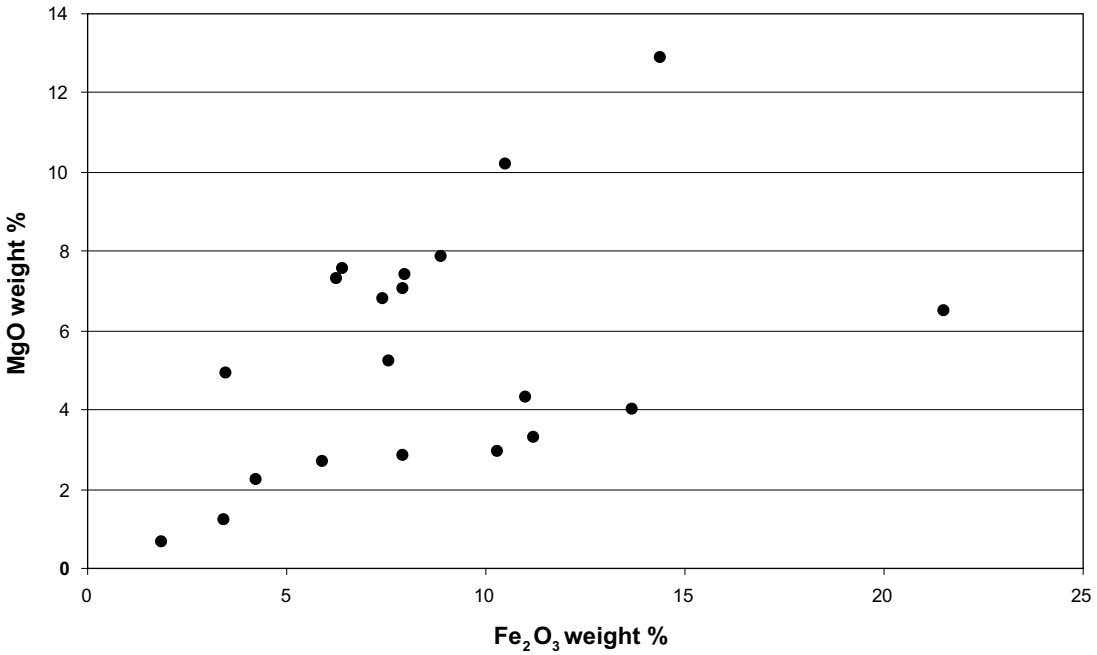


***Figure 3-36.*** *$Fe_2O_3$ versus MgO for bulk samples of fracture fillings/coatings from drill cores KSH01A+B, KSH02 and KSH03A from Simpevarp subarea and KLX03, KLX04, KLX06 and KLX07A+B from Laxemar subarea. Data from SICADA.*

*REEs*

Compared to the host rock, there are fracture fillings both enriched and depleted in REEs, although the general REE trend is similar to that of the host rock with enriched LREE and lower values of HREE. However, there is a larger spread in the REE values in the fracture fillings compared to the host rock. There is for instance enrichment in the light REEs in a couple of samples while the heavy REE concentrations are relatively unchanged (Figure 3-37). In a couple of samples the REEs show lower concentrations than the host rock.

### 3.2.4.1 Geochemistry of selected fracture minerals

The geochemistry of selected fracture minerals from the Oskarshamn site is based on SEM-EDS analyses of pure mineral phases in thin section /Drake and Tullborg 2004, 2005, 2006c and in manuscript/. Since most fractures are a mixture of different mineral phases, the geochemical composition below is to be considered as "end-members" of the different fracture fillings. Trace element analyses of calcite have been carried out by ICP-MS /Drake and Tullborg 2004 and in manuscript/.

*Chlorite and corrensite*

Chlorite and corrensite are the most important $Fe^{2+}$ bearing fracture minerals in the Simpevarp and Laxemar subareas. In corrensite, the Fe content given as FeO is normally between 30 and 45%, the MgO content varies between 2 and 12% and the CaO content is normally between 0.2 and 3%. Chlorite of different composition is formed at several events. The Fe content given as FeO in chlorite varies between 5 and 45%, the MgO content varies between 2 and 23% and CaO is commonly below detection limit (except when chlorite is in mixed-layer clay = corrensite). MnO contents vary between 0.15 to 0.8% in chlorite and corrensite. Chlorite in the altered wall rock and the oldest fracture filling chlorite has a more restricted composition of FeO (20–29%) and MgO (13–20%).

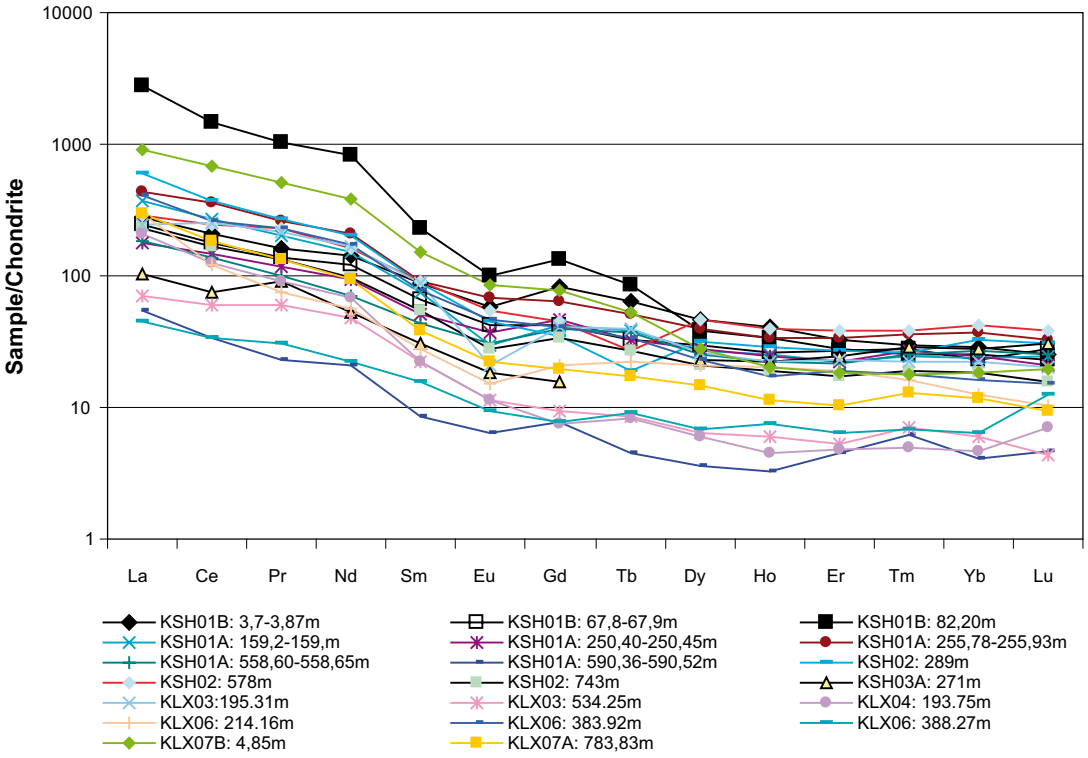


***Figure 3-37.*** *Chondrite normalized REE-pattern for fracture filling material from drill cores KSH01A+B, KSH02 and KSH03A from Simpevarp subarea and KLX03, KLX04, KLX06 and KLX07A+B from Laxemar subarea. Data from SICADA. Chondrite values from /Evansen et al. 1978/.*

*Calcite*

The calcite is a pure $CaCO_3$, with a variable MnO content of up to 2 wt. % but commonly below 1 wt. %. FeO and MgO contents are commonly below 1%. The Sr content varies between different generations of calcite, with high Sr contents (200–450 ppm) in old hydrothermal calcite and low Sr contents (40–150 ppm) in later formed calcite which is common in open fractures. Both U and Th content are commonly low, usually below 0.2 ppm. However, U-contents in late formed calcite are occasionally up to 4 ppm. Another carbonate that has been identified in the Oskarshamn area is REE-carbonate (rich in Ce, La, Nd and Y), which is commonly found along with late formed calcite in open fractures.

*Epidote*

Epidote has a $Fe_2O_3$ content between 10 and 18%, a MnO content between 0 and 0.7%, and a CaO content between 20 and 23%.

*Prehnite*

Prehnite has a $Fe_2O_3$ content between 0.6 and 9%, a MnO content below 0.1%, and a CaO content between 26 and 27%. The Sr content of prehnite is between 40 and 230 ppm.

*Laumontite*

Laumontite has a CaO content between 10.5 and 12% and FeO content below 0.7%. The laumontite in Oskarshamn is often associated with small grains of hematite. The Sr content in laumontite (one sample) is 348 ppm.

*Sulphides*

The sulphide minerals in fractures at the Oskarshamn site are dominantly pyrite which makes up more than 95% of all sulphides. Other identified sulphides are chalcopyrite (~ 1%), galena, sphalerite and very rarely argentite (only identified using SEM).

### 3.2.5 Redox – Fracture fillings

No Mössbauer analyses of fracture fillings have been carried out in the Simpevarp/Laxemar site investigations. However, Mössbauer analyses of chlorite from a fracture filling and from gauge material have been carried out during the Redox experiment at nearby Äspö HRL /Tullborg 1995/. The values from these analyses are thought to be representative also for the candidate area as well and are presented in Table 3-20. The oxidation factor ($Fe^{3+}/Fe_{tot}$) for chlorite varies between 0.329 and 0.437 in the samples. It should be noted that the samples contain trace amounts of epidote which might enhance the oxidation factor. $Fe^{2+}$ makes up more than 55% of the total Fe content in all of the samples.

The redox conditions in fractures with other mineralogy than chlorite can only be estimated. Fractures filled with silicate minerals that exclusively incorporate $Fe^{3+}$, like epidote and prehnite, would give an elevated oxidation factor. Laumontite filled fractures commonly also contain some hematite, so a high oxidation factor can be expected for these fractures as well.

In hydraulically conductive zones, chlorite, calcite, clay minerals and hematite dominate (Section 3.2.3.3). The $Fe_{tot}$ content in fractures with chlorite/corrensite and hematite is commonly between 1.3 and 15%, with a mean value of 6% (calculated from 2 to 15% $Fe_2O_3$ content in bulk fracture fillings) (Section 3.2.4). If a $Fe^{3+}/Fe_{tot}$-ratio of 0.4 is assumed, a $Fe^{2+}$ content of ~ 0.8–6% (mean value 3.6%) in fractures and zones with chlorite/corrensite and hematite is suggested.

**Table 3-20. Mössbauer analyses of chlorite from fracture fillings and gauge material from Äspö HRL, data from /Tullborg 1995/. The samples include trace amounts of epidote. For chlorite in fracture filling "A" and "B" represent samples from the same filling. For gauge material "A" is chlorite coating on coarse fragments and "B" is chlorite as single grains.**

| Sample | Fe-mineral | $Fe^{3+}/Fe_{tot}$ (silicate) |
|---|---|---|
| Chlorite in fracture filling | | |
| KKR0013: 8.8 m A(2) | Chlorite (+epidote) | 0.358 |
| KKR0013: 8.8 m B(2) | Chlorite (+epidote) | 0.329 |
| Mean value (standard deviation) | | 0.344 (0.02) |
| Chlorite in gauge material | | |
| Redox Zone A(3) | Chlorite (+epidote) | 0.437 |
| Tunnel wall B(3) | Chlorite (+epidote) | 0.432 |
| Mean value (standard deviation) | | 0.435 (0.004) |

# 4 Identified missing and pending information

The database comprising fractures and fracture minerals is successively growing, since the number of boreholes increases. This will hopefully fill the gap of data concerning near surface fractures (0–100 m) and will also yield a better representation of fractures with different orientations. For the SR-Can modelling, however, some items are of special importance and these will be addressed below:

## 4.1 pH

To demonstrate that pH in the groundwaters will be maintained in the interval 6 to 10 pH units during the life time of the repository is one of the tasks for the SR-Can modelling. The pH buffering in the groundwater system is usually controlled by the carbonate system and buffering capacity provided by the rock system via carbonate minerals is therefore essential. The crystalline host rocks at both Forsmark and Simpevarp/Laxemar have very low carbonate contents (possibly a few ‰). The fracture coatings, in contrast, usually contain calcite ($CaCO_3$) and Boremap data shows that calcite is documented in more than 25% of the open fractures in both areas. When acid precipitation enters into the soil and further to the bedrock aquifer it will be neutralised by this calcite. Lack of calcite in the uppermost part of the bedrock can be seen in recharge areas with thin soil cover. It is therefore of importance to document the depth distribution of fracture calcite. The amount of available calcite is estimated in this report. This is however based on relatively rough assumptions and more precise calculations would need more information about calcite coating thicknesses and covering proportions. In order to gain the additional information more detailed mapping is needed, which is theoretically achievable but not planned for the moment.

## 4.2 Ion exchange capacity (CEC)

The cation content (Ca+Mg) in the groundwater influences the stability of the bentonite buffer and Ca+Mg values > 40 mg/L in groundwaters is a criteria that assures that bentonite erosion can not take place. Knowledge about the ion exchange capacity along the groundwaters flow paths may therefore be important information, since it may help to interpret the stability and the cation distribution in the groundwaters of the sites. No regular measurements of the cation exchange capacity (CEC) have been carried out within the Transport Program, however, BET surface measurements on fracture coatings and gouge material will be performed. Batch sorption providing $K_d$ values for Sr(II), Cs(I), Ni(II) and Am(III) will be measured on fracture coatings and gouge material.

## 4.3 Redox

It is of importance for the modelling of the long term stability of the canister and also for the potential transport of radionuclides in the groundwater linked to a canister and bentonite buffer failure, to show that reducing capacity is available along the groundwater flow paths. Surface waters are oxidizing but will change to reducing during recharge through the soil cover and/or the near surface bedrock fractures. The $O_2$ reduction can be organic and/or inorganic. During future cold climate conditions (including glaciations) the organic production will be lower than present, and furthermore the hydraulic pressure may be significantly higher forcing potentially oxygenated water to large depth in the bedrock. It is therefore important to show that sufficient

inorganic redox capacity is provided by the fracture coatings and fracture wall rock. Fe(II) is the main reducing agent in the system, but also $S^{2-}$ contribute to the reducing capacity and the presence of unaltered sulphides (mostly pyrite) is taken as an indicator of stable reducing conditions. The amounts of pyrite in the rock is very small (only a few ‰) whereas in the fractures, pyrite and other sulphides are more common but very irregularly distributed. Instead the largest reducing capacity is provided by the Fe(II)-bearing Al-silicates which in the fracture coatings and gouge material are chlorite and clay minerals (corrensite, smectite, mixed layer clays, illite/smectite). In the fresh host rock biotite, hornblende and magnetite are the main hosts for Fe(II), whereas in altered wall rock, chlorite contributes most of the Fe(II). The Fe(II)/Fe(III) ratios for the chlorite and clay minerals are therefore very important for the calculation of the reducing capacity along the flow paths.

In the Simpevarp/Laxemar area the mineralogical and chemical composition including Fe(II)/Fe(III) ratio of altered wall rock and reference rock have been documented. A corresponding study is ongoing in Forsmark. Information of Fe(II)/Fe(III) in the fracture coatings is however sparse and needs to be supplemented for chlorite and clay minerals (corrensite, smectite, mixed layer clay, illite/smectite) from fracture coatings and gouge material together with the Fe content of these minerals. In addition to their oxidation state, the amount of chlorite and clay minerals in the fractures are of importance for estimating the total amount of Fe(II). Similarly to what is described for the carbonates the situation is that the Boremap data are not so detailed and more information on thicknesses of the coatings could make the estimates significantly better. For the moment coating thicknesses < 0.5 mm are not subdivided. A detailed mapping of selected parts of drill cores representing depth from surface to repository levels is possible to carry out, and will provide the necessary abundance of these Fe(II)-containing minerals.

Detailed investigations of drillcores in the upper part of the bedrock (0–100 m) at Laxemar will be conduced for tracing the present depth of the redox zone. This will be done by compilation of detailed core mapping showing the distribution of e.g. Fe-oxides and sulphide minerals. Microscopy, SEM studies, geochemistry and uranium series analyses will also be undertaken.

## 4.4 Uranium

In the Forsmark area high U contents (5–70 µg/L) in groundwaters have been found at depths between 200 to 650 m /SKB 2005a/. Large variation in U content in surface waters are common, but lower uranium content with depth is expected due to decreasing redox potential and decreasing bicarbonate content. The cause of these high U-values is not understood for the moment and more analyses of fracture fillings and groundwater samples are needed. These analyses comprise both U content and U-series isotopes and are presently being carried out. Efforts are also made to identify the U bearing phases hosted in the fracture coatings.

# 5 References


**Byegård J, Gustavsson, E, Tullborg, E-L, 2006.** Data evaluation and retardation model. Preliminary site description Laxemar subarea – version 1.2. SKB R-06-27. Svensk Kärnbränslehantering AB.

**Börjesson S, Gustavsson E, 2005.** Laboratory data from the site investigation programme for the transport properties of the rock. Data delivery for data freeze Laxemar 2.1. Oskarshamn site investigation. SKB P-05-106. Svensk Kärnbränslehantering AB.

**Carlsten S, Gustafson J, Mattsson H, Petersson J, Stephens M B, 2005.** Forsmark site investigation. Geological single-hole interpretation of KFM06A and KFM06B (DS6). SKB P-05-132. Svensk Kärnbränslehantering AB.

**Deer W A, Howie R A, Zussman J, 1992.** An introduction to the rock-forming minerals. 2nd ed. Longman Scientific & Technical. 696 pp.

**Drake H, Tullborg E-L, 2004.** Fracture mineralogy and wall rock alteration, results from drill core KSH01A+B. SKB-P-04-250. Svensk Kärnbränslehantering AB.

**Drake H, Tullborg E-L, 2005.** Fracture mineralogy and wall rock alteration, results from drill cores KAS04, KA1755A and KLX02. SKB-P-05-174. Svensk Kärnbränslehantering AB.

**Drake H, Tullborg E-L, 2006a.** Oskarshamn site investigation. Mineralogical,chemical and redox features of red-staining adjacent to fractures – Results from drill core KLX04. SKB P-06-02, Svensk Kärnbränslehantering AB.

**Drake H, Tullborg E-L, 2006b.** Oskarshamn site investigation. Mineralogical, chemical and redox features of red-staining adjacent to fractures – Results from drill cores KSH01A+B and KSH03A+B. SKB P-06-01. Svensk Kärnbränslehantering AB.

**Drake H, Tullborg E-L, 2006c.** Fracture mineralogy, Results from drill core KSH03A+B. SKB P-06-03. Svensk Kärnbränslehantering AB.

**Drake H, Tullborg E-L, in manuscript.** Fracture mineralogy, Results from drill cores KLX03, KLX04, KLX06, KLX07A, KLX08 and KLX10A. Oskarshamn site investigations, SKB P-06-XX. Svensk Kärnbränslehantering AB.

**Ehrenborg J, Stejskal V, 2004a.** Boremap mapping of core drilled boreholes KSH01A and KSH01B. Oskarshamn site investigation. SKB P-04-01. Svensk Kärnbränslehantering AB.

**Ehrenborg J, Stejskal V, 2004b.** Boremap mapping of core drilled boreholes KSH03A and KSH03B. Oskarshamn site investigation. SKB P-04-132. Svensk Kärnbränslehantering AB.

**Ehrenborg J, Stejskal V, 2004c.** Boremap mapping of core drilled borehole KLX02. Oskarshamn site investigation. SKB P-04-129. Svensk Kärnbränslehantering AB.

**Ehrenborg J, Stejskal V, 2004d.** Boremap mapping of core drilled borehole KSH02. Oskarshamn site investigation. SKB P-04-131. Svensk Kärnbränslehantering AB.

**Ehrenborg J, Stejskal V, 2005.** Boremap mapping of core drilled boreholes KAV04A and KAV04B. Oskarshamn site investigation. SKB P-05-22. Svensk Kärnbränslehantering AB.

**Ehrenborg J, Dahlin P, 2005a.** Boremap mapping of core drilled borehole KLX03. Oskarshamn site investigation. SKB P-05-24. Svensk Kärnbränslehantering AB.

**Ehrenborg J, Dahlin P, 2005b.** Boremap mapping of core drilled borehole KLX04. Oskarshamn site investigation. SKB P-05-23. Svensk Kärnbränslehantering AB.

**Ehrenborg J, Dahlin P, 2005c.** Boremap mapping of core drilled borehole KLX06. Oskarshamn site investigation. SKB P-05-185. Svensk Kärnbränslehantering AB.

**Ehrenborg J, Dahlin P, 2005d.** Boremap mapping of core drilled boreholes KLX07A and KLX07B. Oskarshamn site investigation. SKB P-05-263. Svensk Kärnbränslehantering AB.

**Ehrenborg J, Dahlin P, 2006.** Boremap mapping of core drilled borehole KLX08. Oskarshamn site investigation. SKB P-06-42. Svensk Kärnbränslehantering AB.

**Ehrenborg J, Dahlin P, in manuscript.** Boremap mapping of core drilled boreholes KLX10A, KLX10B and KLX10C. Oskarshamn site investigation. SKB P-06-XXX. Svensk Kärnbränslehantering AB.

**Evansen N M, Hamilton P J, O'Nions R K, 1978.** Rare Earth Abundances in Chondritic Meteorites. Geochimica et Cosmochimica Acta 42, 1199–1212.

**Liedberg L, 2005,** Drill hole KLX06A. Determination of porosity by water saturation and density by buoyancy technique. Oskarshamn site investigation. SKB P-05-127. Svensk Kärnbränslehantering AB.

**Mattsson H, Thunehed H, 2004,** Interpretation of geophysical borehole data and compilation of petrophysical data from KSH02 (80–1,000 m) and KAV01. Oskarshamn site investigation. SKB P-04-77. Svensk Kärnbränslehantering AB.

**Mattsson H, Thunehed H, Triumf C-A, 2004.** Compilation of petrophysical data from rock samples and in situ gamma-ray spectrometry measurements. Stage 2 – 2004 (including 2002). Oskarshamn site investigation. SKB P-04-294. Svensk Kärnbränslehantering AB.

**Persson Nilsson K, Bergman T, Eliasson T, 2004.** Bedrock mapping 2004 – Laxemar subarea and regional model area. Outcrop data and description of rock types. Oskarshamn site investigation. SKB P-04-221. Svensk Kärnbränslehantering AB.

**Petersson J, Wängnerud A, 2003.** Forsmark site investigation. Boremap mapping of telescopic drilled borehole KFM01A. SKB P-03-23. Svensk Kärnbränslehantering AB.

**Petersson J, Wängerud A, Danielsson P, Stråhle A, 2003a.** Forsmark site investigation. Boremap mapping of telescopic drilled borehole KFM03A and core drilled borehole KFM03B. SKB P-03-116. Svensk Kärnbränslehantering AB.

**Petersson J, Wängnerud A, Stråhle A, 2003b.** Forsmark site investigation. Boremap mapping of telescopic drilled borehole KFM02A. SKB P-03-98. Svensk Kärnbränslehantering AB.

**Petersson J, Berglund J, Wängerud A, Danielsson P, 2004a**. Forsmark site investigation. Boremap mapping of telescopic drilled borehole KFM05A. SKB P-04-295, Svensk Kärnbränslehantering AB.

**Petersson J, Tullborg E-L, Mattsson H, Thunehed H, Isaksson H, Berglund J, Lindroos H, Danielsson P, Wängnerud A, 2004b.** Forsmark site investigation. Petrography, geochemistry, petrophysics and fracture mineralogy of boreholes KFM01A, KFM02A and KFM03A+B. SKB P-04-103. Svensk Kärnbränslehantering AB.

**Petersson J, Wängerud A, Berglund J, Danielsson P, 2004c.** Forsmark site investigation. Boremap mapping of telescopic drilled borehole KFM04A. SKB P-04-115. Svensk Kärnbränslehantering AB.

**Petersson J, Berglund J, Wängerud A, Stråhle A, 2005a.** Forsmark site investigation. Petrographic and geochemical characteristics of bedrock samples from boreholes KFM04A–06A, and a whitened alteration rock. SKB P-05-156. Svensk Kärnbränslehantering AB.

**Petersson J, Skogmo G, Berglund J, Wängerud A, 2005b.** Forsmark site investigation. Boremap mapping of telescopic drilled borehole KFM06A and core drilled borehole KFM06B. SKB P-05-101. Svensk Kärnbränslehantering AB.

**Sandström B, Savolainen M, Tullborg E-L, 2004.** Forsmark site investigation. Fracture Mineralogy. Results from fracture minerals and wall rock alteration in boreholes KFM01A, KFM02A, KFM03A and KFM03B. SKB P-04-149. Svensk Kärnbränslehantering AB.

**Sandström B, Tullborg E-L, 2005.** Forsmark site investigation. Fracture mineralogy. Results from fracture minerals and wall rock alteration in KFM01B, KFM04A, KFM05A and KFM06A. SKB P-05-197. Svensk Kärnbränslehantering AB.

**Sandström B, Tullborg E-L, de Torres T, Ortiz J E, 2006.** The occurence and potential origin of asphaltite in bedrock fractures, Forsmark, central Sweden. GFF 128, 233–242.

**Savukoski M, 2004a.** Drill hole KLX04A. Determining of porosity by water saturation and density by buoyancy technique. Oskarshamn site investigation. SKB P-04-268. Svensk Kärnbränslehantering AB.

**Savukoski M, 2004b.** Drill hole KLX02. Determining of porosity by water saturation and density by buoyancy technique. Oskarshamn site investigation. SKB P-04-259. Svensk Kärnbränslehantering AB.

**Savukoski M, Carlsson L, 2004.** Drill hole KSH01A. Determining of porosity by water saturation and density by buoyancy technique. Oskarshamn site investigation. SKB P-04-56. Svensk Kärnbränslehantering AB.

**Savukoski M, 2005a.** Drill hole KLX05A. Determination of porosity by water saturation and density by buoyancy technique. Oskarshamn site investigation. SKB P-05-127. Svensk Kärnbränslehantering AB.

**Savukoski M, 2005b.** Drill hole KLX03A. Determination of porosity by water saturation and density by buoyancy technique. Oskarshamn site investigation. SKB P-05-94. Svensk Kärnbränslehantering AB.

**Sibson R H**, **1977.** Fault rocks and fault mechanisms, Journal of the Geological Society of London 133, 191–213.

**SKB, 2005a.** Hydrogeochemical evaluation for Forsmark model version 1.2. Preliminary site description of the Forsmark area. SKB R-05-17. Svensk Kärbränslehantering AB.

**SKB, 2005b.** Preliminary site description. Forsmark area – version 1.2. SKB R-05-18. Svensk Kärnbränslehantering AB.

**SKB, 2005c.** Preliminary site description, Simpevarp subarea – version 1.2. SKB R-05-08. Svensk Kärnbränlsehantering AB.

**SKB, 2006.** Preliminary site description, Laxemar subarea – version 1.2. SKB R-06-10. Svensk Kärnbränslehantering AB.

**Stephens M B, Lundqvist S, Ekström M, Bergman T, Anderson J, 2003.** Rock types, their petrographic and geochemical characteristics, and a structural analysis of the bedrock based on stage 1 (2002) surface data. SKB P-03-75. Svensk Kärnbränslehantering AB.

**Stephens M B, Lundqvist S, Bergman T, Ekström M, 2005.** Forsmark site investigation. Bedrock mapping. Petrographic and geochemical characteristics of rock types based on Stage 1 (2002) and Stage 2 (2003) surface data. SKB P-04-87. Svensk Kärnbränslehantering AB.

**Tullborg E-L, 1995.** Chapter 4. Mineralogical/Geochemical Investigations in the Fracture Zone. In: Banwart S (ed), The Redox experiment in block scale. SKB PR 25-95-06, p 81–101.

**Wahlgren C-H, Ahl M, Sandahl K-A, Berglund J, Petersson J, Ekström M, Persson P-O, 2004.** Bedrock mapping 2003 – Simpevarp subarea. Outcrop data, fracture data, modal and geochemical classification of rock types, bedrock map, radiometric dating. Oskarshamn site investigation. SKB P-04-102. Svensk Kärnbränlehantering AB.

**Wahlgren C-H, Bergman T, Persson Nilsson K, Eliasson T, Ahl M, Ekström M, 2005.** Bedrock map of the Laxemar subarea and surroundings. Description of rock types, modal and geochemical analyses, including the cored boreholes KLX03, KSH03 and KAV01. Oskarshamn site investigation. SKB P-05-180. Svensk Kärnbränslehantering AB.

**Wahlgren C-H, Bergman T, Ahl M, Ekström M, 2006.** Modal and geochemical analyses of drill core samples 2005 – Classification of rock types in KLX03, KLX04, KLX06, KLX07A, KLX07B, KLX08 and KLX10, Oskarshamn site investigation. SKB P-06-05. Svensk Kärnbränslehantering AB.

# Appendix I

## Minerals mentioned in this report and their chemical formula

| | |
|---|---|
| ***Adularia*** | *$KAlSi_3O_8$ (low T K-feldspar)* |
| ***Albite (Na-Plagioclase)*** | $NaAlSi_3O_8$ |
| ***Allanite*** | $(Ca,Mn,Ce,La,Y,Th)_2(Fe,Ti)(Al,Fe)_2O.OH[Si_2O_7][SiO_4]$ |
| ***Analcime*** | $NaAlSi_2O_6 \cdot H_2O$ |
| ***Apatite*** | $Ca_5(PO_4)_3(OH,F,Cl)$ |
| ***Apophyllite*** | $(K,Ca)Ca_4Si_8O_{20}(F,OH) \cdot 8H_2O$ |
| ***Argentite*** | $Ag_2S$ |
| ***Asphaltite*** | Mixture of hydrocarbons |
| ***Barite*** | $BaSO_4$ |
| ***Biotite*** | $K(Mg,Fe)_3AlSi_3O_{10}(OH)_2$ |
| ***Calcite*** | $CaCO_3$ |
| ***Chalcopyrite*** | $CuFe^{2+}S_2$ |
| ***Chlorite*** | $(Mg,Fe^{2+},Fe^{3+},Al)_3(Si,Al)_4O_{10}(OH)_2$ |
| ***Epidote*** | $Ca_2Al_2Fe(SiO_4)(Si_2O_7)(O,OH)_2$ |
| ***Fluorite*** | $CaF_2$ |
| ***Galena*** | PbS |
| ***Gypsum*** | $CaSO4 \cdot 2H_2O$ |
| ***Harmotome*** | $Ba_{0.8}Na_{0.2}K_{0.1}Al_2Si_6O_{16} \cdot 6H_2O$ (zeolite) |
| ***K-feldspar*** | $KAlSi_3O_8$ |
| ***Hematite*** | $Fe^{3+}{}_2O_3$ |
| ***Laumontite*** | $CaAl_2Si_4O_{12} \cdot 4H_2O$ (zeolite) |
| ***Magnetite*** | $Fe^{2+}(Fe^{+3})_2O_4$ |
| ***Muscovite*** | $KAl_2(Si_3Al)O_{10}(OH,F)_2$ |
| ***Pitchblende*** | $UO_2$ |
| ***Prehnite*** | $Ca_2(Al,Fe^{3+})AlSi_3O_{10}(OH)_2$ |
| ***Pyrite*** | $Fe^{2+}S_2$ |
| ***Quartz*** | $SiO_2$ |
| ***REE-carbonate*** | Ce, Nd, La, Y-rich carbonate |
| ***Sphalerite*** | ZnS |
| ***Titanite*** | $CaTiSiO_5$ |
| ***Clay minerals:*** | |
| ***Corrensite*** | (chlorite-like mixed-layer clay with layers of chlorite and smectite/vermiculite) |
| ***Illite*** | $(K, H_2O)Al_2[(Al,Si)Si_3O_{10}](OH)_2$ |
| ***Smectite*** | $(½Ca,Na)_{0.7}(Al,Mg,Fe)_{4–6}(Si,Al)_8O_{20}(OH)_4 \cdot n\ H_2O$ |
| ***Vermiculite*** | $(Mg,Ca)_{0.6–0.9}(Mg,Fe,Al)_6(Si,Al)_8O_{20}(OH)_4 \cdot n\ H_2O$ |
| ***Saponite*** | $Mg_3(Si_4O_{10})(OH)_2 \cdot nH_2O$ (variety of swelling smectite) |

# Appendix II

## Chemical analyses of fracture fillings – Forsmark

| Borehole | | KFM01A | KFM01A | KFM01A | KFM01A | KFM01A | KFM01A | KFM01A | KFM01B | KFM01B |
|---|---|---|---|---|---|---|---|---|---|---|
| Depth | | 127.40 | 148.40 | 149.18 | 179.35 | 185.35 | 188.1 | 269.90 | 25.30 | 28.65 |
| Minerals | | Ana,Qz, K-fsp,chl | Pre,Corr, Ana,Py | Pre,Corr, Ana,Py | Qz,Ab,Chl Ca,Hm | Pre,Chl,Ill Hm,MLC | Lau,Qz | Pre,Ana Corr,Ca Qz,Py | Asph | K-fsp |
| SiO2 | % | 59.4 | 44.7 | 40.9 | 51.6 | 38.9 | 53.8 | 32.6 | 1.4 | 73.5 |
| Al2O3 | % | 15.3 | 20.3 | 18.9 | 16.7 | 19.4 | 21.5 | 15.0 | 0.3 | 13.1 |
| CaO | % | 0.7 | 17.7 | 12.7 | 3.0 | 9.8 | 11.1 | 19.2 | 2.3 | 0.7 |
| Fe2O3 | % | 10.7 | 6.7 | 10.8 | 11.6 | 10.5 | 1.0 | 10.2 | 0.7 | 2.4 |
| K2O | % | 3.0 | 1.3 | 1.6 | 1.7 | 1.5 | 0.4 | 0.7 | 0.2 | 8.5 |
| MgO | % | 1.5 | 3.4 | 7.8 | 4.5 | 6.2 | 0.2 | 6.5 | < 0.04 | 0.6 |
| MnO | % | 0.1 | 0.1 | 0.2 | 0.2 | 0.1 | 0.0 | 0.2 | 0.0 | 0.0 |
| Na2O | % | 5.1 | 1.1 | 0.4 | 5.1 | 0.2 | 0.3 | 1.2 | < 0.08 | 0.6 |
| P2O5 | % | 0.0 | 0.0 | 0.0 | 0.2 | 0.0 | 0.0 | 0.0 | 0.0 | 0.1 |
| TiO2 | % | 0.1 | 0.0 | 0.0 | 0.9 | 0.0 | 0.0 | 0.0 | 0.0 | 0.2 |
| Summa | % | 96.0 | 95.4 | 93.3 | 95.6 | 86.6 | 88.4 | 85.4 | 4.8 | 99.8 |
| Ba | mg/kg | 554.0 | 180.0 | 340.0 | 161.0 | 76.3 | 128.0 | 117.0 | 16.2 | 1,540.0 |
| Be | mg/kg | 1.3 | 5.5 | 9.9 | 3.8 | 14.7 | 2.1 | 5.0 | < 1 | 2.4 |
| Co | mg/kg | < 6 | < 6 | < 6 | 21.5 | < 10 | < 6 | < 6 | < 10 | < 6 |
| Cr | mg/kg | 18.2 | 24.0 | 17.9 | 21.9 | < 30 | < 10 | 57.0 | < 20 | 27.3 |
| Cs | mg/kg | 32.7 | 9.2 | 3.0 | n.d. | 11.3 | n.d | 8.6 | | 5.9 |
| Cu | mg/kg | 37.2 | 13.8 | 7.1 | 11.4 | 96.2 | 6.2 | 39.7 | 248.0 | 41.7 |
| Ga | mg/kg | 16.7 | 32.5 | 37.9 | 31.4 | 7.4 | 26.7 | 21.6 | < 2 | 13.0 |
| Hf | mg/kg | 2.3 | 0.4 | 0.8 | 2.4 | 0.9 | 0.3 | 0.7 | < 0.2 | 5.6 |
| Mo | mg/kg | < 2 | < 2 | 14.5 | 50.7 | < 5 | < 2 | 5.1 | < 4 | < 2 |
| Nb | mg/kg | 6.7 | 3.2 | 0.9 | 8.7 | < 0.5 | 1.0 | 0.9 | < 0.4 | 9.5 |
| Ni | mg/kg | < 10 | < 10 | < 10 | 19.1 | < 30 | < 10 | 13.8 | < 20 | < 10 |
| Rb | mg/kg | 99.5 | 39.1 | 47.9 | 106.0 | 141.0 | 20.6 | 26.5 | < 4 | 181.0 |
| Sc | mg/kg | 1.6 | < 1 | < 1 | 36.2 | < 3 | < 1 | < 1 | < 2 | 5.6 |
| Sn | mg/kg | 1.6 | 2.5 | < 1 | 6.1 | 2.8 | < 1 | < 1 | 5.2 | 19.6 |
| Sr | mg/kg | 52.3 | 22.6 | 54.0 | 193.0 | 79.7 | 338.0 | 53.0 | 9.0 | 50.4 |
| Ta | mg/kg | 0.5 | 0.4 | 0.1 | 0.8 | < 0.1 | 0.1 | 0.1 | < 0.1 | 0.9 |
| Th | mg/kg | 1.5 | 0.2 | 0.5 | 2.9 | < 0.3 | 0.9 | 1.2 | 0.6 | 14.1 |
| U | mg/kg | 6.7 | 6.7 | 5.5 | 12.1 | 8.4 | 0.5 | 3.4 | 1.4 | 15.8 |
| V | mg/kg | 21.2 | 87.9 | 177.0 | 100.0 | 100.0 | < 2 | 50.0 | 24.8 | 18.6 |
| W | mg/kg | 6.2 | 4.6 | 1.9 | 3.0 | 11.3 | 1.0 | 2.6 | 22.2 | 1.4 |
| Y | mg/kg | 13.1 | 8.9 | 18.0 | 34.3 | 28.2 | 2.1 | 12.3 | 11.4 | 41.9 |
| Zn | mg/kg | 21.8 | 32.1 | 73.7 | 109.0 | 133.0 | < 10 | 93.9 | 94.2 | 78.2 |
| Zr | mg/kg | 47.1 | 2.4 | 6.8 | 97.7 | 6.6 | 12.4 | 10.6 | 12.0 | 211.0 |
| La | mg/kg TS | 30.0 | 4.5 | 10.8 | 41.8 | 45.6 | 6.6 | 25.3 | 4.2 | 114.0 |
| Ce | mg/kg TS | 56.1 | 13.1 | 24.9 | 62.4 | 182.0 | 15.2 | 47.9 | 9.3 | 170.0 |
| Pr | mg/kg TS | 5.1 | 1.4 | 2.4 | 8.3 | 12.0 | 1.5 | 5.2 | < 2 | 24.2 |
| Nd | mg/kg TS | 18.3 | 6.4 | 10.6 | 32.7 | 43.3 | 4.6 | 22.2 | 2.4 | 85.0 |
| Sm | mg/kg TS | 4.0 | 1.7 | 4.2 | 6.4 | 8.7 | 0.817 | 3.3 | < 0.6 | 12.7 |
| Eu | mg/kg TS | 0.5 | 0.2 | < 0.05 | 1.1 | 0.9 | < 0.05 | 0.3 | < 0.08 | 0.8 |
| Gd | mg/kg TS | 3.2 | 1.5 | 3.3 | 6.4 | 10.1 | 1.0 | 2.8 | < 0.6 | 9.1 |
| Tb | mg/kg TS | 0.5 | 0.1 | 0.4 | 0.8 | 1.1 | 0.1 | 0.2 | 0.2 | 1.2 |
| Dy | mg/kg TS | 2.3 | 1.2 | 2.5 | 4.5 | 4.3 | 0.6 | 1.5 | 1.4 | 5.9 |
| Ho | mg/kg TS | 0.5 | 0.2 | 0.5 | 1.0 | 1.0 | 0.1 | 0.3 | < 0.1 | 1.3 |
| Er | mg/kg TS | 1.2 | 0.5 | 1.2 | 3.1 | 3.2 | 0.588 | 0.9 | < 0.2 | 3.4 |
| Tm | mg/kg TS | < 0.1 | 0.1 | 0.2 | 0.5 | < 0.3 | < 0.1 | < 0.1 | < 0.2 | 0.6 |
| Yb | mg/kg TS | 1.5 | 0.9 | 1.1 | 3.3 | 2.2 | < 0.2 | 0.9 | < 0.4 | 4.8 |
| Lu | mg/kg TS | 0.1 | 0.1 | 0.1 | 0.5 | 0.2 | < 0.03 | 0.1 | < 0.06 | 0.8 |

Ab = albite, Amp = amphibole Ana = analcime, Apo = apophyllite, Asph = asphaltite, Chl = chlorite, Corr = corrensite, Hm = hematite, Ill = illite, K-fsp = K-feldspar, Lau = laumontite, MLC = Mixed layer clay, Mus = muscovite, Pl = plagioclase, Pre = prehnite, Qz = quartz, Sme = smectite

| Borehole<br>Depth<br>Minerals | | KFM01B<br>47.90 | KFM01B<br>49.39<br>Asph,qz,<br>K-fsp,chl | KFM01B<br>418.29 | KFM02A<br>118.25<br>Qz,Ab,<br>K-fsp,Ill | KFM02A<br>423.65<br>Qz,Ab<br>K-fsp,Ca<br>Chl | KFM02A<br>476.75<br>Qz,Corr,<br>Apo,Ca | KFM02A<br>516.09<br>Ca,Chl,<br>Corr,Qz<br>Ab,K-fsp | KFM02A<br>893.45<br>Apo,Chl | KFM03A<br>644.17 |
|---|---|---|---|---|---|---|---|---|---|---|
| SiO2 | % | 49.2 | 34.6 | 35.6 | 71.8 | 70.6 | 40.1 | 40.0 | 51.0 | 31.5 |
| Al2O3 | % | 16.5 | 8.7 | 13.1 | 14.2 | 12.5 | 11.9 | 16.4 | 1.2 | 12.8 |
| CaO | % | 1.8 | 0.3 | 6.0 | 0.5 | 0.9 | 6.8 | 12.4 | 22.7 | 8.6 |
| Fe2O3 | % | 15.0 | 1.4 | 15.3 | 2.0 | 5.9 | 14.2 | 9.1 | 1.4 | 22.7 |
| K2O | % | 6.4 | 7.2 | 0.4 | 8.1 | 5.2 | 4.7 | 1.6 | 4.6 | 2.1 |
| MgO | % | 3.2 | 0.2 | 18.5 | 0.8 | 2.3 | 12.1 | 7.7 | 0.8 | 9.6 |
| MnO | % | 0.1 | 0.0 | 0.4 | 0.0 | 0.1 | 0.3 | 0.3 | 0.0 | 0.3 |
| Na2O | % | 1.1 | 0.2 | 0.3 | 1.1 | 2.1 | 0.2 | 2.4 | 0.2 | 1.0 |
| P2O5 | % | 0.3 | 0.0 | 0.2 | 0.1 | 0.1 | 0.1 | 0.1 | 0.0 | 0.1 |
| TiO2 | % | 0.9 | 0.1 | 0.5 | 0.1 | 0.3 | 0.6 | 1.0 | 0.1 | 0.9 |
| Summa | % | 94.5 | 52.7 | 90.3 | 98.7 | 100.0 | 91.0 | 90.9 | 82.2 | 89.6 |
| Ba | mg/kg | 681.0 | 1,480.0 | 33.2 | 1,220.0 | 1,430.0 | 317.0 | 207.0 | 247.0 | 704.0 |
| Be | mg/kg | 4.1 | 0.8 | 2.5 | 2.1 | 1.4 | 1.2 | 5.1 | < 1 | 13.6 |
| Co | mg/kg | 13.6 | < 6 | 80.0 | < 7 | < 6 | 21.6 | 17.8 | < 10 | 43.2 |
| Cr | mg/kg | 25.6 | 15.8 | 244.0 | 242.0 | < 10 | 617.0 | 294.0 | < 20 | 940.0 |
| Cs | mg/kg | 11.2 | n.a. | < 0.1 | 15.7 | 0.3 | 9.7 | 0.4 | 0.3 | 8.4 |
| Cu | mg/kg | | 12.2 | | 20.5 | 16.1 | 606.0 | 37.1 | 1,490.0 | n.a. |
| Ga | mg/kg | 32.5 | < 1 | 37.0 | 32.8 | 42.5 | 30.0 | 32.8 | < 2 | 36.5 |
| Hf | mg/kg | 2.7 | 2.2 | 1.0 | 7.3 | 11.5 | 0.9 | 6.9 | 3.3 | 3.3 |
| Mo | mg/kg | 2.5 | < 2 | < 2 | < 3 | < 2 | < 2 | < 2 | < 5 | 11.6 |
| Nb | mg/kg | 6.4 | 0.5 | 3.2 | 9.8 | 30.4 | 20.6 | 36.1 | 2.8 | 18.0 |
| Ni | mg/kg | 13.7 | 133.0 | 175.0 | < 10 | < 10 | 90.3 | 41.3 | 69.3 | 231.0 |
| Rb | mg/kg | 397.0 | 163.0 | 11.4 | 254.0 | 133.0 | 340.0 | 48.5 | 439.0 | 128.0 |
| Sc | mg/kg | 42.6 | 4.0 | 71.7 | 2.8 | 6.6 | 31.8 | 41.6 | < 2 | 61.7 |
| Sn | mg/kg | 14.0 | < 1 | 9.8 | 1.4 | 3.7 | 25.4 | 16.3 | 21.5 | 11.2 |
| Sr | mg/kg | 81.6 | 17.9 | 31.6 | 50.4 | 60.7 | 27.6 | 359.0 | 20.3 | 128.0 |
| Ta | mg/kg | 0.4 | < 0.06 | 0.3 | 1.1 | 2.7 | 23.1 | 5.2 | 0.2 | 5.3 |
| Th | mg/kg | 5.0 | 7.5 | 5.3 | 2.4 | 10.8 | 1.1 | 7.2 | 4.1 | 11.4 |
| U | mg/kg | 22.1 | 6.1 | 7.2 | 4.5 | 39.7 | 1.4 | 20.9 | 1.7 | 2,200.0 |
| V | mg/kg | 73.0 | 24.8 | 149.0 | 38.2 | 14.6 | 183.0 | 156.0 | 5.2 | 244.0 |
| W | mg/kg | 9.0 | 2.3 | 1.0 | 1.5 | 7.9 | 1.8 | 2.1 | 12.6 | 16.9 |
| Y | mg/kg | 56.9 | 52.9 | 19.0 | 25.4 | 39.1 | 35.4 | 54.2 | 212.0 | 217.0 |
| Zn | mg/kg | 124.0 | 39.0 | 311.0 | 56.5 | 87.5 | 285.0 | 196.0 | 194.0 | 1,210.0 |
| Zr | mg/kg | 152.0 | 116.0 | 18.7 | 250.0 | 353.0 | 24.9 | 197.0 | 87.3 | 102.0 |
| La | mg/kg TS | 88.6 | 31.0 | 9.0 | 12.9 | 38.4 | 43.8 | 37.0 | 815.0 | 105.0 |
| Ce | mg/kg TS | 148.0 | 44.8 | 21.3 | 25.6 | 74.6 | 44.4 | 57.0 | 1,060.0 | 105.0 |
| Pr | mg/kg TS | 17.2 | 3.3 | 2.9 | 3.0 | 7.8 | 4.8 | 6.8 | 97.2 | 13.3 |
| Nd | mg/kg TS | 76.9 | 26.0 | 11.6 | 11.0 | 34.1 | 23.0 | 27.2 | 373.0 | 50.8 |
| Sm | mg/kg TS | 15.8 | < 0.4 | 2.4 | 2.7 | 7.2 | 4.9 | 6.9 | 58.4 | 14.4 |
| Eu | mg/kg TS | 1.8 | 0.3 | 0.6 | 0.4 | 0.9 | < 0.04 | 0.6 | 9.4 | 2.2 |
| Gd | mg/kg TS | 14.2 | 6.5 | 2.5 | 1.7 | 6.3 | 4.7 | 6.4 | 58.8 | 18.9 |
| Tb | mg/kg TS | 2.0 | 1.1 | 0.4 | 0.4 | 1.1 | 0.7 | 1.1 | 7.2 | 4.2 |
| Dy | mg/kg TS | 9.5 | 7.3 | 2.7 | 3.0 | 7.0 | 5.0 | 7.7 | 32.4 | 29.9 |
| Ho | mg/kg TS | 1.8 | 1.5 | 0.5 | 0.8 | 1.5 | 1.1 | 1.7 | 5.6 | 7.2 |
| Er | mg/kg TS | 4.5 | 3.1 | 1.7 | 2.8 | 4.8 | 3.9 | 6.3 | 12.9 | 24.5 |
| Tm | mg/kg TS | 0.7 | 0.5 | 0.3 | 0.5 | 0.8 | 0.5 | 1.1 | 1.5 | 4.0 |
| Yb | mg/kg TS | 4.3 | 2.9 | 1.7 | 3.8 | 4.7 | 5.4 | 9.8 | 6.4 | 30.0 |
| Lu | mg/kg TS | 0.6 | 0.4 | 0.3 | 0.6 | 0.6 | 0.7 | 1.5 | 0.9 | 4.8 |

Ab = albite, Amp = amphibole Ana = analcime, Apo = apophyllite, Asph = asphaltite, Chl = chlorite, Corr = corrensite, Hm = hematite, Ill = illite, K-fsp = K-feldspar, Lau = laumontite, MLC = Mixed layer clay, Mus = muscovite, Pl = plagioclase, Pre = prehnite, Qz = quartz, Sme = smectite

| Borehole<br>Depth<br>Minerals | | KFM03A<br>643.80<br>Ca,Qz,Ab<br>K-fsp,Chl<br>Corr, Hm | KFM03A<br>803.85<br>Qz,Ab,<br>Chl | KFM03B<br>65.2<br>Ca,Qz,Ab<br>K-fsp,Chl<br>Corr, Ill | KFM05A<br>111.56<br>Qz,K-fsp,<br>Asph,Ill<br>< 0.125 m | KFM05A<br>629.21<br>Ca,Qz,Ab<br>Lau,Corr,<br>Hm, Ill | KFM06A<br>145.62<br>Qz,Ab<br>K-fsp,Sme<br>Corr,Py,Ill | KFM06A<br>770.32<br>Ca,Qz,<br>K-fsp<br>Corr | KFM06A<br>357.81<br>Amp,Bi,Pl,<br>Qz,Chl<br>MLC, | KFM07A<br>896.86<br>Qz,Lau<br>Ca,Chl,Ill<br>MLC |
|---|---|---|---|---|---|---|---|---|---|---|
| SiO2 | % | 29.9 | 54.6 | 64.7 | 66.6 | 45.5 | 44.5 | 50.8 | 42.9 | 64.8 |
| Al2O3 | % | 11.3 | 14.0 | 15.7 | 13.1 | 10.5 | 17.2 | 15.2 | 12.8 | 14.7 |
| CaO | % | 12.7 | 1.6 | 1.3 | 0.2 | 5.8 | 0.7 | 9.8 | 5.4 | 3.5 |
| Fe2O3 | % | 17.7 | 15.6 | 4.7 | 3.3 | 13.9 | 14.7 | 4.6 | 18.7 | 4.0 |
| K2O | % | 2.2 | 3.0 | 5.2 | 9.9 | 2.2 | 4.8 | 8.1 | 3.0 | 4.3 |
| MgO | % | 8.1 | 5.0 | 2.3 | 0.6 | 9.4 | 7.4 | 2.1 | 10.7 | 3.0 |
| MnO | % | 0.3 | 0.2 | 0.0 | 0.0 | 0.2 | 0.1 | 0.1 | 0.5 | 0.0 |
| Na2O | % | 1.1 | 3.2 | 3.8 | 0.2 | 1.4 | 0.3 | 1.8 | 1.1 | 0.2 |
| P2O5 | % | 0.0 | 0.1 | 0.5 | 0.0 | 0.0 | 0.0 | 0.0 | 0.2 | 0.1 |
| TiO2 | % | 0.9 | 0.7 | 0.5 | 0.2 | 0.1 | 0.0 | 0.1 | 0.8 | 0.4 |
| Summa | % | 84.2 | 98.0 | 98.7 | 94.1 | 89.0 | 89.7 | 92.6 | 96.1 | 95.1 |
| Ba | mg/kg | 551.0 | 292.0 | 313.0 | 1,770.0 | 419.0 | 215.0 | 797.0 | 335.0 | 205.0 |
| Be | mg/kg | 11.1 | 3.2 | 2.9 | 1.2 | 3.7 | 14.5 | 3.4 | 3.0 | 1.9 |
| Co | mg/kg | 38.3 | 10.9 | 13.6 | < 6 | < 7 | 211.0 | < 6 | 39.9 | < 6 |
| Cr | mg/kg | 816.0 | 74.1 | 17.0 | 413.0 | 1,760.0 | 19.0 | 36.2 | 896.0 | 17.7 |
| §Cs | mg/kg | 5.0 | 2.8 | 7.1 | 2.6 | 1.7 | 14.1 | 0.9 | 4.4 | 8.3 |
| Cu | mg/kg | 249.0 | 114.0 | 162.0 | < 6 | 18.9 | 77.6 | 208.0 | 8.1 | 9.4 |
| Ga | mg/kg | 29.8 | 88.9 | 11.2 | 12.8 | 47.2 | 70.5 | 27.6 | 13.4 | < 1 |
| Hf | mg/kg | 2.7 | 8.1 | 3.4 | 3.7 | 3.8 | 1.2 | 3.7 | 2.1 | 3.1 |
| Mo | mg/kg | < 2 | 8.13 | < 2 | 2.4 | < 3 | 8.1 | 5.9 | < 2 | < 2 |
| Nb | mg/kg | 33.6 | 54.0 | 30.5 | 9.8 | 3.2 | 7.9 | 17.1 | 32.8 | 6.4 |
| Ni | mg/kg | 183.0 | 52.0 | < 10 | < 10 | 19.5 | 109.0 | 18.4 | 144.0 | < 10 |
| Rb | mg/kg | 116.0 | 118.0 | 135.0 | 326.0 | 86.8 | 259.0 | 186.0 | 157.0 | 301.0 |
| Sc | mg/kg | 47.4 | 17.5 | 12.8 | 8.1 | 3.2 | 151.0 | 4.4 | 52.4 | 11.0 |
| Sn | mg/kg | 5.8 | 15.4 | 9.0 | 12.9 | 4.2 | 93.1 | 8.4 | 22.8 | 3.3 |
| Sr | mg/kg | 110.0 | 69.6 | 74.9 | 15.8 | 102.0 | 53.2 | 490.0 | 63.0 | 64.9 |
| Ta | mg/kg | 4.1 | 3.4 | 4.3 | 0.7 | 0.3 | 0.8 | 1.6 | 5.0 | 0.9 |
| Th | mg/kg | 6.8 | 1.3 | 8.1 | 9.8 | 6.9 | 2.1 | 14.7 | < 0.1 | < 0.1 |
| U | mg/kg | 2,310.0 | 3.3 | 14.5 | 3.3 | 69.4 | 17.8 | 12.8 | 14.9 | 2.9 |
| V | mg/kg | 195.0 | 74.2 | 35.1 | 19.1 | 22.0 | 430.0 | 32.9 | 234.0 | 55.4 |
| W | mg/kg | 11.5 | 4.0 | 4.7 | 1.8 | 8.0 | 0.6 | 6.1 | 1.6 | 68.3 |
| Y | mg/kg | 198.0 | 34.2 | 39.5 | 39.7 | 134.0 | 104.0 | 90.0 | 73.1 | 25.9 |
| Zn | mg/kg | 234.0 | 158.0 | 148.0 | 110.0 | 201.0 | 96.3 | 170.0 | 287.0 | 54.8 |
| Zr | mg/kg | 91.0 | 287.0 | 125.0 | 133.0 | 104.0 | 26.3 | 105.0 | 39.6 | 129.0 |
| La | mg/kg TS | 70.8 | 8.4 | 12.0 | 46.9 | 201.0 | 3.8 | 24.9 | 28.2 | 16.1 |
| Ce | mg/kg TS | 73.3 | 21.1 | 15.9 | 95.9 | 1,090.0 | 14.6 | 46.7 | 50.4 | 32.3 |
| Pr | mg/kg TS | 10.4 | 6.7 | 3.3 | 11.3 | 41.9 | 1.8 | 6.3 | 5.8 | 4.2 |
| Nd | mg/kg TS | 40.6 | 14.6 | 14.4 | 38.2 | 191.0 | 7.9 | 23.2 | 26.4 | 19.7 |
| Sm | mg/kg TS | 12.7 | 4.1 | 3.0 | 7.4 | 39.8 | 3.8 | 5.2 | 6.3 | 4.1 |
| Eu | mg/kg TS | 2.2 | 0.6 | 0.8 | 0.5 | 3.1 | 0.4 | 0.4 | 0.7 | 0.8 |
| Gd | mg/kg TS | 19.5 | 0.9 | 4.5 | 6.6 | 47.7 | 7.6 | 6.9 | 4.2 | 2.8 |
| Tb | mg/kg TS | 4.1 | < 0.1 | 0.8 | 1.0 | 4.8 | 1.4 | 1.5 | 1.2 | 0.6 |
| Dy | mg/kg TS | 31.4 | 4.7 | 5.5 | 5.8 | 15.6 | 10.6 | 11.5 | 7.4 | 3.2 |
| Ho | mg/kg TS | 7.2 | 1.1 | 1.2 | 1.1 | 2.6 | 2.4 | 2.7 | 1.8 | 0.7 |
| Er | mg/kg TS | 23.7 | 3.0 | 3.9 | 3.1 | 4.9 | 9.0 | 8.4 | 6.4 | 1.9 |
| Tm | mg/kg TS | 4.2 | 0.7 | 0.7 | 0.5 | 0.4 | 1.4 | 1.4 | 1.2 | 0.3 |
| Yb | mg/kg TS | 28.7 | 3.8 | 4.7 | 3.2 | 3.2 | 11.2 | 9.9 | 9.9 | 2.3 |
| Lu | mg/kg TS | 4.9 | 0.5 | 0.7 | 0.4 | 0.4 | 1.7 | 1.2 | 1.8 | 0.4 |

Ab = albite, Amp = amphibole Ana = analcime, Apo = apophyllite, Asph = asphaltite, Chl = chlorite, Corr = corrensite, Hm = hematite, Ill = illite, K-fsp = K-feldspar, Lau = laumontite, MLC = Mixed layer clay, Mus = muscovite, Pl = plagioclase, Pre = prehnite, Qz = quartz, Sme = smectite

| Borehole | | KFM08A | KFM08A | KFM08A |
|---|---|---|---|---|
| Depth | | 495.13 | 686.67 | 918.84 |
| Minerals | | Qz,K-fsp Ill,Chl,Pre | Ca,Mus Qz,Chl MLC | Qz,Pl,Ca Lau,Chl,Hm Ill,MLC |
| SiO2 | % | 60.5 | 46.9 | 51.4 |
| Al2O3 | % | 16.6 | 21.9 | 16.5 |
| CaO | % | 0.7 | 6.2 | 4.4 |
| Fe2O3 | % | 6.8 | 5.7 | 9.8 |
| K2O | % | 7.3 | 7.3 | 3.9 |
| MgO | % | 3.5 | 1.8 | 6.2 |
| MnO | % | 0.1 | 0.1 | 0.1 |
| Na2O | % | 0.3 | 1.2 | 1.1 |
| P2O5 | % | 0.0 | 0.0 | 0.2 |
| TiO2 | % | 0.2 | 0.4 | 0.9 |
| Summa | % | 95.9 | 91.3 | 94.4 |
| Ba | mg/kg | 589.0 | 2,040.0 | 195.0 |
| Be | mg/kg | 4.2 | 9.8 | 7.0 |
| Co | mg/kg | < 6 | < 6 | 18.3 |
| Cr | mg/kg | 26.4 | 258.0 | 85.1 |
| Cs | mg/kg | 6.1 | 17.6 | 12.1 |
| Cu | mg/kg | 18.2 | 73.5 | 17.1 |
| Ga | mg/kg | 18.9 | 35.7 | < 1 |
| Hf | mg/kg | 2.9 | 1.6 | 2.1 |
| Mo | mg/kg | < 2 | < 2 | < 2 |
| Nb | mg/kg | 12.9 | 10.5 | 6.3 |
| Ni | mg/kg | < 10 | < 10 | 15.0 |
| Rb | mg/kg | 589.0 | 342.0 | 295.0 |
| Sc | mg/kg | 11.2 | 13.9 | 34.8 |
| Sn | mg/kg | 3.9 | 13.1 | 20.3 |
| Sr | mg/kg | 42.1 | 48.2 | 136.0 |
| Ta | mg/kg | 3.2 | 0.6 | 0.6 |
| Th | mg/kg | 0.5 | < 0.1 | < 0.1 |
| U | mg/kg | 8.0 | 164.0 | 20.5 |
| V | mg/kg | 87.0 | 93.8 | 187.0 |
| W | mg/kg | 48.4 | 68.6 | 7.8 |
| Y | mg/kg | 521.0 | 62.4 | 37.4 |
| Zn | mg/kg | 77.2 | 51.9 | 109.0 |
| Zr | mg/kg | 80.4 | 73.4 | 92.7 |
| La | mg/kg TS | 12.5 | 62.3 | 19.2 |
| Ce | mg/kg TS | 37.9 | 110.0 | 37.2 |
| Pr | mg/kg TS | 7.1 | 13.8 | 4.2 |
| Nd | mg/kg TS | 50.1 | 55.0 | 20.9 |
| Sm | mg/kg TS | 23.0 | 9.9 | 3.1 |
| Eu | mg/kg TS | 2.7 | 0.5 | 1.3 |
| Gd | mg/kg TS | 34.6 | 7.6 | 3.0 |
| Tb | mg/kg TS | 6.2 | 1.4 | 0.6 |
| Dy | mg/kg TS | 40.0 | 7.7 | 3.7 |
| Ho | mg/kg TS | 8.9 | 1.6 | 0.9 |
| Er | mg/kg TS | 27.0 | 3.6 | 2.6 |
| Tm | mg/kg TS | 3.8 | 0.6 | 0.4 |
| Yb | mg/kg TS | 26.9 | 4.2 | 3.2 |
| Lu | mg/kg TS | 4.0 | 0.5 | 0.5 |

Ab = albite, Amp = amphibole Ana = analcime, Apo = apophyllite, Asph = asphaltite, Chl = chlorite, Corr = corrensite, Hm = hematite, Ill = illite, K-fsp = K-feldspar, Lau = laumontite, MLC = Mixed layer clay, Mus = muscovite, Pl = plagioclase, Pre = prehnite, Qz = quartz, Sme = smectite.

# Appendix III

## Chemical analyses of fracture fillings – Oskarshamn

| Borehole<br>Depth<br>Minerals | | KSH01B<br>3.7–3.87 m<br>Qz, Ca, Corr, Sme, (Chl) | KSH01B<br>67.8–67.9 m<br>Qz, K-fsp, Ab, Chl, Ca, MLC, (Ill) | KSH01B<br>82.20 m<br>Qz, K-fsp, Ab, Ca, Chl, Chl, MLC | KSH01A<br>159.2 m<br>Qz, K-fsp, Ab, Ca, Chl, Amp, Corr | KSH01A<br>250.40–250.45 m<br>Qz, K-fsp, Ca, Chl, Hm, (Ill) | KSH01A<br>255.78–255.93 m<br>Qz, K-fsp, Ca, Chl, Hm, Corr |
|---|---|---|---|---|---|---|---|
| SiO2 | % | 24.57 | 47.86 | 49.15 | 40.60 | 46.58 | 43.16 |
| Al2O3 | % | 7.29 | 14.19 | 16.79 | 11.50 | 14.58 | 15.49 |
| CaO | % | 19.02 | 6.67 | 3.24 | 8.73 | 4.18 | 3.78 |
| Fe2O3 | % | 11.35 | 8.48 | 11.32 | 14.72 | 10.85 | 10.64 |
| K2O | % | 0.73 | 3.82 | 5.69 | 1.79 | 4.48 | 4.36 |
| MgO | % | 11.72 | 4.48 | 4.68 | 4.86 | 8.62 | 11.28 |
| MnO | % | 0.48 | 0.18 | 0.19 | 0.19 | 0.25 | 0.22 |
| Na2O | % | 0.19 | 2.84 | 1.82 | 1.62 | 0.25 | 0.65 |
| P2O5 | % | < 0.01 | 0.33 | 0.42 | 0.34 | 0.23 | 0.43 |
| TiO2 | % | 0.05 | 1.35 | 1.07 | 0.99 | 1.31 | 1.61 |
| Total | % | 75.4 | 90.2 | 94.4 | 85.4 | 91.3 | 91.6 |
| Ba | mg/kg | 165 | 598 | 1,290 | 9,720 | 1,210 | 964 |
| Be | mg/kg | 7.8 | 4.5 | 7.54 | 3.04 | 4.35 | 5.55 |
| Co | mg/kg | 14.8 | 16.4 | 24.7 | < 6 | 21.7 | 23.8 |
| Cr | mg/kg | < 10 | 116 | 78.4 | 144 | 94.2 | 67.9 |
| Cs | mg/kg | 3.37 | 9.2 | 36.9 | 1.62 | 2.23 | 2.86 |
| Cu | mg/kg | 390 | 41.5 | 190 | 43.7 | 387 | 351 |
| Ga | mg/kg | 17 | 17.3 | 31.1 | 15.8 | 18 | 23.9 |
| Hf | mg/kg | 0.439 | 8.63 | 5.88 | 5.82 | 5.3 | 8.37 |
| Mo | mg/kg | < 3 | < 4 | < 2 | 17.7 | 9.32 | < 2 |
| Nb | mg/kg | 1.19 | 16.3 | 21.2 | 16 | 13 | 27.3 |
| Ni | mg/kg | 13.7 | 28.6 | 28.6 | < 10 | 22.5 | 26.2 |
| Rb | mg/kg | 23 | 121 | 201 | 42.8 | 108 | 90.1 |
| Sc | mg/kg | 10.4 | 23.6 | 51.3 | 21.7 | 20.4 | 27.8 |
| Sn | mg/kg | 10.8 | 3.74 | 18.9 | 9.52 | 21.8 | 17.5 |
| Sr | mg/kg | 132 | 190 | 198 | 259 | 461 | 153 |
| Ta | mg/kg | 0.184 | 1.19 | 2.93 | 1.29 | 0.96 | 2.22 |
| Th | mg/kg | 0.255 | 5.88 | 12.1 | 7.47 | 4.95 | 7.93 |
| U | mg/kg | 2.33 | 4.86 | 22.7 | 9.46 | 9.56 | 19.7 |
| V | mg/kg | 111 | 183 | 359 | 163 | 183 | 261 |
| W | mg/kg | 2.49 | 5.49 | 16.9 | 2.75 | 38.3 | 3.48 |
| Y | mg/kg | 74 | 38.9 | 58.4 | 39.4 | 37.3 | 57.2 |
| Zn | mg/kg | 356 | 168 | 313 | 133 | 360 | 485 |
| Zr | mg/kg | 6.18 | 310 | 241 | 232 | 234 | 339 |
| La | mg/kg | 67.4 | 59.2 | 673 | 92.2 | 43.7 | 107 |
| Ce | mg/kg | 131 | 114 | 926 | 170 | 93.7 | 227 |
| Pr | mg/kg | 15.6 | 13.4 | 98.8 | 19.6 | 11.4 | 24.8 |
| Nd | mg/kg | 67.3 | 58.3 | 387 | 71.9 | 43.8 | 98.3 |
| Sm | mg/kg | 13.5 | 10.1 | 35.5 | 11.7 | 7.87 | 14 |
| Eu | mg/kg | 3.37 | 2.48 | 5.82 | 1.72 | 2.18 | 3.92 |
| Gd | mg/kg | 16.9 | 8.6 | 26.9 | 8.68 | 9.42 | 12.9 |
| Tb | mg/kg | 2.4 | 1.21 | 3.16 | 1.43 | 1.22 | 1.92 |
| Dy | mg/kg | 11.9 | 7.54 | 9.59 | 6.91 | 7.02 | 10 |
| Ho | mg/kg | 2.33 | 1.47 | 1.92 | 1.42 | 1.37 | 1.91 |
| Er | mg/kg | 5.39 | 4.52 | 4.61 | 3.7 | 3.7 | 5.51 |
| Tm | mg/kg | 0.749 | 0.722 | 0.644 | 0.618 | 0.701 | 0.934 |
| Yb | mg/kg | 4.68 | 3.83 | 4.19 | 3.91 | 4 | 6.03 |
| Lu | mg/kg | 0.637 | 0.699 | 0.587 | 0.623 | 0.523 | 0.818 |

Ab = albite, Amp = amphibole, Apo = apophyllite, Chl = chlorite, Corr = corrensite, Ep = epidote, Hm = hematite, Ill = illite, K-fsp = K-feldspar, Lau = laumontite, MLC = Mixed layer clay, Mus = muscovite, Pre = prehnite, Qz = quartz, Sme = smectite, Ta = talc.

| Borehole<br>Depth<br>Minerals | | KSH01A<br>558.60–558.65 m<br>Qz, K-fsp,<br>Ca, Chl,<br>Hm, Corr | KSH01A<br>590.36–590.52 m<br>Qz, K-fsp,<br>Ab, Chl,<br>MLC, Ill | KSH02<br>289 m<br>Qz, K-fsp,<br>Ab, Ca, Chl,<br>Hm, Corr | KSH02<br>578 m<br>Chl, Qz,<br>K-fsp, Ab,<br>Hm, Corr, (Ta) | KSH02<br>743 m<br>Qz, K-fsp,<br>Ab, Hm,<br>Chl, Corr | KSH03A<br>271 m<br>Not<br>analysed |
|---|---|---|---|---|---|---|---|
| SiO2 | % | 44.02 | 26.28 | 44.3 | 39.3 | 48.5 | 54.8 |
| Al2O3 | % | 14.07 | 9.88 | 13 | 15.8 | 15.9 | 16.2 |
| CaO | % | 2.20 | 18.32 | 2.28 | 2.9 | 1.73 | 0.962 |
| Fe2O3 | % | 11.41 | 9.16 | 21.5 | 14.4 | 10.5 | 11 |
| K2O | % | 3.40 | 1.12 | 2.75 | 2.62 | 3.64 | 5.22 |
| MgO | % | 12.27 | 12.54 | 6.48 | 12.9 | 10.2 | 4.3 |
| MnO | % | 0.33 | 0.46 | 0.189 | 0.339 | 0.233 | 0.097 |
| Na2O | % | 1.54 | 0.60 | 2.29 | 0.966 | 2.9 | 1.23 |
| P2O5 | % | 0.14 | 0.08 | 0.28 | 0.417 | 0.227 | 0.538 |
| TiO2 | % | 0.78 | 0.22 | 0.998 | 1.51 | 0.737 | 1.38 |
| Total | % | 90.2 | 78.7 | 94.1 | 91.2 | 94.6 | 95.7 |
| Ba | mg/kg | 840 | 518 | 1,040 | 511 | 621 | 906 |
| Be | mg/kg | 5.05 | 3.98 | 3.89 | 9.8 | 6.09 | 7.56 |
| Co | mg/kg | 19.9 | 14.4 | 16 | 19.9 | 21.7 | 16.9 |
| Cr | mg/kg | 22.7 | 41.9 | 93.8 | 77.7 | 73.1 | 67.3 |
| Cs | mg/kg | 2.82 | 0.378 | 4.58 | 5.87 | 1.17 | 19.3 |
| Cu | mg/kg | 504 | 121 | 132 | 930 | 19 | 270 |
| Ga | mg/kg | 17.1 | 20.2 | 91.5 | 98.9 | 31.7 | 83.5 |
| Hf | mg/kg | 2.84 | 1.27 | 6.51 | 11.9 | 4.08 | 10.8 |
| Mo | mg/kg | < 4 | < 2 | < 2 | < 2 | < 2 | < 2 |
| Nb | mg/kg | 11.7 | 3.08 | 17.7 | 24.3 | 10.8 | 28.3 |
| Ni | mg/kg | < 20 | 22.7 | 28.2 | 32.7 | 27.7 | 35.4 |
| Rb | mg/kg | 98.2 | 27.1 | 96.8 | 87.6 | 87.8 | 326 |
| Sc | mg/kg | 27.6 | 5 | 24.5 | 25.9 | 20.2 | 14 |
| Sn | mg/kg | 3.16 | < 1 | 10.1 | 41.7 | 2.54 | 12 |
| Sr | mg/kg | 229 | 165 | 386 | 186 | 355 | 87.8 |
| Ta | mg/kg | 1.04 | 0.179 | 1.23 | 1.88 | 0.596 | 2.63 |
| Th | mg/kg | 3.82 | 1.45 | 6.68 | 13.8 | 8.31 | 15.8 |
| U | mg/kg | 9.77 | 0.909 | 11.3 | 8.31 | 6.98 | 23.2 |
| V | mg/kg | 253 | 147 | 332 | 122 | 114 | 94.8 |
| W | mg/kg | 1.89 | 0.953 | 7.04 | 8.64 | 7.41 | 7.75 |
| Y | mg/kg | 35.9 | 6.2 | 43.1 | 64.6 | 33.4 | 36.1 |
| Zn | mg/kg | 523 | 384 | 377 | 1,130 | 470 | 236 |
| Zr | mg/kg | 118 | 52.3 | 250 | 487 | 166 | 504 |
| La | mg/kg | 44.6 | 13.4 | 145 | 71.3 | 55.7 | 25.6 |
| Ce | mg/kg | 86.9 | 21.5 | 235 | 157 | 107 | 48 |
| Pr | mg/kg | 9.69 | 2.2 | 26 | 21.9 | 12.8 | 8.83 |
| Nd | mg/kg | 33.1 | 9.81 | 96.2 | 77.4 | 46 | 24.9 |
| Sm | mg/kg | 6.81 | 1.31 | 13.7 | 13.9 | 8.36 | 4.69 |
| Eu | mg/kg | 1.8 | 0.367 | 2.6 | 3.18 | 1.63 | 1.07 |
| Gd | mg/kg | 8.13 | 1.57 | 7.18 | 9.17 | 6.82 | 3.22 |
| Tb | mg/kg | 1.37 | 0.168 | 0.714 | 1.01 | 1.01 | < 0.1 |
| Dy | mg/kg | 6.36 | 0.926 | 8.1 | 11.9 | 5.33 | 5.78 |
| Ho | mg/kg | 1.25 | 0.183 | 1.65 | 2.26 | 1.06 | 1.25 |
| Er | mg/kg | 3.6 | 0.743 | 4.52 | 6.26 | 2.82 | 4.04 |
| Tm | mg/kg | 0.657 | 0.159 | 0.675 | 0.971 | 0.493 | 0.73 |
| Yb | mg/kg | 4.42 | 0.674 | 5.37 | 7.03 | 3.07 | 4.56 |
| Lu | mg/kg | 0.642 | 0.118 | 0.78 | 0.974 | 0.399 | 0.768 |

Ab = albite, Amp = amphibole, Apo = apophyllite, Chl = chlorite, Corr = corrensite, Ep = epidote, Hm = hematite, Ill = illite, K-fsp = K-feldspar, Lau = laumontite, MLC = Mixed layer clay, Mus = muscovite, Pre = prehnite, Qz = quartz, Sme = smectite, Ta = talc.

| Borehole<br>Depth<br>Minerals | | KLX03<br>195.31 m<br>Qz, K-fsp, Ab, Amp, Chl, Ca, MLC | KLX03<br>534.25 m<br>Not analysed | KLX04<br>193.75 m<br>Qz, K-fsp, Chl, Ca, MLC | KLX06<br>214.16 m<br>Fl, Qz, K-fsp, Ab, Chl, MLC | KLX06<br>383.92 m<br>Qz, K-fsp, Ab, Chl, Ill, Ep, Hm | KLX06<br>388.27 m<br>Qz, K-fsp, Mus, Chl, (Ep), MLC | KLX07B<br>4.85 m<br>Qz, K-fsp, Chl, Ill, Corr | KLX07A<br>783.83 m<br>Qz, K-fsp, Ab, Ca, Chl, Corr |
|---|---|---|---|---|---|---|---|---|---|
| SiO2 | % | 48.3 | 9.57 | 62.1 | 40.4 | 43.8 | 53.8 | 49.5 | 54.1 |
| Al2O3 | % | 12.4 | 2.85 | 17.4 | 10.5 | 19.5 | 23.8 | 17.1 | 15.6 |
| CaO | % | 5.98 | 34.1 | 2.6 | 25.1 | 5.83 | 1.64 | 2.14 | 3.57 |
| Fe2O3 | % | 11.2 | 1.87 | 4.25 | 3.45 | 13.7 | 3.5 | 8.87 | 6.27 |
| K2O | % | 1.91 | 0.632 | 8.15 | 6.83 | 5.39 | 6.86 | 5.28 | 4.43 |
| MgO | % | 3.29 | 0.649 | 2.21 | 1.22 | 4.01 | 4.94 | 7.88 | 7.28 |
| MnO | % | 0.135 | 0.0227 | 0.108 | 0.0537 | 0.225 | 0.0747 | 0.261 | 0.163 |
| Na2O | % | 2.56 | 0.685 | 0.254 | 0.595 | 0.228 | 0.3 | 2.08 | 2.65 |
| P2O5 | % | 0.652 | 0.163 | 0.0775 | 0.037 | 0.482 | 0.195 | 0.314 | 0.217 |
| TiO2 | % | 1.38 | 0.238 | 0.228 | 0.0948 | 1.37 | 0.511 | 0.676 | 0.663 |
| Total | % | 87.8 | 50.8 | 97.4 | 88.3 | 94.5 | 95.6 | 94.1 | 94.9 |
| Ba | mg/kg | 15,400 | 219 | 1,020 | 2,330 | 550 | 422 | 1,750 | 618 |
| Be | mg/kg | 4.64 | < 0.7 | 13 | 4.87 | 237 | 13 | 75.2 | 7.31 |
| Co | mg/kg | < 6 | 19.4 | < 6 | < 6 | 11.4 | 7.94 | 36.5 | 6.58 |
| Cr | mg/kg | 93.9 | 149 | 36.2 | 12 | 118 | 31.8 | 34.4 | < 10 |
| Cs | mg/kg | 1.12 | < 0.1 | 35.8 | 8.34 | 103 | 62.3 | 12.1 | 1.23 |
| Cu | mg/kg | 6.51 | < 7 | 9.98 | 7.19 | 27.2 | 21.1 | 460 | 14.5 |
| Ga | mg/kg | 13.3 | < 1 | 32.9 | 5.63 | 34.9 | 23.6 | 29.2 | 19.4 |
| Hf | mg/kg | 13 | 2.22 | 2.12 | 8.94 | 6.21 | 4.9 | 3.72 | 4.96 |
| Mo | mg/kg | 7.14 | < 3 | < 2 | < 2 | < 2 | < 2 | < 2 | < 2 |
| Nb | mg/kg | 21.4 | 3.55 | 3.92 | 2.38 | 15.4 | 9.25 | 5.22 | 12.5 |
| Ni | mg/kg | < 10 | < 10 | < 10 | < 10 | 25.3 | 21.2 | 35.8 | < 10 |
| Rb | mg/kg | 33.1 | 17.8 | 231 | 119 | 415 | 348 | 137 | 87.9 |
| Sc | mg/kg | 9 | 1.85 | 2.35 | 4.74 | 20.3 | 3.12 | 16.7 | 7.12 |
| Sn | mg/kg | 9.61 | 4.72 | 5.73 | 6.46 | 14.4 | 4.12 | 7.67 | 11.2 |
| Sr | mg/kg | 717 | 325 | 899 | 54.1 | 1,870 | 402 | 485 | 590 |
| Ta | mg/kg | 6.13 | 0.364 | 0.456 | 1.28 | 1.32 | 0.996 | 0.593 | 1 |
| Th | mg/kg | 9.13 | 2.26 | 3.6 | 4.29 | 10 | 19.7 | 8.31 | 13.9 |
| U | mg/kg | 6.11 | 1.1 | 2.56 | 7.95 | 16.4 | 6.33 | 10.7 | 6.85 |
| V | mg/kg | 173 | 33.3 | 96.9 | 104 | 114 | 72.9 | 128 | 87.2 |
| W | mg/kg | 24.3 | 0.802 | 0.96 | 5.78 | 18.5 | 5.61 | 5.03 | 2.9 |
| Y | mg/kg | 50.1 | 11.5 | 10.6 | 93.3 | 36.2 | 13.2 | 44.9 | 22.3 |
| Zn | mg/kg | 407 | 180 | 218 | 312 | 552 | 267 | 1,900 | 559 |
| Zr | mg/kg | 700 | 98.1 | 84.7 | 32.5 | 323 | 235 | 190 | 227 |
| La | mg/kg | 60.1 | 17 | 50.3 | 73.1 | 99.3 | 11 | 220 | 73.5 |
| Ce | mg/kg | 163 | 38.7 | 78.6 | 77.3 | 168 | 21.7 | 438 | 117 |
| Pr | mg/kg | 20.6 | 5.79 | 8.83 | 7.12 | 22.1 | 2.94 | 49.2 | 13 |
| Nd | mg/kg | 80 | 22.6 | 31.8 | 26.4 | 81.8 | 10.7 | 182 | 45.1 |
| Sm | mg/kg | 13.4 | 3.48 | 3.48 | 4.33 | 11.8 | 2.43 | 23.6 | 5.94 |
| Eu | mg/kg | 1.23 | 0.655 | 0.658 | 0.885 | 2.66 | 0.546 | 4.99 | 1.29 |
| Gd | mg/kg | 8.29 | 1.92 | 1.55 | 4.23 | 8.47 | 1.58 | 15.6 | 3.96 |
| Tb | mg/kg | 1.49 | 0.319 | 0.314 | 0.828 | 1.27 | 0.335 | 1.98 | 0.639 |
| Dy | mg/kg | 6.6 | 1.63 | 1.54 | 5.28 | 5.76 | 1.74 | 7.14 | 3.74 |
| Ho | mg/kg | 1.25 | 0.337 | 0.251 | 1.13 | 0.973 | 0.423 | 1.15 | 0.639 |
| Er | mg/kg | 3.87 | 0.865 | 0.786 | 3.13 | 3.18 | 1.07 | 3.06 | 1.74 |
| Tm | mg/kg | 0.573 | 0.178 | 0.125 | 0.415 | 0.453 | 0.177 | 0.452 | 0.327 |
| Yb | mg/kg | 3.65 | 0.994 | 0.769 | 2.09 | 2.65 | 1.05 | 3.05 | 1.94 |
| Lu | mg/kg | 0.506 | 0.109 | 0.181 | 0.261 | 0.384 | 0.313 | 0.502 | 0.242 |

Ab = albite, Amp = amphibole, Apo = apophyllite, Chl = chlorite, Corr = corrensite, Ep = epidote, Hm = hematite, Ill = illite, K-fsp = K-feldspar, Lau = laumontite, MLC = Mixed layer clay, Mus = muscovite, Pre = prehnite, Qz = quartz, Sme = smectite, Ta = talc.